TRIBHUVAN UNIVERSITY

INSTITUTE OF E NGINEERING

PULCHOWK CAMPUS

THESIS NO: PUL080MSMSE015

HYBRID BIO-BASED EPOXY COMPOSITES FOR CLIMATE-RESILIENT SMART URBAN INFRASTRUCTURE

by

SACHIN GHIMIRE

A THESIS

SUBMITTED TO THE DEPARTMENT OF APPLIED SCIENCES AND CHEMICAL ENGINEERING

IN PARTIAL FULFILLMENT OF THE REQUIREMENTS FOR THE

DEGREE OF MASTER OF SCIENCE IN MATERIAL SCIENCE AND ENGINEERING

DEPARTMENT OF APPLIED SCIENCES AND CHEMICAL ENGINEERING

LALITPUR, NEPAL

MAY 2026

COPYRIGHT

BOARD OF EXAMINATION AND CERTIFICATE OF APPROVAL

This thesis work entitled **"Hybrid Bio-Based Epoxy Composites for Climate-Resilient Smart Urban Infrastructure"** by **Sachin Ghimire** (Roll No.: 080MSMSE015, Exam Roll No: 12360) under the supervision of **Asst. Prof. Dr. Chhabi Lal Gnawali** in the Department of Applied Sciences and Chemical Engineering, Pulchowk Campus, Institute of Engineering (IOE), Tribhuvan University (T.U.), is hereby submitted for the partial fulfilment of the Masters of Science (M.Sc.) degree in Material Science and Engineering. This thesis work has been accepted and forwarded to the Controller of Examination, Institute of Engineering, Tribhuvan University, Nepal for the legal procedure.

……..

Asst. Prof. Dr. Chhabi Lal Gnawali

Supervisor

Department of Applied Sciences and Chemical engineering

Pulchowk Campus, Institute of Engineering

Tribhuvan University

……..

Professor Dr. Rinita Rajbhandari

External Examiner

Department of Applied Sciences and Chemical engineering

Pulchowk Campus, Institute of Engineering

Tribhuvan University

……

Professor Dr. Sahira Joshi

Head of Department

Department of Applied Sciences and Chemical Engineering

Pulchowk Campus, Institute of Engineering

Tribhuvan University

RECOMMENDATION

This is to recommend that Sachin Ghimire (Roll No.: PUL080MSMSE015, Exam Roll No: 12360), has carried out thesis work entitled **"Hybrid Bio-Based Epoxy Composites for Climate-Resilient Smart Urban Infrastructure"** as part of the requirements for the Master of Science (M.Sc.) degree in Materials Science and Engineering under my supervision in the Department of Applied Sciences & Chemical Engineering, Pulchowk Campus, Institute of Engineering, Tribhuvan University, Kathmandu, Nepal.

He has fulfilled all the requirements laid down by the Institute of Engineering (IOE), Tribhuvan University (T.U.), Nepal for the submission of the thesis for the partial fulfilment of Masters of Science (M.Sc.) degree in Materials Science and Engineering.

…….

Asst. Prof. Dr. Chhabi Lal Gnawali

Supervisor

Department of Applied Sciences and Chemical Engineering

Pulchowk Campus

Institute of Engineering

Tribhuvan University

DECLARATION

This thesis entitled "**Hybrid Bio-Based Epoxy Composites for Climate-Resilient Smart Urban Infrastructure**" is submitted to the Department of Applied Sciences & Chemical Engineering, Pulchowk Campus, Institute of Engineering, Tribhuvan University, Nepal for the partial fulfillment of the requirements for the Master of Science (M.Sc.) degree in Materials Science and Engineering. This thesis work was carried out under the supervision of Assistant Professor Dr. Chhabi Lal Gnawali, Department of Applied Sciences and Chemical Engineering, Institute of Engineering, Pulchowk Campus, Tribhuvan University, Nepal.

I declare that the work presented in this thesis is original and has not been submitted previously for the award of any other degree.

…….

Sachin Ghimire

Roll No 080MSMSE015

Exam Roll No: 12360

LETTER OF FORWARD

Date: May, 2026

On the recommendation of Dr. Chhabi Lal Gnawali, this thesis submitted by Sachin Ghimire (Roll No.: 080MSMSE015, Exam Roll No: 12360), entitled "**Hybrid Bio-Based Epoxy Composites for Climate-Resilient Smart Urban Infrastructure**" is forwarded by the Department of Applied Sciences and Chemical Engineering, Pulchowk Campus, for the approval to the Evaluation Committee, Institute of Engineering (IOE), Tribhuvan University (T.U.), Nepal.

The candidate has fulfilled all the requirements laid down by the Institute of Engineering (IOE), Tribhuvan University (T.U.), Nepal for the thesis work.

……..

Professor Dr. Sahira Joshi

Head of Department

Department of Applied Sciences and Chemical Engineering

Pulchowk Campus

Institute of Engineering

Tribhuvan University

THIS THESIS WORK IS DEDICATED TO MY WIFE (SNEHA DHAKAL), FATHER (BINDU RAJ GHIMIRE) AND MOTHER (SARASWATI GHIMIRE).

ACKNOWLEDGEMENTS

I am deeply grateful to my supervisor, Assistant Professor Dr. Chhabi Lal Gnawali, Department of Applied Sciences and Chemical Engineering, Pulchowk Campus, Tribhuvan University for his guidance, motivation and support throughout my thesis work. I also sincerely thank Dr. Sahira Joshi, Head of Department, Dr. Ganesh Kumar Shrestha, Program Coordinator and Assistant Professor Purnima Mulmi for their mentorship and for fostering a supportive academic environment. Furthermore, I acknowledge the Nanomaterials Laboratory for providing the necessary experimental facilities, Amrit Science Campus for supporting FTIR analysis.

I also express my sincere appreciation as this research project was funded by the Implementation of Urban Ecosystem-based Adaptation Research Activities Program implemented by the Nepal Academy of Science and Technology (NAST)-Nepal Climate Change Knowledge Management Centre (NCCKMC) in collaboration with Kathmandu Valley Development Authority (KVDA). The program is a part of the Urban Ecosystem-based Adaptation for Climate-resilient Development in the Kathmandu Valley, Nepal (Kathmandu Urban EbA Project) approved by the Global Environment Facility (GEF) with Least Developed Countries Fund (LDCF) and being executed by the KVDA with the technical oversight of the United Nations Environment Programme (UNEP).

I would like to appreciate Bibek Ghimire, Prabhakar Thapa Magar, Kushal Chuwain Subedi, Ashman Karki and Bipana Ojha Khatri for their valuable feedback and technical assistance. Finally, I express my deepest gratitude to my family for their unwavering support, encouragement and inspiration. Their patience and belief in me have been a constant source of strength and I owe the successful completion of this thesis to them.

Supported By:

…….

Sachin Ghimire

Roll No.: 080MSMSE015

Exam Roll No: 12360

LIST OF ACRONYMS AND ABBREVIATION

AMS	Accelerator Mass Spectrometry
ASTM	American Society for Testing and Materials
B	DGEBA + ESO + Biochar formulation
BB	DGEBA + ESO + Biochar + Beeswax hybrid formulation
BC	Biochar (Sugarcane Bagasse-derived)
BET	Brunauer-Emmett-Teller (surface area measurement)
BPA	Bisphenol A
BW	Beeswax
CBC	Bio-based Carbon Content
CED	Cumulative Energy Demand
CF	Carbon Footprint
DGEBA	Diglycidyl Ether of Bisphenol A
DMA	Dynamic Mechanical Analysis
EbA	Ecosystem-based Adaptation
EBC	European Biochar Certificate
ECH	Epichlorohydrin
EEW	Epoxide Equivalent Weight
EIS	Electrochemical Impedance Spectroscopy
ESO	Epoxidised Soybean Oil
EVO	Epoxidised Vegetable Oil
FTIR	Fourier-Transform Infrared Spectroscopy
GWP	Global Warming Potential

IBI	International Biochar Initiative
ISO	International Organisation for Standardisation
IV	Iodine Value
LCA	Life Cycle Assessment
MCDM	Multi-Criteria Decision Making
NIS	Negative Ideal Solution
OOC	Oxirane Oxygen Content
P	Neat DGEBA formulation (Petroleum benchmark)
PCA	Principal Component Analysis
PE	DGEBA + ESO formulation
PIS	Positive Ideal Solution
RH	Relative Humidity
SDG	Sustainable Development Goal
SEM	Scanning Electron Microscopy
SMI	Sustainable Material Index
Tg	Glass Transition Temperature
TOPSIS	Technique for Order of Preference by Similarity to Ideal Solution
UV	Ultraviolet
UV-A	Ultraviolet A
VOC	Volatile Organic Compound
WCA	Water Contact Angle
WUI	Waste Utilisation Index

LIST OF SYMBOLS

Symbol	Meaning
–	Subtraction
%	Percentage
°	Degree (Unit of Angle)
°C	Degree Celsius
+	Addition
<	Less than
>	Greater than
~	Approximately equal to
cm^{-1}	Wavenumber
Co	Cobalt
eq/kg	Equivalent(s) per kilogram
eV	Electronvolt
g	Gram
g/L	Gram per Liter
g/L	Grams per litre (Unit of Density)
h	Hours
K	Kelvin
kHz	kilohertz
kV	kilovolt
L	Litre
m	Metre

m^2/g	Square metres per gram (Unit of Specific Surface Area)
mg	Milligram
mL	Millilitre
mN/m	Millinewton per metre (Unit of Surface Tension)
mol	Mole
mPa.s	Millipascal-second (Unit of Viscosity)
MΩ.cm	Megohm-cemtimeter (Unit of Resistivity)
N	Normality
nm	Nanometre
pH	Potential of Hydrogen
phr	Parts per hundred resin
rpm	Revolutions per minute
s	Second
SCB	Sugarcane Bagasse
Sw.	Swelling percent
Tg	Glass Transition Temperture
wt%	Weight percentage
ΔM	Percentage Mass Change
µA	Microampere
µL/s	MicroLitre per second
µm	Micrometre
τ	Tortuosity Factor

ABSTRACT

A bio-based epoxy hybrid (BB) combining epoxidised soybean oil (ESO), sugarcane bagasse biochar and purified beeswax outperforms fossil-based DGEBA in durability and sustainability for South Asian mid-altitude concrete coatings, a region facing monsoonal rainfall, Ultaviolet exposure, freeze-thaw cycling and acid rain in succession. Conventional DGEBA carries a cradle-to-gate global warming potential of roughly 6–8.5 kg CO_2eq/kg footprint and relies on petrochemicals. The BB formulation introduces 15 phr of ESO, 2.5 wt% biochar and 0.75 wt% beeswax into DGEBA matrix. The water contact angle decreases from around 73° (neat DGEBA) to 68.1° (PE and B) and finally rises to around 71° (BB), confirming hydrophobicity. Across natural weathering, freeze-thaw (30 cycles, −20 to +60 °C), acid/base (0.01 N H_2SO_4/NaOH) and water immersion tests, BB recorded the lowest mass gain, 0.28% in natural exposure, swelling 0.11% under freeze-thaw, 0.66% under acid, 0.06% under base, 0.98% under water immersion. Entropy-weighted TOPSIS ranks BB as optimal formulation (closeness coefficient = 1.000) and principal component analysis isolates BB in the superior quadrant. Sustainability improves monotonically from neat DGEBA to BB as the VOC mass fraction falls by 59% (from 8.53% to 3.49%), the cradle-to-gate carbon footprint falls to 9.30 kg CO_2eq/kg and the Integrated Sustainable Material Index rises from 0.0000 to 0.9896. Waste Utilisation Index confirms circular economy benefits using locally sourced agro-industrial residues. Thus, the Sample BB hybrid offers scientifically validated, climate-resilient performance for urban reinforced concrete coatings as protective coatings, while eliminating dependence on imported petrochemical feedstocks and aligning with SDGs 9, 11, 12 and 13.

Keywords: *Hybrid bio-based epoxy; Waste valorisation; Circular economy; Sustainable Material Index*

TABLE OF CONTENTS

LIST OF FIGURES

LIST OF TABLES

LIST OF EQUATIONS

1 INTRODUCTION

1.1 Urban Infrastructure in a Climate-Stressed World

Cities have emerged as the dominant form of human settlement in the twenty-first century and their continued expansion places extraordinary pressure on both the materials that construct them and the natural systems that sustain them (Creutzig et al., 2024; Hardoy et al., 2013). Over half the world's population already lives in urban areas and the United Nations projects this proportion will reach 68% by 2050, implying the addition of approximately 2.5 billion new urban residents over the next three decades ("Urban Systems and Other Settlements," 2023). Translating that demographic shift into built form demands an unprecedented output of new construction: roads, bridges, transit corridors, retaining structures, utility networks and the millions of square metres of building stock needed to house, educate and employ those populations (Acharya, 2021). The construction and built environment sector already accounts for around 40% of total global energy-related CO_2 emissions each year when operational energy use and the embodied carbon in construction materials are combined (Li et al., 2026). The required new floor space at roughly 230 billion square metres by 2050, an area equivalent to rebuilding a city the size of New York every month for three decades. Against that scale of material demand, the chemical composition of construction products can no longer be treated as a secondary concern ("Buildings," 2023).

The problem is compounded by the simultaneous deterioration of the service environment in which existing and new infrastructure must function (Yang & Frangopol, 2019). Climate change has intensified freeze-thaw cycling in mid-altitude and high-altitude regions, extended peak temperature durations in subtropical and equatorial zones, altered precipitation patterns in ways that expose facades and pavements to more frequent saturation-and-drying cycles and raised ambient concentrations of airborne pollutants that attack both concrete substrates and the polymer coatings applied to protect them (Cao et al., 2022; "Freeze–Thaw Environment," 2025; Guler & Akbulut, 2025). Polymer-based materials such as resins, adhesives, protective coatings and composite matrices are particularly sensitive to these shifts because their degradation mechanisms, including hydrolysis, photo-oxidation, thermal fatigue and environmental stress cracking, are directly accelerated by heat, moisture and ultraviolet radiation (Broughton & Maxwell, 2007; Chaffey et al., 2025). Standard accelerated-weathering test protocols that were calibrated against historical climate envelopes may substantially

underestimate the in-service durability of materials now entering construction supply chains (Duan et al., 2017).

Nepal, the geographical setting of this research, presents these converging pressures in concentrated form. Kathmandu Valley and other rapidly urbanising Nepali cities occupy mid-altitude elevations where the Himalayan climate generates pronounced diurnal and seasonal temperature swings, intense monsoonal rainfall, high ultraviolet radiation flux and winter frost events shows a combination that challenges both concrete substrates and the polymer systems used to protect and bond them (Ishtiaque et al., 2017). Simultaneously, Nepal's agricultural sector produces large volumes of biomass by-products that currently find little value-added application (Kafle et al., 2024). Sugarcane mills in the Terai region generate substantial quantities of bagasse, the fibrous residue remaining after juice extraction, much of which is disposed of through open burning that contributes directly to particulate air pollution (Amaresh et al., 2024). Apiaries across the hill and mountain districts produce beeswax as a routine by-product of honey harvesting, yet large-scale utilisation of this material in technical applications remains limited (Gebrekristos et al., 2023). The coincidence of a pressing material need and an available set of renewable feedstocks creates a locally compelling rationale for bio-based composite development that mirrors the global imperative to transition construction materials away from fossil-derived chemistry (Cosentino et al., 2024; Ndikumana, Tanane, Youness, et al., 2025).

1.2 The Conventional Epoxy Problem: Performance, Toxicology and Environmental Burden

Epoxy resins occupy a structurally indispensable position in modern construction. They serve as adhesives bonding composite layers in fibre-reinforced structural elements, as protective coatings on steel and concrete substrates exposed to aggressive environments, as grout and repair mortars in concrete rehabilitation work and as matrix polymers in fibre-reinforced composites for bridge decks, walkways and facade panels (Makinde-Isola et al., 2025; Spee et al., 2006). Their functional credentials are considerable: properly formulated and applied DGEBA-based systems deliver adhesion strengths exceeding 20 MPa on prepared steel, tensile moduli of 3.0–4.5 GPa in cured neat formulations, glass transition temperatures of 80–120 °C depending on stoichiometry and post-cure schedule and broad resistance to solvents, dilute acids and alkalis (Bajpai et al., 2021; Khan & Chavan, 2019; Kumar et al., 2016; Pham & Marks, 2004). The global epoxy resin market is valued at approximately USD 14.32 billion in

2025 and is projected to reach USD 23.89 billion by 2034 reflecting the material's continued indispensability across construction, automotive, aerospace and electronics sectors (Fortune Business Insights, 2026).

The dominant commercial epoxy chemistry involves the condensation of bisphenol A (BPA) with epichlorohydrin (ECH) to produce diglycidyl ether of bisphenol A (DGEBA), which is subsequently cured by polyamine or polyamide hardeners (Shankar et al., 2023). Both BPA and ECH are petrochemical derivatives manufactured through energy-intensive processes and their production carries a cumulative environmental burden that is difficult to reconcile with contemporary sustainability targets (Altuwair, 2018; Yang et al., 2025). The cradle-to-gate global warming potential of 6.0–8.5 kg CO_2-eq/kg of DGEBA resin, calculated across the propylene oxidation, allyl chloride and epichlorohydrin synthesis steps (Kouznetsov & Vargas Méndez, 2022; Wang et al., 2021). The ECH production route generates approximately 0.85–1.2 kg of chlorinated organic by-products per kilogram of ECH manufactured, creating a significant waste stream alongside the primary product (Chen, 2025; Madej & Kiss, 2023).

Beyond production emissions, the toxicological profile of these raw materials has attracted mounting regulatory scrutiny. BPA is an acknowledged endocrine-disrupting chemical that mimics oestrogen at low nanomolar concentrations; the European Food Safety Authority has progressively tightened its tolerable daily intake limits and the European Chemicals Agency (2017) lists BPA as a Substance of Very High Concern under REACH regulation (Buoso et al., 2025; Hafezi & Abdel-Rahman, 2019). BPA is released from incompletely cured DGEBA matrices during thermal degradation and can leach into water when epoxy-coated surfaces contact aqueous environments, raising occupational and post-installation exposure concerns (Kajiyama et al., 2025). Epichlorohydrin is separately classified by the International Agency for Research on Cancer (1999) as a probable human carcinogen (Group 2A), is a recognised skin sensitiser and is listed as a reproductive toxin under European CLP regulations. Residual ECH concentrations in commercial epoxy resins, typically 0.5–2 ppm after purification, can rise dramatically during fire events or high-temperature processing (Hafezi & Abdel-Rahman, 2019; Ighalo et al., 2024).

The end-of-life profile of conventional thermoset epoxies compounds the case for change. Once cured, three-dimensionally crosslinked DGEBA networks cannot be thermoplastically reprocessed or dissolved by conventional solvent systems (Memon et al., 2022; Zhao et al., 2023). Their practical end-of-life pathway is landfill or incineration showing neither of which is compatible with the circular economy frameworks now codified in policy instruments including the European Green Deal's Construction Products Regulation and the United Nations

Sustainable Development Goals, particularly SDG 9 (industry, innovation, and infrastructure), SDG 11 (sustainable cities), and SDG 12 (responsible production and consumption) (Ofori, 2023). Comparative life cycle assessments demonstrate the scale of what substituting bio-based alternatives could achieve: Published life-cycle assessment data indicate that replacing 50% of DGEBA with a bio-based epoxide can reduce cumulative energy demand by 28–35% and global warming potential by 22–30% relative to a fully fossil-based benchmark. A fully bio-based resin derived from epoxidised linseed oil and a citric-acid hardener carried a 40–55% lower carbon footprint than a comparable DGEBA/amine system (Faroque et al., 2025). These figures make clear that bio-based routes represent a genuinely impactful industrial transition, not merely an academic exercise.

1.3 Bio-based Epoxy Resins: Opportunities and Constraints

The search for bio-derived alternatives to DGEBA has generated a rich chemistry landscape over the past two decades. Epoxidised vegetable oils (EVOs) constitute the most commercially advanced class of bio-epoxide. They are synthesised by converting the carbon-carbon double bonds present in unsaturated fatty acid chains of plant triglycerides into three-membered oxirane rings via chemical or enzymatic epoxidation (Lai et al., 2022). The resulting materials retain the inherent flexibility of long aliphatic fatty acid chains while introducing the epoxide functionality necessary for polymerisation with amine, anhydride or other co-reactive hardeners (Álvarez et al., 2025). Among commercially studied EVOs, which include epoxidised soybean oil (ESO), epoxidised linseed oil, epoxidised palm oil and epoxidised castor oil, ESO has attracted the widest attention. This is partly a function of supply: global soybean production exceeds 360 million tonnes annually and ESO is already manufactured in hundreds of thousands of tonnes per year as a PVC plasticiser, meaning no new manufacturing infrastructure is required to redirect it toward materials applications (Kulikov et al., 2025; Niedermann et al., 2014).

Beyond the EVO platform, several other bio-epoxide chemistries have been developed to address the thermomechanical shortcomings that EVOs exhibit in neat form. Lignin-derived epoxides, synthesised by glycidylation of the phenolic hydroxyl groups in lignocellulosic by-products, benefit from the inherent rigidity of their aromatic backbone and yield cured glass transition temperatures (Tg) of 90–160 °C which is substantially higher than the 30–80 °C typical of neat EVO systems (Álvarez et al., 2025; Capretti et al., 2023; Van de Velde et al., 2021). Isosorbide diglycidyl ether, derived from starch via sorbitol dehydration, achieves Tg

values of 100–150 °C owing to its rigid bicyclic structure, positioning it as a direct structural substitute for DGEBA in thermally demanding applications (Hammami et al., 2025; Zhang et al., 2026). Itaconic acid, produced by fungal fermentation of sugars and rosin-derived diepoxides from pine resin represent further platforms that introduce useful combinations of stiffness, reactivity and renewable carbon content (Niehoff et al., 2023; Okabe et al., 2009).

Despite this chemical diversity, a recurring technical limitation constrains the practical utility of neat bio-based epoxy systems in structurally demanding construction applications (Sowińska-Baranowska et al., 2026; Xia et al., 2025a). EVOs in particular suffer from what the literature terms the "dangling chain effect": flexible aliphatic segments between crosslink junctions introduce molecular mobility that reduces network stiffness, resulting in glass transition temperatures that are insufficient for outdoor or thermally exposed service environments (Radi et al., 2013). Strategies to compensate for this include blending EVOs with stiffer bio-epoxide molecules, using high-functionality hardeners that raise crosslink density and incorporating rigid particulate fillers that physically restrict chain motion (Di Mauro et al., 2020; Paramarta & Webster, 2016; Yuan Zhang et al., 2024). The hybrid formulation approach adopted in the present study pursues the third of these strategies, using sugarcane bagasse biochar as a reinforcing filler to elevate stiffness and Tg while beeswax and honey-derived components address waterproofing and self-healing function respectively.

1.4 Epoxidised Soybean Oil: Chemistry, Properties, and Construction Relevance

Soybean oil is among the most widely produced vegetable oils in the world, with annual output exceeding 60 million tonnes across the major producing nations of the Americas and Asia. Its triglyceride composition dominated by linoleic acid (C18:2, approximately 52–58%), oleic acid (C18:1, 23–25%), linolenic acid (C18:3, 7–8%), palmitic acid (C16:0, ~11%) and stearic acid (C18:0, ~4%) gives an average of approximately 4.6 carbon-carbon double bonds per triglyceride molecule, making it highly amenable to epoxidation. The prevailing industrial epoxidation route is the Prilezhaev peracid method, in which hydrogen peroxide and a carboxylic acid (typically acetic acid) generate a peracid in situ that transfers active oxygen electrophilically to each double bond, forming an oxirane ring without introducing halogenated by-products (Xia & Larock, 2010). The resulting ESO carries an oxirane oxygen content of approximately 6.0–7.2% and an epoxide equivalent weight of 230–280 g/eq, parameters that govern both its reactivity with hardeners and the crosslink density of the resulting thermoset network (Auvergne et al., 2014).

When cured with amine or anhydride hardeners, ESO forms a loosely crosslinked flexible thermoset. The long aliphatic chain segments flanking each oxirane group act as molecular spacers that generate free volume and allow segmental motion, producing networks with elongations at break of 10–40% and fracture toughness characteristics that are superior to brittle DGEBA-based systems. However, these same structural features limit the achievable stiffness: tensile moduli of neat ESO thermosets typically fall below 1.5 GPa and glass transition temperatures are often below 50 °C, which falls short of the 80–100 °C threshold commonly cited for structural construction applications (Kumar et al., 2016). This stiffness-toughness trade-off is a well-documented feature of fatty acid-derived thermosets and represents the primary material challenge that filler reinforcement must address (Fidanovski et al., 2018).

In construction-relevant studies, ESO-based systems have been evaluated for waterproof coatings, fibre-reinforced biocomposites, wood consolidants, adhesives and cementitious repair mortars. These investigations consistently confirm that ESO formulations can meet durability requirements in moderate-stress environments particularly where flexibility, adhesion to porous substrates and low-temperature processability are valued but they struggle to achieve the combination of high tensile strength, elevated Tg and prolonged outdoor durability without targeted modification (Liu et al., 2018). In the context of smart urban infrastructure, where materials must additionally maintain stable dielectric properties for sensor integration, keep water absorption below 1–2% and ideally retain some capacity for autonomous damage repair, the performance gap of unmodified ESO is more pronounced still. A carefully designed hybrid composite strategy is required to bridge this gap while preserving the renewable provenance and reduced environmental footprint that motivate the use of ESO in the first place (Hosni, 2026).

1.5 Natural Additives: Beeswax and Sugarcane Bagasse Biochar

1.5.1 Beeswax: Hydrophobic Character and Waterproofing Function

Beeswax is a complex lipid material secreted by Apis mellifera honeybees, composed of approximately 35–40 wt.% long-chain monoesters (C40–C46 esters of C16 acids and C24–C36 alcohols), 14–15 wt.% hydrocarbons (predominantly heptacosane and nonacosane, C27–C33), 12–15 wt.% diesters and hydroxyesters, and 8–9 wt.% free fatty acids, principally palmitic acid (Hepburn et al., 2014). This predominantly non-polar, saturated composition confers an exceptionally hydrophobic character: smooth beeswax films exhibit water contact

angles of 100–110° and the material possesses a melting point of 62–65 °C together with a low density of approximately 0.95–0.96 g/cm³ (Shabeer et al., 2025). These properties, combined with its renewable origin and biological safety, make beeswax an attractive candidate for moisture barrier applications in polymer composites where synthetic hydrophobic agents would introduce petrochemical content (Adak et al., 2025; Vijayan et al., 2023).

In polymer matrices, beeswax functions differently depending on its loading level. At concentrations of 2–5 wt.%, it acts as an internal plasticiser that reduces cure shrinkage stresses and lowers mixture viscosity during processing, facilitating void-free casting. At higher loadings of 5–15 wt.%, it forms discrete hydrophobic micro-domains within the cured network that extend the diffusion path for water molecules and reduce bulk moisture uptake substantially (Dobrosielska et al., 2023). Incorporating beeswax microparticles at 5–20 wt.% into a bio-epoxy matrix based on cardanol and ESO reduced 24-hour water absorption from 3.4% to below 0.8%, with only a 6–12% reduction in flexural strength, a result that highlights the favourable balance achievable between waterproofing enhancement and mechanical property retention. A systematic decrease in moisture diffusivity in beeswax-modified coatings and attributed it to the formation of a hydrophobic percolating network within the polymer matrix (Neznakomova et al., 2025). Beyond its moisture barrier role, beeswax encapsulates a latent thermal energy storage capacity (latent heat of fusion approximately 170–180 J/g) that may contribute to temperature buffering in building envelope components, an ancillary benefit of potential relevance to urban heat island mitigation (Amberkar & Mahanwar, 2023). The melting behaviour of beeswax also introduces a thermally activated self-healing mechanism: when surface temperatures approach 62–65°C, as they routinely do on sun-exposed building surfaces in tropical and subtropical climates, the beeswax phase liquefies and can flow into micro-cracks, sealing them as the surface cools (Buchwald & Greenberg, 2008; Khamdaeng et al., 2016).

1.5.2 Sugarcane Bagasse Biochar: Production, Properties, and Reinforcing Mechanisms

Biochar is the carbonaceous solid produced by the thermochemical decomposition of biomass under limited oxygen conditions (a process termed pyrolysis) conducted typically at temperatures between 300 and 700 °C (Amalina et al., 2022). Sugarcane bagasse, the fibrous residue remaining after juice extraction in sugar mills, represents one of the most abundant agricultural by-products worldwide, with annual generation estimated at 500–600 million tonnes (Ndikumana, Tanane, Aichi, et al., 2025). Pyrolysis converts this waste stream into a stable carbonaceous material while simultaneously sequestering a substantial fraction of the

biomass carbon in a recalcitrant form that persists in composites for decades providing a quantifiable carbon sequestration co-benefit to the resulting material (Ganesan et al., 2025). This waste-to-resource pathway aligns with the principles of circular economy and urban ecosystem-based adaptation, converting an environmental liability into a functional construction material.

Sugarcane bagasse biochar produced at pyrolysis temperatures of 500–600 °C typically exhibits a carbon content of 70–80 wt.%, a highly porous structure with BET surface area of 150–400 m^2/g depending on activation conditions, a rich surface chemistry featuring carboxyl, hydroxyl, lactone and anhydride functional groups derived from partial oxidation of the aromatic carbon framework and a bulk density of 0.25–0.45 g/cm^3. This combination of high surface area, surface reactivity and low density makes bagasse biochar an attractive filler for polymer composites, where it can act simultaneously as a mechanical reinforcement, a thermal stability modifier and an interfacial coupling agent (Iwuozor et al., 2022). In epoxy systems specifically, biochar particles interact with the matrix through physical interlocking between the irregular particle surfaces and cured polymer chains, through covalent or hydrogen-bond-mediated coupling between surface oxygenated groups and epoxide rings or amine molecules during cure and at loadings above a critical threshold of approximately 3–5 wt.% for micron-sized particles through the formation of a rigid percolating network that restricts molecular mobility and elevates the effective Tg of the composite (Bade et al., 2026; Bartoli et al., 2022). The practical mechanical improvements achievable through biochar addition to bio-epoxy matrices are well evidenced in recent literature. The incorporation of 3 wt.% chemically activated wood biochar into an ESO/amine system improved tensile strength by 28%, flexural modulus by 34% and thermal onset degradation temperature by 22 °C relative to the neat ESO control (Das et al., 2021; Prakash et al., 2021). Pyrolysis temperature strongly governs the surface functional group density of sugarcane bagasse biochar, with higher temperatures generally increasing aromaticity while reducing the concentration of reactive surface oxygenates a finding that has direct implications for the optimisation of biochar preparation conditions in the present study (Banik et al., 2018; Sathyabama & Firdous, 2025). The existing application of bagasse and bagasse biochar in building materials, including particle boards, lightweight panels and cement composites, has demonstrated their potential in non-load-bearing components (Ahmad et al., 2025; Samanth et al., 2025). However, their incorporation into bio-based epoxy composites with co-functioning natural additives such as beeswax has not been explored.

1.6 Hybrid Bio-based Composites: Design Rationale and Multi-functional Performance

1.6.1 The Case for Hybrid Additive Strategies

The term "hybrid composite" refers to a material system in which two or more reinforcing or modifying phases, differing in chemical nature, geometry or scale, are combined within a single matrix to achieve a property profile that exceeds the arithmetic average of the individual constituents a phenomenon sometimes described as a positive hybrid effect. In the context of bio-based epoxy composites for construction, hybrid design serves a particularly strategic function: it allows the formulator to compensate for the inherent limitations of the bio-based matrix through the targeted selection of complementary additives, while maintaining overall environmental credentials. Single-additive bio-composites whether reinforced with biochar alone or modified with beeswax alone have demonstrated partial improvements in specific properties but none has simultaneously addressed the full performance requirements like mechanical reinforcement, moisture resistance and self-healing capability that smart urban infrastructure applications demand (Y. Zhang et al., 2024).

Recent research in polymer science indicates that combining multiple bio-additives can produce synergistic improvements that exceed what any individual component contributes in isolation (Marturano et al., 2023). Beeswax, when dispersed as micro-domains within a partially compatible polymer matrix, reduces moisture ingress through the hydrophobic barrier effect, while simultaneously acting as a thermally responsive phase that melts and flows at temperatures routinely encountered on sun-exposed construction surfaces in tropical climates (Janesch et al., 2020; Naderizadeh et al., 2019). Sugarcane bagasse biochar provides the mechanical stiffness and thermal stability that ESO alone cannot achieve, through the physical and chemical matrix-filler interactions (Bartoli et al., 2022; Dahal et al., 2019). The hypothesis driving the present thesis is that a composite formulation integrating additives within an Epoxy matrix can combine these functional contributions in a manner that is not predictable from binary-additive studies that the simultaneous presence of a epoxidized vegetable oil, a rigid porous filler and a hydrophobic wax phase within a single thermoset network will produce a property combination, characterised by adequate stiffness, low moisture uptake and thermally activatable healing, that none of the individual components enables alone.

1.6.2 Waterproofing and Moisture Resistance

For materials used in outdoor urban infrastructure, bridge deck coatings, pavement sealers, facade cladding adhesives and roof membranes that sustained moisture resistance is a primary performance criterion. Water ingress into epoxy composites occurs through two principal mechanisms: Fickian diffusion of water molecules through the bulk polymer network and capillary uptake along filler-matrix interfaces and micro-cracks. Bio-based epoxy systems are generally more susceptible to water absorption than their DGEBA counterparts because the ester groups of triglyceride-derived matrices are susceptible to hydrolytic attack, and the polar hydroxyl groups generated during amine curing provide sites for water clustering and plasticisation (Di Mauro et al., 2020). Beeswax incorporation addresses the diffusion mechanism by creating a hydrophobic tortuous path that obstructs water molecule ingress, an effect well documented by contact angle measurements on beeswax-modified surfaces (Janesch et al., 2020; Naderizadeh et al., 2019). Biochar particles, depending on surface activation state, contribute to moisture management by adsorbing water at particle surfaces and simultaneously extending the diffusion path length through physical tortuosity effects (Bartoli et al., 2022). Together, the synergistic action of beeswax hydrophobisation and biochar diffusion barrier effect is hypothesised to reduce equilibrium water uptake of the composite to below 1.0 wt.%, a threshold as the boundary for acceptable moisture performance in structural coating applications.

1.6.3 Thermomechanical Reinforcement

The thermomechanical property enhancements attainable through biochar reinforcement of ESO-based composites are central to the viability of the proposed hybrid system for construction applications. Dynamic mechanical analysis studies on biochar-filled bio-epoxy systems consistently reveal increases in storage modulus at ambient temperature and a shift in the tan delta peak as well as indicative of Tg to higher temperatures with increasing filler loading, up to an optimum content beyond which particle agglomeration diminishes the reinforcing effect (Bartoli et al., 2022; Dahal et al., 2019). The primary mechanism is the restriction of long-range polymer chain motion by the high-surface-area biochar networkwhich is analogous to the well-established reinforcing action of nanosilica in conventional epoxy but achievable with a bio-derived, low-cost agricultural by-product (Das et al., 2021). Concurrently, beeswax addition at modest concentrations of 2–5 wt.% is expected to improve fracture toughness by acting as a crack-deflection agent: wax micro-domains can absorb crack-

tip energy through micro-plastic deformation, dissipating energy that would otherwise drive brittle fracture propagation (Dobrosielska et al., 2023). The simultaneous optimisation of modulus, strength, toughness and Tg through a combined biochar-beeswax strategy represents a meaningful contribution to the bio-epoxy composite literature, where the two modifications have previously only been investigated independently.

1.6.4 Self-healing Mechanisms in Bio-based Epoxy Systems

Self-healing materials have attracted sustained research interest since pioneering demonstrations that microencapsulated healing agents embedded in epoxy composites could autonomously recover a significant proportion of original fracture toughness after damage. Two broad strategies have been explored: extrinsic self-healing, which relies on embedded capsules or vascular networks containing healing agents released upon damage and intrinsic self-healing, achieved through reversible covalent chemistries (Diels-Alder reactions, disulfide exchange) or supramolecular interactions (hydrogen bonding, ionic associations) built into the polymer backbone (Liu et al., 2018; Memon et al., 2022). Intrinsic self-healing is particularly attractive in bio-based systems because it does not require the synthesis of petroleum-derived healing agents for encapsulation. ESO-based vitrimers incorporating Diels-Alder adducts between furfuryl-functionalised fatty acid chains and bismaleimide crosslinkers could recover up to 85% of initial tensile strength after 30 minutes of thermal treatment at 120 °C shows a result that establishes proof of concept for thermally driven healing in soybean oil-derived matrices (Cerdan et al., 2024; Safaei et al., 2023; Xu et al., 2021).

The present thesis pursues a distinct, less-studied healing pathway: the exploitation of beeswax micro-domains as thermally activated micro-encapsulants that melt at temperatures routinely achieved on sun-exposed building surfaces in tropical climates (55–75 °C), releasing honey-phase healing agent into micro-cracks where its high viscosity and progressive sugar crystallisation upon cooling provides crack-filling action. The rheological characteristics of honey shows viscosity of 2,000–10,000 mPa·s at 25 °C, decreasing to 100–500 mPa·s at 60 °C which provide a physical basis for this mechanism. While the healing efficiency of this bio-mimetic mechanism requires experimental quantification, the conceptual foundation is grounded in independently documented rheological and thermal data. Importantly, no prior study has integrated all three components: ESO, sugarcane bagasse biochar and beeswax in a single composite formulation and the potential in an epoxy system has not been reported.

1.7 Climate-Smart Urban Infrastructure: Performance Requirements and the Nepal Context

The concept of climate-smart or smart urban infrastructure encompasses materials and systems that not only fulfil their structural function but actively respond to environmental conditions in ways that extend service life, reduce maintenance costs and improve occupant comfort (Bokhad et al., 2024). For polymer-based construction materials, climate resilience translates into specific measurable requirements: thermal stability across the operational temperature envelope of the deployment region (typically −20 °C to +60 °C for temperate and tropical urban environments), water absorption below 1–2% to prevent dielectric interference with embedded sensors and to avoid hydrolytic degradation of load-bearing interfaces, ultraviolet resistance to prevent photo-oxidative yellowing and surface chalking and ideally some capacity for autonomous damage repair to extend service life without manual intervention (Lebedev et al., 2019; Mittal et al., 2025; Srinivasa et al., 2025).

Bio-based epoxy composites face a particular challenge under UV radiation exposure. The ester chromophores present in ESO chains absorb UV-A radiation in the 315–400 nm range, initiating photo-oxidative chain scission reactions that degrade both the mechanical properties and visual appearance of the material over time (Ci et al., 2025; Jin et al., 2023). The UV-absorbing aromatic functionalities inherent in the graphitic domains of biochar, offer potential passive photoprotection mechanisms that may slow this degradation pathway suggests a hypothesis that warrants systematic investigation through accelerated weathering testing (Papadopoulou et al., 2024). The freeze-thaw cycling encountered at mid-altitude Himalayan locations such as Kathmandu introduces a further durability challenge: water absorbed into the composite during the wet monsoon season can expand during winter freeze events, generating internal pressure sufficient to propagate micro-cracks at filler-matrix interfaces (Millán Ramírez et al., 2023). The low equilibrium moisture uptake targeted by the beeswax-biochar combination in the present formulation is therefore a prerequisite not only for tropical applications but also for the temperate highland conditions of Nepal.

Nepal's specific socioeconomic context reinforces the relevance of this research direction. The country's construction sector relies heavily on imported materials whose supply chains are vulnerable to the geopolitical and logistical disruptions that land-locked Himalayan geography creates. Developing bio-based composite materials from domestically available agricultural and apicultural by-products, sugarcane bagasse from Terai-region mills and beeswax from hill and mountain apiaries, would reduce dependence on imported petrochemicals while

simultaneously creating economic value from waste streams. The urban buildings of Kathmandu and other growing Nepali cities, many of which use non-load-bearing partition and cladding components that are accessible to bio-composite replacement, represent a realistic near-term application context (Khadka & Chalotra, 2022; Mesta et al., 2022). The potential for improved thermal comfort through the insulating properties of natural fibres and the latent heat buffering contribution of beeswax is particularly pertinent in a setting where energy access is constrained and space heating and cooling costs are significant for urban households.

At a broader scale, this work aligns with the urban ecosystem-based adaptation (EbA) agenda that the United Nations Environment Programme and national development frameworks in South Asia have articulated as a response to climate vulnerability in rapidly urbanising regions (Cohen-Shacham et al., 2016; Seddon et al., 2020). Urban EbA integrates nature-based solutions including the use of biological materials into infrastructure design to simultaneously enhance climate resilience, reduce the urban heat island effect and support biodiversity. The partial biodegradability of bio-based composites at the end of their service life, relative to conventional glass-fibre-reinforced plastics or petrochemical foam panels, offers an end-of-life pathway that imposes a lower burden on already-stressed municipal solid waste management systems in cities like Kathmandu. This combination of performance, provenance and end-of-life characteristics positions the hybrid bio-composite concept as a contribution not only to materials science but to the broader agenda of sustainable urban development in rapidly changing climate conditions (Sherpa, 2024).

1.8 Problem Statement and Research Questions

1.8.1 Problem Statement

Urban infrastructure in rapidly expanding South Asian cities faces an escalating multi-hazard climate environment characterised by intense monsoonal rainfall, freeze-thaw cycling at mid-altitude elevations, elevated ultraviolet irradiance and progressive acidification of precipitation (Akinsanola et al., 2025). Reinforced concrete structures, which constitute the dominant building typology in Nepal's Kathmandu Valley, are routinely protected with diglycidyl ether of bisphenol-A (DGEBA) epoxy coatings. Despite their widespread adoption, conventional DGEBA-based systems carry a cradle-to-gate global warming potential of 6–8.5 kg CO_2eq/kg, rely exclusively on petrochemical feedstocks whose supply is geopolitically vulnerable in a landlocked Himalayan context and raise chronic endocrine disruption and occupational health concerns attributable to bisphenol-A residuals (Nikafshar et al., 2017; Spee et al., 2006; Yang

& Frangopol, 2019). These environmental and socioeconomic burdens motivate the development of bio-based alternatives.

Epoxidised soybean oil (ESO) presents a promising bio-based matrix, yet in isolation it yields thermosets of insufficient mechanical stiffness and elevated moisture uptake, limiting its deployment in structural and protective coating applications (Niedermann et al., 2014; Xia & Larock, 2010). Sugarcane bagasse biochar, an abundant agro-industrial by-product of Nepal's Terai sugar mills, offers particle-level stiffness and diffusion-barrier functionality (Zafeer et al., 2023), while purified beeswax from hill apiaries provides a hydrophobic phase capable of sealing surface and sub-surface moisture ingress pathways (Vijayan et al., 2023). However, the hypothesis that these three bio-derived components can be synergistically integrated within a DGEBA/polyamine matrix to deliver climate-resilient performance that simultaneously surpasses the petroleum benchmark on durability, sustainability and circular economy dimensions has not been experimentally investigated. No prior study has characterised the ternary ESO-biochar-beeswax system under the combined multi-hazard exposure conditions representative of South Asian mid-altitude urban infrastructure, nor evaluated it through entropy-weighted multi-criteria decision analysis against a comprehensive sustainability index. This knowledge gap constitutes the central problem addressed by the present research.

1.8.2 Research Questions

The following research questions were formulated to operationalise the study objectives and guide the experimental programme:

1.8.2.1 Central Research Question

How can locally sourced Nepali agro-industrial and apicultural by-products (sugarcane bagasse, soybean oil and beeswax) be transformed into a hybrid bio-based epoxy composite that achieves multi-hazard durability, hydrophobicity and sustainability, thereby offering a viable climate-resilient alternative to petroleum-based DGEBA epoxies for protective urban infrastructure coatings in South Asia's mid-altitude environment?

1.8.2.2 Secondary Research Questions

- Can sugarcane bagasse biochar, epoxidised soybean oil, and purified beeswax be successfully extracted or synthesised from locally sourced Nepali agro-industrial and apicultural feedstocks, and do the resulting precursor materials meet the compositional

and functional requirements necessary for incorporation into a DGEBA-based epoxy composite system?

- What are the chemical structural characteristics of the synthesised hybrid bio-based epoxy composites, and does FTIR spectroscopy confirm the successful incorporation and curing of all bio-derived additives (ESO, biochar, beeswax) within the DGEBA polyamine network?
- How does the progressive incorporation of ESO, sugarcane bagasse biochar and beeswax affect the hydrophobic character and water absorption behaviour of the composite formulations and does the hybrid BB system achieve moisture uptake within acceptable thresholds for protective coating applications?
- How does the BB hybrid composite perform relative to the DGEBA petroleum benchmark and single-additive control formulations under multi-hazard durability stresses like freeze-thaw cycling, acid and alkali chemical exposure, water immersion, and natural environment weathering which represents of South Asian mid-altitude urban infrastructure service conditions?
- What are the sustainability credentials of the hybrid composite relative to the petroleum benchmark, as assessed through bio-based carbon content, volatile organic compound emission, cradle-to-gate carbon footprint, cumulative energy demand, waste utilisation index and integrated sustainable material index?

1.9 Research Objectives

1.9.1 General Objective

To develop and characterize a hybrid bio-epoxy composite materials integrating epoxidized soybean oil, sugarcane bagasse biochar and beeswax for climate-resilient protective urban infrastructure coatings in South Asia's mid-altitude environment.

1.9.2 Specific Objectives

- To extract and prepare sugarcane bagasse biochar from sugarcane bagasse waste, epoxidized soybean oil from vegetable oil (e.g. Soybean oil) and purified beeswax from apiculture waste (beeswax),
- To synthesize and characterize hybrid bio-based epoxy composites,
- To evaluate hydrophobicity properties,

- To assess sustainability and durability metrics of protective coatings for urban infrastructure application in South Asia's mid-altitude environment.

1.10 Study Area

The research was conducted in Kathmandu Valley located in central Nepal through agro-industrial and apicultural activities which generate abundant sugarcane bagasse and honey bee byproducts. Material sourcing, synthesis, testing and characterization was carried out at Pulchowk Campus, Institute of Engineering, Tribhuvan University with the help of various collaboration with other institutions and labs. Final sample was tested in urban buildings applications for various properties.

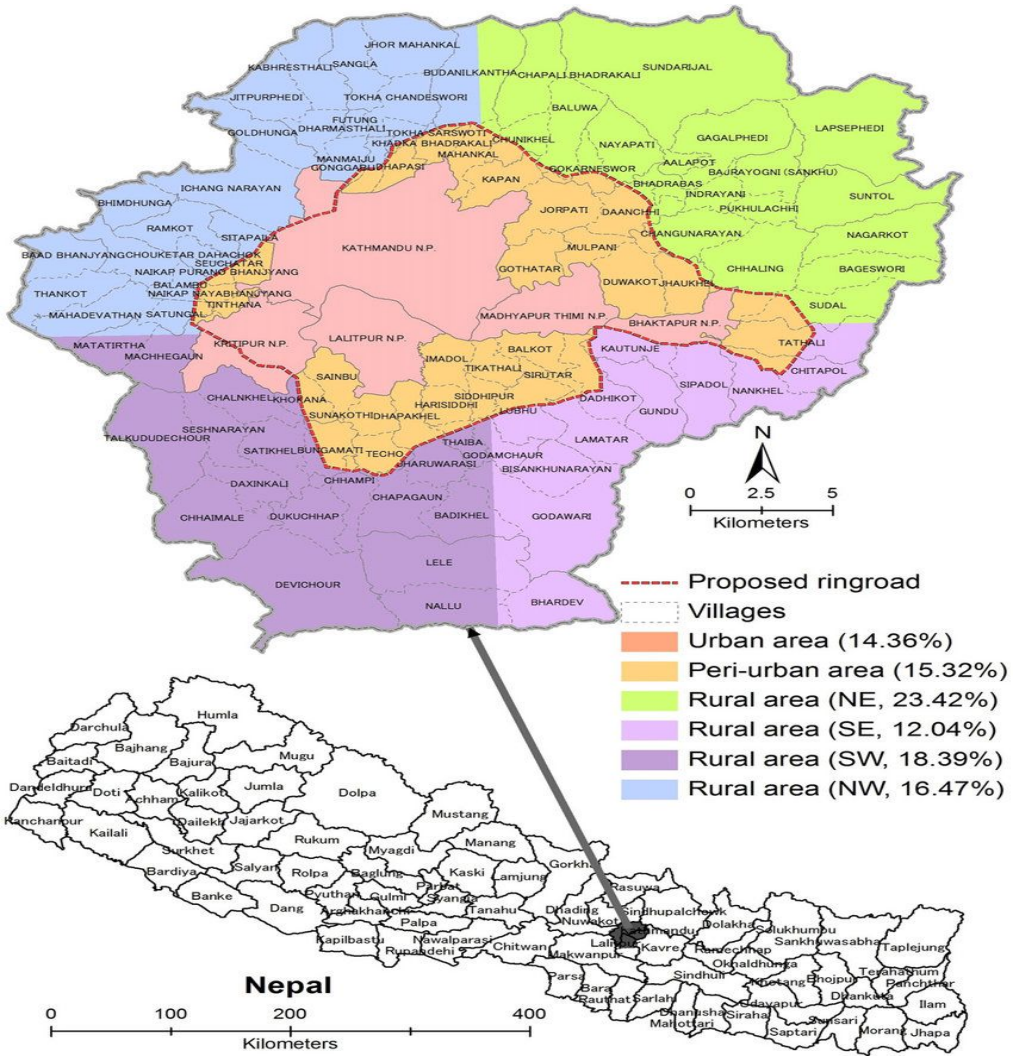

Figure 1-1Kathmandu Valley (Thapa & Murayama, 2012)

1.11 Organization of the Thesis Study

This thesis is organised into five chapters, a reference list and three appendices, structured to progress logically from conceptual framing through experimental investigation to analytical synthesis.

1 Introduction establishes the research context by situating the study within the dual challenges of climate-stressed urban infrastructure and the environmental burden of conventional petrochemical epoxy systems. It introduces the component materials such as ESO, sugarcane bagasse biochar and beeswax which articulates the hybrid composite design rationale, describes the Nepal study context and presents the problem statement, research questions and objectives that govern the experimental programme.

2 Literature Review surveys the scientific foundation underpinning each component and methodology of the study. It reviews the following: chemistry, classification and curing mechanisms of epoxy resins, the properties and performance of epoxidised vegetable oils as bio-based matrices, the production, surface chemistry and composite reinforcement behaviour of biochar derived from sugarcane bagasse, the functional attributes of beeswax as a hydrophobic modifier, standard climate resilience testing protocols for polymer coatings and sustainability assessment frameworks for bio-based construction materials. The chapter concludes by identifying the research gaps that the present study addresses.

3 Materials and Methods provides a detailed account of the experimental programme. It describes the procurement and local sourcing of raw materials, the in-situ peracetic acid synthesis and quality verification of ESO, the aqueous thermal and methanol-extraction purification of beeswax and the slow pyrolysis production of sugarcane bagasse biochar. The composite fabrication protocol for all four formulations (P, PE, B, BB) is presented, followed by the characterisation methods like FTIR spectroscopy, wettability analysis, sustainability assessment and multi-protocol durability testing with full specification of instruments, standards and data analysis procedures.

4 Results and Discussion presents and interprets the complete experimental dataset across four domains. FTIR spectroscopy results confirm the molecular identity of all precursor materials and the successful curing and additive incorporation in all composite formulations. Wettability analysis reports water contact angle and water absorption data across the formulation series. The sustainability assessment quantifies bio-based carbon content, VOC reduction, carbon footprint, cumulative energy demand, waste utilisation index and integrated sustainable material index (SMI). The multi-parameter durability assessment reports freeze-

thaw, acid resistance, alkali resistance, water immersion and natural environment weathering results, followed by entropy-weighted TOPSIS, principal component analysis and hierarchical clustering to derive a rigorous composite performance ranking.

5 Conclusion and Recommendations synthesizes the principal findings of the study, evaluates their significance relative to the research questions and objectives, acknowledges the limitations of the current experimental scope and proposes a structured programme of future work to advance the BB composite toward practical engineering deployment.

The References section documents are all cited sources in APA format. Appendix I provides evidence of conference paper submission acceptance. Appendix II presents a photographic record of key laboratory procedures. Appendix III contains the plagiarism check report confirming the originality of the thesis.

2 LITERATURE REVIEW

2.1 Epoxy Resins: Definition, Classification, and Chemical Structure

Epoxy resins are a broad and versatile class of thermosetting polymers defined by the presence of one or more epoxide (oxirane) functional groups in their molecular structure. It is a three-membered heterocyclic ring comprising two carbon atoms and one oxygen atom, with the formal name 1,2-epoxide or oxirane (Jin et al., 2015; Pham & Marks, 2004). These strained, electrophilic rings are the reactive loci through which epoxy resins participate in polymerisation: nucleophilic species such as amines, anhydrides, thiols or phenols open the ring by attacking either of the two ring carbons, forming a covalent bond while generating a secondary hydroxyl group as a by-product. The resulting three-dimensional thermoset network, once fully crosslinked, cannot be remoulded or dissolved, making epoxy resins quintessential thermosetting polymers with outstanding combinations of mechanical performance, chemical resistance, adhesion to a wide variety of substrates and electrical insulating properties (Auvergne et al., 2014; Pham & Marks, 2004).

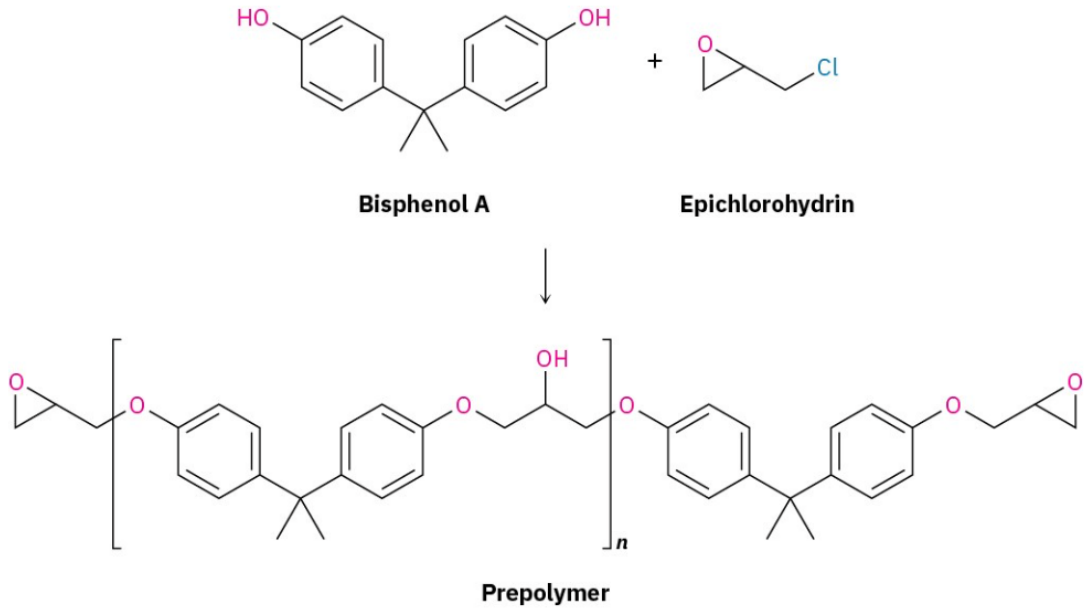

Figure 2-1 Formation of Epoxy Resin Prepolymer (LibreTexts, 2023)

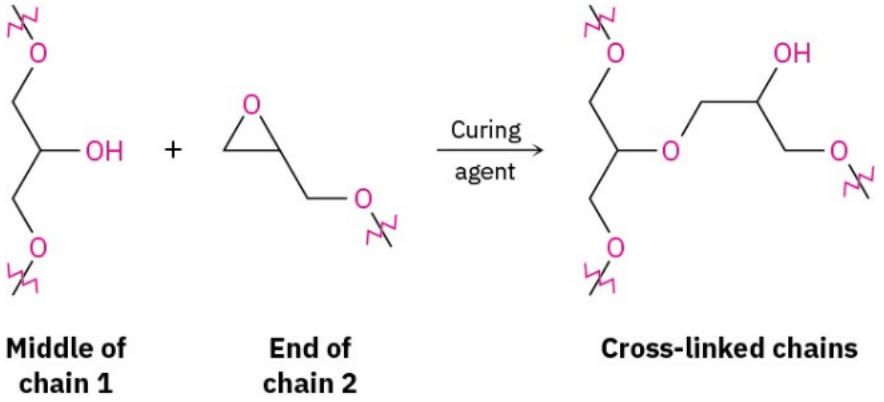

Figure 2-2 Formation of Epoxy Resin (LibreTexts, 2023)

The systematic name for the epoxide functional group is 2,3-epoxypropyl or glycidyl ether when linked through an oxygen to an aromatic ring, giving the parent fragment the structure –O–CH_2–CH(O–)–CH_2. In the commercially dominant diglycidyl ether of bisphenol A (DGEBA), two such glycidyl ether groups flank a bisphenol A central unit, yielding the structure: $CH_2(O)CH–CH_2–O–C_6H_4–C(CH_3)_2–C_6H_4–O–CH_2–CH(O)CH_2$, where the oxirane O bridges the two terminal carbons of each glycidyl group. The molecular weight of the monomeric DGEBA unit is 340 g/mol, with an epoxide equivalent weight (EEW) of 170 g/mol (the mass of resin per epoxide group). Commercial DGEBA products typically carry some degree of oligomeric chain extension, giving EEW values of 175–200 g/mol for liquid resins and substantially higher values for solid grades (Jin et al., 2015).

2.1.1 Classification of Epoxy Resins

Epoxy resins can be classified by several criteria: by their chemical origin (petroleum-derived versus bio-based), by their physical state at ambient temperature (liquid versus solid), by their functionality (difunctional, trifunctional or tetrafunctional), by their backbone chemistry (bisphenol, novolac, aliphatic, cycloaliphatic or heterocyclic) and by their intended application (structural, coating, adhesive or encapsulant) (Sindane et al., 2025; Y. Zhang et al., 2024). The following classification by backbone chemistry is most instructive for understanding structure-property relationships relevant to the present research.

2.1.1.1 Bisphenol-Based Epoxy Resins

Bisphenol A diglycidyl ether (DGEBA) is the archetypal and commercially dominant bisphenol-type epoxy resin, synthesised through the reaction of bisphenol A with epichlorohydrin in the presence of sodium hydroxide (Pham & Marks, 2004). The resulting

monomer or oligomeric chain contains two terminal glycidyl ether groups and one central isopropylidene bisphenyl unit. The rigid aromatic rings and the tetrasubstituted carbon of the isopropylidene bridge impart excellent mechanical stiffness and a glass transition temperature of 80–120 °C in fully cured formulations with amine hardeners. Bisphenol F diglycidyl ether (DGEBF), in which the isopropylidene bridge is replaced by a simple methylene (–CH_2–) link, offers lower viscosity and comparable performance. Also, novolac epoxies, produced from phenol-formaldehyde resins, provide higher functionality (3–5 epoxide groups per molecule) and correspondingly higher crosslink density, thermal resistance and chemical durability (Jin et al., 2015; Pham & Marks, 2004).

2.1.1.2 Aliphatic and Cycloaliphatic Epoxy Resins

Aliphatic epoxy resins lack aromatic ring structures and are derived from the direct epoxidation of olefinic double bonds in aliphatic chains or cyclic olefins using peracid reagents. Examples include diglycidyl ether of 1,4-butanediol (DGBA), poly(propylene glycol) diglycidyl ether, and epoxidised linseed oil. These materials offer low viscosity, UV stability (no chromophoric aromatic rings), flexibility and low viscosity, making them suitable as reactive diluents or toughening modifiers in DGEBA blends. Cycloaliphatic epoxies, such as 3,4-epoxycyclohexylmethyl 3,4-epoxycyclohexane carboxylate (ECC), feature epoxide groups directly on saturated cyclic rings, providing outstanding electrical properties and UV resistance (Aalto-Korte et al., 2015; Pham & Marks, 2004). Their high Tg values (up to 160 °C with anhydride cure) make them preferred in demanding outdoor electrical and optical applications.

2.1.1.3 Glycidylamine Epoxy Resins

Glycidylamine epoxies are produced by the glycidylation of primary or secondary amines with epichlorohydrin. Tetraglycidyl 4,4'-diaminodiphenyl methane (TGDDM) is the most widely used representative, carrying four epoxide groups and offering very high crosslink density when cured with aromatic diamines such as 4,4'-diaminodiphenyl sulfone (DDS). The resulting networks achieve glass transition temperatures of 200–250 °C and are the matrix resins of choice in advanced structural composites for aerospace applications where thermal performance at high altitude is paramount (Sun et al., 2022). However, their higher toxicity, cost and processing complexity make them unsuitable for general civil construction applications.

2.1.1.4 Bio-based Epoxy Resins: Classification and Representative Structures

Bio-based epoxy resins encompass any epoxide-functional material whose carbon backbone is derived from renewable biological feedstocks rather than petroleum. The most commercially significant family is epoxidised vegetable oils (EVOs), discussed in detail in Section 2.3. Other important classes include: (a) lignin-based epoxies, produced by glycidylation of the phenolic hydroxyl groups of lignin extracted from lignocellulosic biomass, which benefit from the inherent rigidity of the aromatic backbone and yield Tg values of 90–160 °C (Li et al., 2018), (b) isosorbide diglycidyl ether (ISDGE), derived from starch via sorbitol dehydration and glycidylation, whose rigid bicyclic dioxabicyclo[2.2.1] heptane framework delivers Tg values of 100–150°C and represents the closest direct structural substitute for DGEBA from a renewable source (Hong et al., 2014), (c) itaconic acid diepoxide, produced from the glycidylation of itaconic acid obtained by fungal fermentation of sugars (Hajian & Yusoff, 2015) and (d) rosin-derived diepoxides, including dehydroabietic acid glycidyl ester, produced from pine resin (abietic acid) through oxidative functionalisation (Mantzaridis et al., 2013). Each class presents specific combinations of thermal performance, reactivity, and renewable carbon content that position it within different segments of the bio-based construction polymer market.

2.2 Epoxy Resin Chemistry: Curing Mechanisms and Network Formation

The transformation of a liquid epoxy resin into a crosslinked thermoset solid occurs through a cure reaction in which the epoxide ring is opened by a co-reactive hardener molecule, forming covalent bonds at each ring-opening event. The selection of hardener chemistry profoundly determines not only the cure kinetics and processing window but also the ultimate network structure, glass transition temperature, mechanical properties, and chemical resistance of the cured material (Pham & Marks, 2004).

2.2.1 Amine Curing Agents: Chemistry and Mechanism

Amine hardeners are the most widely used curing agents for epoxy resins in construction applications and polyamine-based systems form the basis of all formulations investigated in the present study. Primary amines ($–NH_2$) react with epoxide groups through a two-step mechanism: the first N–H bond adds across the oxirane ring in an exothermic ring-opening reaction to give a secondary amine bearing a pendant hydroxyl group (step 1) and the resulting secondary amine (–NH–) reacts with a second epoxide group to give a tertiary amine crosslink

(step 2). This bifunctional reactivity means that each primary amine nitrogen can crosslink two epoxide groups, generating a densely branched three-dimensional network when the stoichiometry of amine N–H groups to epoxide groups is approximately unity (Abe, 2015).

The cure kinetics of amine-epoxy systems depend strongly on temperature, catalyst (accelerator) presence and the electronic and steric character of the amine. Aliphatic amines such as diethylenetriamine (DETA, $H_2N–CH_2CH_2–NH–CH_2CH_2–NH_2$) and triethylenetetramine (TETA) react rapidly with DGEBA at ambient temperature, enabling room-temperature cure schedules practical for field construction applications. The exotherm of the ring-opening reaction is approximately 100–120 kJ/mol per epoxide group opened, which can lead to thermal runaway in thick-section laminates if insufficient thermal management is applied. Aromatic amines such as 4,4'-methylenedianiline (MDA) and 4,4'-diaminodiphenyl sulfone (DDS) react more slowly due to the reduced nucleophilicity of the amine group deactivated by resonance with the aromatic ring as they require elevated-temperature post-cure schedules of 150–180 °C to achieve full conversion and develop their characteristic high Tg values of 150–200 °C (Jin et al., 2015; Pramanik et al., 2014).

The FTIR spectrum of a fully cured amine-epoxy system exhibits characteristic absorption features that serve as diagnostic markers for network formation. The epoxide ring vibration at 820–840 cm^{-1}, prominent in the uncured resin, disappears completely upon full cure as all epoxide groups are consumed. The broad N–H stretching absorptions of the primary amine hardener at 3280–3380 cm^{-1} diminish progressively during cure as the N–H groups react with epoxide. The secondary alcohol C–O–H stretching near 3400–3500 cm^{-1} grows as ring-opening generates hydroxyl groups. Ether C–O–C stretching at 1100–1250 cm^{-1}, arising from the aliphatic ether linkages formed by epoxide ring-opening, intensifies as the network builds. The DGEBA aromatic C=C stretching at 1507 cm^{-1} remains largely unchanged throughout cure and serves as an internal reference band for normalising the spectra (Gu et al., 2009; Jin et al., 2015).

2.2.2 Anhydride Curing Agents

Anhydride hardeners, exemplified by phthalic anhydride, methyl nadic anhydride (MNA) and methyltetrahydrophthalic anhydride (MTHPA) react with epoxide groups through a more complex mechanism involving initial esterification of the anhydride with the hydroxyl groups generated from the first epoxide ring-opening, followed by further ring-opening by the carboxylate intermediates . Anhydride-cured systems generally require tertiary amine or Lewis acid catalysts and elevated cure temperatures (100–150°C), but produce thermosets with

excellent chemical resistance (particularly toward hydrolytic attack) and moderate glass transition temperatures of 80–150 °C depending on anhydride structure. The generally lower exotherm compared to amine cure makes anhydrides particularly suitable for thick-section casting and their lower volatility reduces occupational exposure concerns. Methyl nadic anhydride-cured ESO produced glass transition temperatures of up to 68 °C, a significant improvement over amine-cured equivalents, confirming the utility of anhydride hardeners for thermomechanical optimisation of bio-based epoxy systems (Matějka et al., 1983; Teleky & Vodnar, 2019).

2.3 Epoxidised Vegetable Oils as Bio-Based Epoxy Matrices

The chemistry underpinning epoxidised vegetable oils (EVOs) is inseparable from the structural character of plant triglycerides. These naturally occurring esters consist of a glycerol backbone esterified with three fatty acid chains of varying length and degree of unsaturation and it is precisely the carbon-carbon double bonds (C=C) distributed along those chains that serve as the reactive sites for the epoxidation reaction. By converting each C=C into a strained three-membered oxirane ring, chemists transform a commodity food oil into a reactive monomer capable of participating in thermoset network formation (Abbasov et al., 2018; Auvergne et al., 2014). This conceptually elegant transformation has driven sustained research interest in EVO-based polymers since at least the 1990s and the literature has matured to the point where structure-property relationships are well documented across a range of oil types, epoxidation conditions and curing chemistries (Abbasov et al., 2018).

Among the peracid routes available for converting unsaturated triglycerides into epoxides, the Prilezhaev in-situ method holds the dominant position in industrial practice. In this procedure, acetic acid and hydrogen peroxide react under heterogeneous acid catalysis to generate peracetic acid directly within the reaction mixture; the peracid then transfers its electrophilic active oxygen to each double bond, forming the oxirane ring without generating halogenated by-products or requiring the operator to handle isolated peracid solutions. The degree of epoxidation achievable by this route is governed by the initial iodine value of the starting oil, the stoichiometry of the reagents and the reaction temperature and duration. Commercial-grade ESO produced to high conversion carries an oxirane oxygen content of approximately 6.0–7.2 wt% and an epoxide equivalent weight (EEW) of 220–280 g/eq, parameters that govern both the reactivity of the resin with hardener molecules and the crosslink density of the resulting thermoset network (Cogliano et al., 2024).

Soybean oil occupies a privileged position in the EVO literature for reasons that are simultaneously chemical and logistical. Its fatty acid profile is dominated by linoleic acid (C18:2, approximately 52–58 wt%), with meaningful proportions of oleic acid (C18:1, 23–25 wt%) and linolenic acid (C18:3, 7–8 wt%), translating into an average of approximately 4.5–4.6 double bonds per triglyceride molecule. This degree of unsaturation produces comparatively high oxirane functionality upon complete epoxidation and a corresponding high crosslink potential when the product is cured with amine or anhydride hardeners. At the same time, global soybean production consistently exceeds 360 million tonnes per year and ESO is already manufactured at hundreds of thousands of tonnes annually as a PVC plasticiser, meaning no dedicated new manufacturing infrastructure is required to redirect it toward polymer matrix applications (Rajyaguru et al., 2022).

The fundamental thermomechanical limitation of ESO-based thermosets is well established and represents the central material challenge that the present study addresses. When ESO is cured with conventional aliphatic polyamine or polyamide hardeners, the resulting network contains long, flexible aliphatic segments between crosslink junctions which is an unavoidable consequence of the fatty acid chain architecture. These segments introduce molecular mobility, create free volume and depress both the glass transition temperature (Tg) and the elastic modulus of the cured material. Reported Tg values for neat ESO/amine systems typically fall in the range of 5–45 °C, while tensile moduli seldom exceed 1.2 GPa. By contrast, fully cured DGEBA/amine systems deliver Tg values of 80–120 °C and moduli of 3.0–4.5 GPa, establishing a performance gap that has driven two decades of formulation research aimed at elevating EVO-based systems toward structural serviceability (Baroncini et al., 2016; Chow, 2011).

Several strategies have been pursued to bridge this thermomechanical gap. The most widely reported is partial blending of ESO with DGEBA, which introduces the rigid bisphenol A unit into the network without entirely sacrificing renewable content. An ESO:DGEBA blend at 70:30 w/w, cured with a polyamide hardener, achieved a tensile strength of approximately 45 MPa and a Tg of around 62 °C while retaining a bio-carbon content above 60% indicated performance adequate for many coating and adhesive applications. A complementary approach involves the use of high-functionality anhydride hardeners that increase crosslink density and restrict chain mobility even within a pure EVO matrix. A third strategy (central to the present thesis) employs rigid particulate fillers to physically restrict polymer chain mobility and stiffen the network, an approach whose viability in biochar-reinforced ESO systems is discussed extensively in Section 2.4 (Jin et al., 2023).

2.4 Biochar: Definition, Production, and Physical Architecture

Biochar is a carbon-rich, porous solid material produced by the thermochemical decomposition of organic biomass under severely oxygen-limited or completely anoxic conditions, a process broadly described as pyrolysis. Unlike combustion, which oxidises organic carbon to CO_2 and water in the presence of excess oxygen, pyrolysis thermally decomposes biomass in the absence of oxygen, yielding three co-products: a solid carbonaceous char (biochar), a condensable liquid fraction (bio-oil or pyroligneous acid) and non-condensable gases (syngas, primarily CO, CO_2, CH_4 and H_2). The operating temperature window (typically 300–700 °C) determines not only the mass yield of each fraction but also the chemical and physical character of the resulting biochar (Dahal et al., 2019; Das et al., 2021).

The International Biochar Initiative (IBI) and the European Biochar Certificate (EBC) define biochar formally as 'a solid material obtained from the thermochemical conversion of biomass in an oxygen-limited environment' and distinguish it from other charcoal products by its intended use for soil amendment, carbon sequestration, and materials applications rather than fuel. This definitional distinction is important for the present research: the biochar used as a composite filler is characterised by its structural and surface chemical properties as a functional material rather than its energy content as a combustion fuel (Köves et al., 2024).

2.4.1 Chemistry and Surface Functional Groups of Biochar

At the lower end of the pyrolysis temperature range (300–400°C), biochar retains a comparatively high concentration of oxygen-containing surface functional groups such as hydroxyl (–OH), carboxyl (–COOH), carbonyl (C=O) and lactone (–O–C=O) moieties which are derived from incomplete aromatisation of the original lignocellulosic polymer framework consisting of cellulose, hemicellulose, and lignin. The cellulose fraction of biomass, structurally composed of β-1,4-linked D-glucose units in linear chains, undergoes dehydration, depolymerisation and retro-aldol fragmentation at temperatures above 250°C, producing levoglucosan and furfural intermediates that subsequently condense into aromatic ring structures. Hemicellulose, a branched heteropolysaccharide of pentose and hexose sugars, decomposes at lower temperatures (220–315°C) and contributes to the development of oxygenated surface functional groups. Lignin, an amorphous aromatic polymer of hydroxyphenylpropane units, is the most thermally stable of the three biomass components, decomposing progressively from 280 °C to beyond 500 °C and contributing polycyclic aromatic structures to the biochar skeleton (Zhao et al., 2026).

As pyrolysis temperature rises toward 600–700 °C, the graphitic carbon skeleton becomes progressively more condensed through aromatisation, condensation and the elimination of heteroatom-containing side groups. Surface functional group density declines through dehydration and condensation reactions and both electrical conductivity and aromatic ring cluster size increase. This progressive graphitisation is detectable by Raman spectroscopy: the D band at approximately 1350 cm^{-1}, associated with disordered sp^3-hybridised carbon at defect sites and ring edges, and the G band at approximately 1580 cm^{-1}, associated with ordered sp^2-hybridised graphitic carbon, together characterise the degree of structural order. The I_D/I_G ratio decreases as temperature increases, indicating progressive ordering of the carbon framework. The practical consequence for polymer composite formulation is that moderate-temperature biochar (400–550 °C) presents the most favourable balance between surface reactivity as required for interfacial coupling with epoxy and amine groups and structural rigidity (Jia et al., 2018).

2.4.2 Porous Architecture and BET Surface Area of Biochar

One of the most distinctive and functionally important attributes of biochar as a polymer filler is its highly developed porous architecture, inherited from and templated by the cellular structure of the parent biomass. The three-dimensional pore network of biochar encompasses macropores (diameter > 50 nm), mesopores (2–50 nm) and micropores (< 2 nm), with the relative proportions determined by the botanical characteristics of the feedstock, the pyrolysis temperature and any post-treatment activation procedures. BET (Brunauer-Emmett-Teller) surface area, determined from nitrogen gas adsorption-desorption isotherms at 77 K, is the standard measure of total accessible surface area and typically ranges from 50–150 m^2/g for untreated agricultural biochar to 400–1500 m^2/g for steam- or chemically activated biochar (Aboughaly et al., 2023).

Sugarcane bagasse biochar produced at moderate pyrolysis temperatures of 450–500 °C exhibits BET surface areas of 150–400 m^2/g, highly irregular particle morphology inherited from the fibrous vascular structure of the parent bagasse and a low bulk density of 0.25–0.45 g/cm^3. This high specific surface area is critical to the reinforcing mechanism in thermoset composites: it multiplies the interfacial area across which stress can be transferred from the loaded polymer matrix to the stiffer filler skeleton and it increases the probability that individual matrix polymer chains will be simultaneously adsorbed at multiple contact points on the biochar surface, restricting long-range segmental motion and elevating the effective

glass transition temperature of the composite above that of the unfilled matrix (Zafeer et al., 2023).

The pore network geometry of biochar also plays a decisive role in its moisture barrier function within polymer composites. Randomly oriented, irregular pores with high tortuosity shows characteristic of the vascular canal system of fibrous agricultural residues and impose a tortuous diffusion path on molecules attempting to traverse the composite. The effective diffusivity D_{eff} of water and chemical penetrants through the composite is related to the bulk diffusivity D_0 through the polymer matrix by the Nielsen tortuosity model:

$$D_{eff} = D_0/\tau \qquad \text{—— Equation 1}$$

where $\tau = 1 + (L/2W)\varphi$ is the tortuosity factor, L/W is the aspect ratio of the filler particle and φ is the filler volume fraction. For randomly distributed particles such as biochar at 5 wt% loading, empirical tortuosity values of τ = 2–5 are commonly reported, reducing effective diffusivity to 20–50% of the unfilled matrix value a substantial improvement in barrier performance (Sparavigna, 2023).

Micropore filling by the polymer matrix during composite fabrication is a critical factor modulating this diffusion-barrier effect. At low viscosity during the pre-gel stage of cure, the liquid resin can penetrate into the mesopore and macropore network of the biochar, forming an interpenetrating structure in which polymer chains are intimately constrained by the pore walls, a configuration that restricts chain mobility, enhances interfacial adhesion, and creates a continuous barrier from particle exterior to particle interior. Incomplete pore filling, which occurs at high viscosity or with extremely fine micropores, leaves residual void volume that can serve as water sorption sites, counteracting the diffusion-barrier effect (Lala et al., 2018).

2.4.3 Sugarcane Bagasse Biochar as a Polymer Filler: Literature Evidence

The study incorporated chemically activated sugarcane bagasse biochar at loadings of 1–7 wt% into an ESO/DGEBA matrix at 70:30 w/w, cured with an aromatic amine hardener. At the optimum loading of 3 wt%, tensile strength improved by 28%, flexural modulus by 34% and the onset degradation temperature (T5%) measured by thermogravimetric analysis shifted upward by 22 °C relative to the unfilled control. Scanning electron microscopy of fracture surfaces revealed that irregular biochar particles deflected advancing crack fronts, forcing crack paths to traverse longer and more tortuous routes before reaching critical size, thereby dissipating additional fracture energy. The same study recorded a 22% reduction in equilibrium water uptake at optimum loading, attributed to both the physical tortuosity imposed on

diffusing water molecules by the dispersed particle network and the intrinsic hydrophobicity of the aromatic graphitic domains present in the biochar (Jamilatun et al., 2023).

The systematic investigation of sugarcane bagasse biochar produced across a temperature range of 250–700 °C, quantifying the progressive increase in carbon content from approximately 45 wt% at 250 °C to approximately 80 wt% at 700 °C and demonstrating that the density of oxygenated surface functional groups peaked at 400–500 °C before declining through condensation at higher temperatures. This finding directly informs the optimisation of pyrolysis conditions for the present study's filler preparation. The finding that intermediate pyrolysis temperatures (450–550 °C) maximise the concentration of reactive surface functional groups capable of coupling with epoxide and amine species in the matrix establish a consistent guidance principle for polymer composite filler preparation from agricultural biochar (Banik et al., 2018; Dahal et al., 2019; Jamilatun et al., 2023).

Capretti et al. (2023) demonstrated through electron microscopy and contact angle analysis that biochar particle surface chemistry and dispersion quality are the primary determinants of composite barrier performance, rather than bulk loading level alone. Their finding that bath sonication of biochar in a liquid epoxy aliquot produces substantially more uniform particle distribution than dry blending while avoiding the localised thermal degradation associated with high-intensity probe sonication (Capretti et al., 2023). Almond shell biochar in flax-epoxy composites and reported that 10 wt% loading reduced water uptake by approximately 28% relative to the unreinforced control, confirming the generality of the biochar barrier effect across different feedstock types and composite matrix chemistries (Bade et al., 2026).

Beyond mechanical reinforcement and moisture barrier function, biochar fillers contribute additional functional attributes with direct relevance to the climate-resilience objectives of this study. The partially graphitic aromatic structure of moderate-to-high-temperature biochar absorbs ultraviolet radiation in the UV-A and UV-B spectral regions, a property that has been exploited in polymer stabilisation to suppress photo-oxidative chain scission in the host matrix (Bartoli et al., 2022; Jin et al., 2023). For ESO-based coatings, whose ester chromophores absorb UV-A radiation and initiate degradation through photo-oxidative reactions, this passive photoprotective role of dispersed biochar particles may represent a meaningful durability benefit that warrants investigation under accelerated weathering conditions. Biochar in alkaline cement environments undergoes progressive surface oxidation, providing a mechanistic basis for the elevated mass loss observed in raw biochar composites under alkaline exposure conditions (Belanger et al., 2022; Wu et al., 2025).

2.5 Beeswax as Bio-Derived Functional Modifier

Beeswax is biosynthesised by the abdominal wax glands of worker honeybees of the genus Apis and serves as the structural material from which the hexagonal honeycomb cells of the hive are constructed. Its chemical composition reflects this load-bearing and waterproofing function: the material is predominantly non-polar, consisting of approximately 35–40 wt% long-chain monoesters derived from C16 fatty acids and C24–C36 monohydric alcohols to produce C40–C46 ester molecules; 14–15 wt% saturated and mono-unsaturated hydrocarbons, principally odd-chain alkanes in the C27–C33 range; 12–15 wt% diesters and hydroxy esters; and 8–9 wt% free fatty acids with palmitic acid (C16:0) predominating (Buchwald & Greenberg, 2008). This saturated, largely non-polar constitution confers a water contact angle of 100–110° on smooth beeswax surfaces, a low surface energy of approximately 30–35 mN/m, a sharp melting transition at 62–65 °C, and a density of approximately 0.95–0.96 g/cm³ shows properties that collectively make it an exceptionally effective natural moisture barrier and thermally responsive functional material (Bogdanov, 2016; Buchwald & Greenberg, 2008; Janesch et al., 2020).

The incorporation of beeswax into polymer coatings and composites reveals two concentration-dependent functional regimes. At low loadings of 2–5 wt%, beeswax acts principally as a processing aid: its low melting point causes it to liquefy during the elevated-temperature cure of thermoset resins, reducing mixture viscosity and improving wettability of filler particle surfaces, while also diminishing cure shrinkage stresses. At higher loadings of 5–15 wt%, the wax crystallises upon cooling into discrete hydrophobic micro-domains distributed through the cured polymer network. These domains act as physical barriers to water molecule diffusion by increasing the tortuosity of the transport path through the composite, and by reducing the surface energy in the immediate vicinity of the polymer-air interface through partial surface migration of low-molecular-weight wax fractions during curing. The 15 wt% loading reduced 24-hour water absorption from 3.4 wt% in the unfilled composite to below 0.8 wt%, while retaining 85–88% of the tensile strength of the unfilled control (Hosni, 2026; Janesch et al., 2020; Naderizadeh et al., 2019).

The comprehensive analysis of wax-modified polymer coatings in which beeswax and synthetic paraffin waxes were compared across a range of polymer matrices. Beeswax-modified epoxy coatings consistently achieved water contact angles of 95–130°, with moisture uptake 40–65% lower than unmodified equivalents. The authors attributed the moisture resistance effect not only to the bulk hydrophobicity of the wax phase but also to the formation

of a percolating hydrophobic micro-network within the cured matrix at loadings above approximately 8 wt%. This percolation geometry implies that moisture resistance does not increase linearly with wax loading but exhibits a pronounced threshold behaviour above the percolation concentration, which has direct implications for the optimisation of beeswax loading in the present composite system. The water contact angles exceeding 110° and significantly reduced water vapour transmission rates in beeswax-coated substrates, attributing performance to the fine crystalline microstructure of beeswax that produces a near-defect-free hydrophobic film (Janesch et al., 2020; Naderizadeh et al., 2019).

An ancillary but functionally significant property of beeswax is its latent thermal energy storage capacity. The solid-liquid phase transition at 62–65 °C is accompanied by an enthalpy of fusion of approximately 170–180 J/g, meaning that wax-containing composites can absorb and release substantial quantities of thermal energy during the melting and crystallisation cycle (Buchwald & Greenberg, 2008). In building envelope materials, this buffering capacity attenuates internal surface temperature fluctuations and may contribute to thermal comfort regulation in naturally ventilated buildings, a benefit particularly pertinent in the Nepali urban context where space conditioning energy is costly. More directly relevant to the performance hypothesis of the present study is the fact that the same thermal transition enabling latent heat storage also releases the wax phase as a low-viscosity liquid at temperatures routinely achieved on sun-exposed building surfaces. Infrared surface temperature measurements on unshaded masonry facades in tropical and subtropical climates regularly record peak values of 55–75 °C, squarely within the range at which beeswax transitions from solid to mobile liquid, providing the thermodynamic basis for passive, sunlight-driven wax mobility in surface cracks (Naderizadeh et al., 2019).

2.6 Climate Resilience Testing of Polymer Coatings

The concept of climate resilience applied to infrastructure protective coatings encompasses the sustained retention of mechanical integrity, adhesion, barrier performance and surface optical properties across the full range of environmental conditions encountered throughout service life. For polymer coatings in Nepal's urban infrastructure context, that range is notably demanding: ultraviolet irradiance is elevated at Kathmandu's altitude of approximately 1,400 m, where reduced atmospheric UV attenuation yields UV indices of 9–12 during summer months, relative humidity oscillates from below 30% in winter to above 90% during the June–September monsoon season, air temperatures span from sub-zero on winter nights to above 35

°C in summer and coatings on bridges, retaining walls and road infrastructure may also contact dilute acids, alkalis and chloride-bearing road dust (Mailhot et al., 2005).

Freeze-thaw durability testing evaluates the vulnerability of coatings applied to cementitious substrates to the volumetric expansion of absorbed water during freezing. For coatings with residual moisture uptake above approximately 2–3 wt%, the hydraulic pressure generated by the 9% volumetric expansion of water upon freezing can exceed the tensile strength of the coating-substrate interface, propagating delamination from any pre-existing microdefects. The beeswax-biochar combination targeted in the present study aims to reduce equilibrium moisture uptake well below this threshold, conferring a corresponding improvement in freeze-thaw resistance over unmodified ESO controls. Epoxy coatings applied to concrete subjected to 100 freeze-thaw cycles retained 75–80% of initial chloride permeability reduction, while formulations without filler showed full permeability recovery within 50 cycles (Millán Ramírez et al., 2023).

Chemical resistance to dilute sulphuric acid is critical for coatings applied in industrial and urban environments subject to acid rain, effluent, or biological sulphur oxidation. Bio-derived coatings incorporating glycerol-based polyester and epoxidised acrylate soybean oil and reported excellent adhesion, flexibility, and solvent resistance comparable to reference commercial formulations, positioning bio-based chemistries as viable replacements for conventional epoxy coatings in protective applications. The chemical resistance of epoxy coatings filled with waste glass particles in 5% H_2SO_4 and 5% NaOH over 120 days, establishing that particle-reinforced systems consistently outperformed unfilled controls in both swelling suppression and mass stability, consistent with the barrier enhancement mechanism (Møller et al., 2017; Xia et al., 2025b).

2.7 Sustainability Assessment of Bio-Based Construction Polymer Materials

The sustainability case for bio-based polymer materials in construction rests on quantitative evidence that their environmental burden is meaningfully lower than that of the fossil-derived systems they are intended to replace. Life Cycle Assessment (LCA), conducted in accordance with ISO 14040/14044, provides the most internationally recognised framework for making this quantification. A cradle-to-gate LCA boundary (encompassing raw material extraction, agricultural production, transport and polymer synthesis, but excluding the use phase and end-of-life management) is the most common choice for comparing candidate materials at the specification stage (Firoozi et al., 2025). The cradle-to-gate global warming potential of 6.0–

8.5 kg CO_2-equivalent per kilogram for DGEBA resin. Replacing 50% of DGEBA with a bio-based epoxide reduced cumulative energy demand by 28–35% and global warming potential by 22–30% and a fully bio-based resin carried a carbon footprint 40–55% lower than a comparable DGEBA/amine system (Moussa & Young, 2014).

Bio-based carbon content determination by accelerator mass spectrometry (AMS), standardised in ASTM D6866, provides the regulatory-compliant basis for distinguishing biogenic from fossil carbon in polymer materials. Modern biogenic carbon, fixed from atmospheric CO_2 by living biomass within approximately the past 50 years, carries the contemporary radiocarbon signature ($^{14}C/^{12}C$ ratio) of atmospheric carbon dioxide, while fossil carbon from petroleum or coal feedstocks is essentially devoid of radiocarbon through radioactive decay over geological timescales. The AMS result directly establishes the fraction of the material's carbon inventory that is attributable to renewable feedstocks, forming the numerical basis for bio-content claims under programmes such as the USDA BioPreferred designation and the EU Ecolabel for construction products (Barrio et al., 2021; Hermansson et al., 2019; Quintana et al., 2018).

End-of-life performance is increasingly integrated into sustainability assessments following the codification of circular economy principles in policy instruments. Conventional thermoset epoxies, once cured into irreversibly crosslinked three-dimensional networks, cannot be thermoplastically reprocessed or dissolved by conventional solvent systems; their practical end-of-life pathway is landfill or incineration, neither of which recovers material value or aligns with circular economy objectives. Bio-based thermosets offer incremental improvement through the renewable provenance of their feedstocks and the marginally higher biodegradability of aliphatic ester linkages relative to the aromatic ether linkages in DGEBA. The valorisation of waste-derived biochar and apiary beeswax into construction materials represents a particularly compelling circular economy contribution, as both materials currently impose negative environmental externalities (bagasse through open burning and beeswax through underutilisation) that the composite application pathway eliminates (Phan et al., 2026).

Multi-criteria decision-making (MCDM) methods, including the Technique for Order of Preference by Similarity to Ideal Solution (TOPSIS) with entropy-based weighting, have emerged as powerful tools for objective material selection in construction engineering contexts. Entropy-based weighting derives criterion weights objectively from the information content of the decision matrix without expert subjectivity, representing the degree of discrimination between alternatives provided by each criterion. The application of these computational approaches to bio-based epoxy durability data, as carried out in the CBM submission

component of this research, enables objective formulation ranking that is free from the implicit weighting subjectivity of purely descriptive comparison, producing actionable guidance for formulation selection in construction engineering contexts (Ashby, 2000; Rane et al., 2023).

2.8 Research Gaps and Positioning of the Present Study

The literature surveyed in the preceding sections establishes a robust evidence base for each individual component of the hybrid composite formulation developed in this thesis, while simultaneously revealing the absence of studies that integrate them into a unified system oriented toward climate-resilient urban infrastructure applications. The literature lacks a study that integrates ESO, sugarcane bagasse biochar and beeswax into a single formulated composite system and investigates their combined effects on the full triad of performance criteria comprising thermomechanical properties, moisture resistance and durability under climate-relevant stresses while also evaluating the resulting material through entropy-weighted TOPSIS/PCA/clustering computational analysis and a comprehensive sustainability assessment framework.

Prior investigations have examined binary additive combinations in isolation, biochar or beeswax, each paired separately with bio-epoxy matrices but the hypothesis driving the present study is that the simultaneous presence of a rigid porous filler and a hydrophobic wax phase within the ESO network will produce property combinations that none of the individual components enables in isolation. The synergistic dual-barrier mechanism: hydrophobic surface sealing by beeswax combined with tortuous diffusion paths imposed by biochar, is a novel mechanistic concept grounded in independently documented individual component behaviours but requiring experimental verification in the three-component system studied here.

From a methodological standpoint, the application of entropy-weighted TOPSIS with PCA and hierarchical clustering to bio-based epoxy durability data represents a methodological novelty in this research domain. Previous formulation comparisons have relied on direct graphical or tabular presentation of individual property metrics without objective multi-criteria aggregation, making it impossible to identify the globally optimal formulation across a multi-dimensional performance space. The MCDM approach adopted here resolves this gap and provides a quantitative, reproducible ranking framework applicable to future bio-based composite development.

The present study therefore occupies a defined and unoccupied position in the bio-epoxy composite literature, contributing: (i) the first documented investigation of the three-

component ESO/sugarcane bagasse biochar/beeswax system with DGEBA base matrix (ii) the first application of entropy-weighted TOPSIS/PCA/hierarchical clustering to a bio-based epoxy durability dataset (iii) a comprehensive sustainability assessment framework validated against four independent metrics and (iv) an engineering-relevant performance evaluation contextualised for South Asian mid-altitude urban infrastructure under combined monsoon, freeze-thaw and acid-exposure conditions. The next chapter states the specific research methods that operationalise this positioning.

2.9 Summary

The literature reviewed in this chapter establishes a robust scientific foundation for the hybrid bio-based epoxy composite developed in this thesis, while simultaneously mapping the knowledge gaps that motivate the experimental programme. Epoxy resins based on the DGEBA prepolymer dominate construction protective coatings by virtue of their high crosslink density, chemical resistance and adhesion, but their reliance on bisphenol-A chemistry carries endocrine disruption risks and a cradle-to-gate carbon footprint of 6–8.5 kg CO_2eq/kg (Bajpai et al., 2021; Faroque et al., 2025; Hafezi & Abdel-Rahman, 2019). Amine curing agents produce thermoset networks through sequential ring-opening reactions that determine the final crosslink density and mechanical and chemical performance of the cured film (Abe, 2015).

Epoxidised vegetable oils, particularly ESO, offer a bio-based matrix component with renewable feedstock provenance and a substantially lower environmental burden than DGEBA. Their flexible aliphatic fatty acid chains introduce toughening contributions but reduce glass transition temperature and increase moisture uptake when used as the sole epoxide source, necessitating co-matrix or additive strategies to restore mechanical performance for construction applications. Partial substitution of DGEBA with ESO has consistently reduced cumulative energy demand and global warming potential by 22–35% in comparative LCA studies, with the improvement scaling with the ESO substitution ratio (Abbasov et al., 2018; Capretti et al., 2023; Cogliano et al., 2024; Faroque et al., 2025).

Biochar produced from sugarcane bagasse by slow pyrolysis at 450–550°C presents a well-characterised particulate filler with high specific surface area (150–400 m^2/g), a partially graphitic aromatic carbon skeleton and a surface functional group chemistry dominated by oxygenated species capable of interfacial chemical coupling with epoxide and amine groups during cure. Its incorporation into bio-epoxy matrices at loadings of 2–5 wt% has been shown to improve tensile and flexural modulus, elevate glass transition temperature through chain

mobility restriction, and reduce equilibrium moisture uptake through combined tortuosity and hydrophobicity effects. Pyrolysis temperature governs the trade-off between surface reactivity and structural rigidity, with moderate temperatures (400–550°C) providing the most favourable balance for polymer composite applications (Samanth et al., 2025; Sozio et al., 2026; Wu et al., 2025; Zafeer et al., 2023).

Beeswax is a chemically complex natural wax consisting primarily of long-chain monoesters, hydrocarbons, and free fatty acids, conferring water contact angles of 100–110° and a melting transition at 62–65°C. At loadings of 2–15 wt% in polymer matrices, beeswax micro-domains create hydrophobic tortuous diffusion barriers that reduce moisture uptake by 40–65% relative to unmodified controls. Its latent heat storage capacity at the solid-liquid phase transition additionally provides passive thermal buffering relevant to tropical building envelopes. Critically, the thermal activation of beeswax at surface temperatures of 55–75°C, routinely achieved on sun-exposed masonry in South Asian climates, provides a physical basis for a thermally driven crack-filling mechanism that represents an underexplored pathway to quasi-intrinsic self-healing in bio-epoxy systems (Bogdanov, 2016; Buchwald & Greenberg, 2008; Cerdan et al., 2024).

Climate resilience testing of polymer coatings in Nepal's multi-hazard environment requires a concurrent evaluation of freeze-thaw resistance, acid and alkaline chemical resistance, UV exposure tolerance and sustained water immersion performance. Established ASTM and ISO gravimetric protocols provide reproducible metrics for each exposure mode and multi-criteria decision-making approaches (specifically entropy-weighted TOPSIS with PCA and hierarchical clustering) enable the objective aggregation of multi-dimensional performance data into a single, traceable composite ranking (Akinsanola et al., 2025; Ashby, 2000; "Freeze–Thaw Environment," 2025).

Sustainability assessment frameworks grounded in ISO 14044 life cycle assessment principles, supplemented by bio-based carbon content determination per ASTM D6866 and circular economy metrics, provide the quantitative basis for comparing bio-based and fossil-derived composites across environmental burden, renewable content, VOC emission and end-of-life recoverability dimensions. Waste valorisation of agro-industrial residues such as sugarcane bagasse and beekeeping co-products into functional construction materials represents a particularly high-impact circular economy contribution in developing-country contexts where open burning and underutilisation currently dominate their end-of-life pathways (Ahmad et al., 2025; Barrio et al., 2021; Chen, 2025; Faroque et al., 2025).

Collectively, the literature confirms the scientific viability of each component of the proposed hybrid system while revealing a critical absence: no prior study has combined ESO, sugarcane bagasse biochar and beeswax in a single composite formulation and subjected it to multi-hazard climate testing under conditions representative of South Asian mid-altitude urban infrastructure. The following chapter describes the materials, synthesis procedures and characterisation methods employed to address this gap.

3 MATERIALS AND METHODS

3.1 Overview

The experimental programme follows a structured sequential architecture that moves from the synthesis and quality verification of individual precursor materials, through formulation design and composite fabrication, to comprehensive multi-domain characterisation and statistical optimisation. This structure ensures that performance outcomes measured in the composite evaluation phase are attributable to controlled compositional variables rather than to batch-to-batch variation in starting material quality (Azanaw, 2025).

3.2 Materials

All chemical reagents were of analytical reagent (AR) grade or better unless explicitly noted. Agricultural feedstocks soybean oil, sugarcane bagasse and beeswax were sourced locally in Nepal from producers in the Terai region and Kathmandu Valley respectively. Local sourcing was deliberate as it reflects the thesis commitment to demonstrating material viability within the constraints of supply chains accessible to developing-country research institutions and it supports the circular economy argument that bio-based construction materials should valorise locally available agricultural by-products rather than depend on imported bio-chemicals whose transport footprint partially offsets their feedstock sustainability advantage.

3.3 Synthesis of Epoxidised Soybean Oil (ESO)

The synthesis of ESO constitutes the chemical foundation of this research, as it is the primary bio-based epoxide component in all non-benchmark formulations. The method adopted is the Prilezhaev in-situ peracetic acid epoxidation, conducted with a heterogeneous acid catalyst (conc. H_2SO_4) to suppress competing ring-opening hydrolysis of the freshly formed epoxide groups. This procedure closely follows the protocols, with stoichiometric adjustments based on the measured iodine value of the soybean oil batch used in each synthesis (Cogliano et al., 2024).

3.3.1 Stoichiometric Calculation

The number of moles of olefinic double bonds (C=C) per gram of soybean oil is calculated from the measured iodine value (IV) using the established conversion:

$$\text{Moles of C=C per gram of oil} = \text{IV} \times 0.01786 \qquad \text{—— Equation 2}$$

For a batch with IV = 126 g I_2/100 g (as measured for the batches used in this work by Wijs titration per ASTM D5768)(Samanta et al., 2023):

Moles C=C = 1.26 × 0.01786 = 0.480 mol per 100 g of oil (0.48 mol C=C per 100 g oil)

The reagent quantities required for 100 g of soybean oil are then calculated as follows. A 1:1.5 molar ratio of H_2O_2 to C=C is employed to ensure adequate peracid availability for full conversion without excessive over-oxidation. A molar acetic acid to H_2O_2 ratio of 0.5 is used, as the peracetic acid generation equilibrium is sufficiently favourable under heterogeneous acid catalysis that a sub-stoichiometric acetic acid quantity is adequate:

Required moles of H_2O_2 = 0.480 × 1.5 = 0.72 mol → Volume of 30% H_2O_2 = (0.72 × 34.01) / (1.11 × 0.30) ≈ 73 mL (we use 55 mL of 50% H_2O_2)

Amount of glacial acetic acid = (0.48 × 0.5 × 60.05) / (1.05 g/mL) ≈ 14 mL (we take 30 mL for practical margin)

Amount of conc. H_2SO_4 (catalyst supplement) ≈ 0.5 mL (we take 1 mL for adequate acid catalysis)

The final reagent volumes (for 100 g soybean oil) used in practice are: 100 mL soybean oil (base material), 30 mL glacial acetic acid (for double-bond conversion margin), 55 mL of 30–50% H_2O_2 (to ensure full conversion) and 1 mL concentrated H_2SO_4 (catalytic amount). These quantities reflect safety-adjusted practical volumes consistent with the calculations from the research notebooks and the laboratory flowchart.

3.3.2 Experimental Procedure of ESO Synthesis

The reaction is carried out in a 500 mL four-necked round-bottom flask equipped with a reflux condenser, a mechanical stirrer (300 rpm), a dropping funnel and a calibrated thermometer inserted into a thermostatic water bath. The step-by-step procedure, as executed in the laboratory is as follows:

Step 1 Preparation of In-Situ Peracetic Acid:

Soybean oil (100 g) is charged to the reaction flask. Glacial acetic acid (30 mL) is added and the mixture is heated to 55°C with stirring. The acid-catalyst 1ml conc. H_2SO_4 is added. The resulting slurry is equilibrated at 55 °C for 10 minutes to ensure uniform temperature distribution before the oxidant is introduced. The chemical equilibrium governing peracetic acid formation in the presence of the acid catalyst conc. H_2SO_4 is:

$$CH_3COOH + H_2O_2 \rightleftharpoons CH_3COOOH + H_2O \qquad \text{—— Equation 3}$$

Step 2 Controlled Addition of Hydrogen Peroxide:

Hydrogen peroxide (55 mL of 30% aqueous solution, or equivalent to 0.72 mol H_2O_2) is charged into the dropping funnel and added dropwise to the stirring oil-acid-catalyst mixture over a period of 30 minutes. The addition rate is regulated to maintain the reaction temperature below 70 °C, monitored continuously by the calibrated thermometer. The exothermic nature of the peracid formation and the subsequent epoxidation of C=C bonds necessitates this controlled addition; excursions above 70 °C risk accelerating epoxide ring-opening hydrolysis, reducing the oxirane oxygen content of the product.

Step 3 Reaction and Progress Monitoring:

Following complete H_2O_2 addition, the reaction temperature is raised to 65 °C and maintained for 6–8 hours with continuous mechanical stirring. Progress is monitored by withdrawing 0.5 mL aliquots at hourly intervals and measuring the residual iodine value by Wijs titration. Reaction is considered complete when the rate of IV reduction falls below 0.5 g I_2/100 g per hour, typically between 6 and 8 hours.

Step 4 Work-Up and Purification:

The reaction mixture is cooled to 40 °C and the filtrate (crude ESO in acetic acid/water/organic phase mixture) is transferred to a separating funnel. The organic layer is washed sequentially with 5 wt% sodium carbonate solution (2 × 50 mL, to neutralise residual acetic acid and peracetic acid), then with deionised water (3 × 50 mL) until the aqueous wash phase tests neutral by pH paper (pH 6.5–7.0). The organic layer is separated and dried over anhydrous magnesium sulphate (approximately 10 g per 100 mL of product) for one hour with occasional swirling. The drying agent is removed by filtration is removed under reduced pressure (50 °C, 20 mbar) on a rotary evaporator. The ESO product is recovered as a pale yellow, viscous liquid.

Step 5 Quality Control:

The purified ESO is characterised before use in composite fabrication as the analytical determination of FTIR spectrum (4000–400 cm^{-1}, 64 scans, 4 cm^{-1} resolution) confirms epoxide formation (820–840 cm^{-1}) and disappearance of C=C (3010 cm^{-1}).

3.4 Purification of Beeswax

Raw beeswax cakes received from the local Nepali apiary were irregular yellow-brown lumps exhibiting visible contamination by propolis (dark resinous material deposited by bees), pollen granules, wax-moth cocoon remnants and dust particulates embedded during hive extraction and handling. This heterogeneous contamination, if not removed, would introduce

compositional variability between batches and could create stress concentration points at particulate inclusions within the composite matrix. A two-stage purification procedure was therefore developed and validated, drawing on the aqueous thermal clarification method (Buchwald & Greenberg, 2008; Naderizadeh et al., 2019; Neznakomova et al., 2025).

3.4.1 Stage 1 Aqueous Thermal Clarification

The raw beeswax is weighed (typically 200–300 g per batch) into a borosilicate glaass 1 L beaker. Deionised water (equal volume to the wax mass, approximately 200–300 mL) is added to the beaker. The mixture is placed on a hotplate and heated to 70–75 °C with continuous stirring until the wax has completely melted and a homogeneous molten wax-in-water suspension forms. This temperature range is critical: it is sufficiently above the beeswax melting point (62–65 °C) to ensure complete liquefaction, but below the boiling point of water, avoiding excessive evaporation and the fire hazard associated with overheating wax. The suspension is maintained at 70–75 °C for 15 minutes to allow heat-soluble impurities to migrate into the aqueous phase. The mixture is then allowed to cool undisturbed to room temperature (typically 22–25 °C), during which the wax resolidifies as a solid cake floating above the aqueous phase. The cake is recovered by decantation and the dark-coloured aqueous phase (containing water-soluble impurities, pollen component and some propolis-derived compounds) is discarded. This stage removes gross impurities and is compatible with further processing steps. The aqueous purification method is consistent with the procedure, who demonstrated that simple aqueous heating at 70–75 °C removes the majority of gross impurities from crude beeswax and is adequate for subsequent analytical characterisation(Bogdanov, 2016; Buchwald & Greenberg, 2008; Dobrosielska et al., 2023). The method avoids organic solvents, making it a greener purification option consistent with the environmental ethos of the overall research programme.

3.4.2 Stage 2 Methanol Extraction for Decontamination

Where the Stage 1 product retains visible colour or contains measurable quantities of residual propolis-derived phenolic compounds (assessed by FTIR absorption in the 1600–1650 cm^{-1} aromatic C=C stretching region), a methanol extraction is performed. The Stage 1 purified wax is melted at 65 °C and treated with methanol (1:3 wt:vol) under continuous stirring for 30 minutes to extract polar contaminants including residual propolis phenolics, beeswax-associated pesticide residues and coloured natural pigments. The methanol phase is separated by centrifugation (3000 rpm, 10 min) and the residual methanol is removed from the wax phase

by brief oven drying at 50 °C. The ‘wet decontaminated wax’ is then dispersed in water at 70 °C for 30 minutes, decanted, and dried as in Stage 1 to yield the final purified beeswax. This procedure aligns with protocols (Luna et al., 2021).

3.5 Production of Sugarcane Bagasse Biochar

Sugarcane bagasse biochar was produced from locally sourced bagasse residue by laboratory-scale slow pyrolysis conducted in a muffle furnace. The procedure follows modifications tailored to the available laboratory equipment and the specific surface chemistry requirements for compatibility with an epoxy composite matrix (Noor & Abdullah, 2026).

3.5.1 Pre-Treatment of Bagasse

Raw sugarcane bagasse, received from a local sugar mill in the form of compressed fibrous bales, was first washed with deionised water to remove residual sucrose and water-soluble impurities. The washed bagasse was then dried in a forced-air oven at 50 °C for 24 hours. The dried material was mechanically ground in a jaw crusher and sieved to collect the fraction passing a 300 micron mesh screen (Gnawali et al., 2023). This dried powder fraction was stored in sealed containers at ambient temperature and relative humidity below 40% until use.

3.5.2 Slow Pyrolysis Procedure in Muffle Furnace

Biochar formation was carried out in a muffle furnace at a target pyrolysis temperature of 450 °C for a holding time of 2 hours. The pre-treated, dried bagasse powder was weighed into ceramic crucibles in four separate sample preparations to evaluate both sample size effects and the reproducibility of the pyrolysis process.

The crucibles (previously cleaned by washing with deionised water and then with ethanol and dried in an oven for several minutes) were placed in the muffle furnace at ambient temperature. The furnace was ramped at approximately 5 °C/minute (Shrestha et al., 2022) to the target temperature of 450 °C and held for 2 hours before natural cooling under static air conditions.

3.6 Composite Fabrication Protocol

The composite fabrication sequence is:

(1) ESO and DGEBA are weighed to the target ratio and combined in a glass beaker, heated to 60 °C with overhead stirring at 500 rpm for 10 minutes to achieve a homogeneous viscous blend,

(2) pre-melted beeswax (liquefied at 70 °C in a separate vessel) is added to the ESO-DGEBA blend at 70 °C and stirred for 5 minutes, then cooled to 50 °C,
(3) biochar (pre-dried at 120 °C for 12 hours and pre-dispersed in 5 mL of DGEBA by 15-minute bath sonication at 40 kHz)(Capretti et al., 2023) is added and the suspension mixed at 3000 rpm for 5 minutes using a high-shear mixer,
(4) the stoichiometric mass of polyamine hardener is added and mixed by hand for 5 minutes followed by overhead stirring at 300 rpm for 10 minutes,
(5) the formulation is degassed under vacuum (50 mbar) for 5 minutes to remove entrained air bubbles. The degassed formulation is cast or applied within 15 minutes of hardener addition. Curing follows a two-stage schedule: 25 °C for 72 hours under ambient conditions (RH 50 ± 5%), followed by post-cure at 80 °C for 2 hours in a forced-air oven (Kumar et al., 2019).

3.7 Characterisation Techniques

The Various characterization techniques and test are performed. The characterization and various tests to be performed are mentioned below:

3.7.1 FTIR Spectroscopy Characterization

Fourier-transform infrared spectroscopy was performed on all precursor materials and cured composite specimens using an ATR-FTIR spectrometer (PerkinElmer Spectrum IR version 10.6.2) over the range 4000–400 cm^{-1} at Amrit Campus. FTIR of Liquid precursors (ESO, unhardened DGEBA, amine hardener), solid precursors (beeswax, biochar) and cured composite specimens characterized.

3.7.2 Wettability Analysis (Water Contact angle Test and Water Absorption Test)

Water contact angles were measured using a Biolin Scientific OneAttension optical goniometer operating in sessile drop mode. Polished flat specimens (25 × 75 × 1 mm, surface-finished with 1200-grit silicon carbide paper to provide a reproducible surface texture) were cleaned with isopropanol, dried at 60 °C for 1 hour and conditioned at 23 ± 1 °C and 50 ± 5% RH for 24 hours before measurement. A 10 µL droplet of deionised water (resistivity >18 MΩ·cm, surface tension 72.8 mN/m at 20 °C) was deposited on the specimen surface via a precision microsyringe at a dispensing rate of 1 µL/s. Images of the droplet profile were captured at 1 frame per second for 10 seconds after deposition and the contact angle on both sides of the droplet was extracted from the profile images by the Young-Laplace fitting algorithm of the

OneAttension 4.3.1 software. At least five droplets were measured at different locations on each specimen and the mean ± standard deviation was reported. The instrument temperature and humidity were maintained at 23 °C and 50% RH throughout measurement.

3.7.3 Sustainability Assesment (Bio-based content, VOC, Circularity, Carbon and Energy Footprint)

The sustainability assessment framework followed a four-metric approach encompassing bio-based carbon content (calculated by mass-balance procedure guided by ASTM D6866 principles), VOC content (ASTM D2369 gravimetric method at 110 °C for 60 minutes), cradle-to-gate carbon footprint and cumulative energy demand (ISO 14044 process-based mass-balance using published proxy factors from the ecoinvent 3 database framework) and a Waste Utilisation Index (WUI, four-indicator geometric mean). An Integrated Sustainable Material Index was computed by min-max normalisation of all four metric dimensions followed by equal-weight aggregation.

3.7.4 Durability Assessment (Freeze-Thaw, Chemical Resisitance, Biodegradability, Natural Environment Exposure)

The durability assessment programme encompassed eight gravimetric protocols conducted on glass-slide-cast specimens:
(1) natural environment weathering (15 days outdoor exposure at IOE Pulchowk Campus),
(2) freeze-thaw cycling (30 cycles, −20 °C / +60 °C),
(3) acid resistance (0.01 N H_2SO_4, pH ≈ 2.3, 15 days immersion),
(4) base resistance (0.01 N NaOH, pH ≈ 12, 15 days immersion) and
(5) deionised water immersion (15 days).
All specimen masses were corrected for the glass slide substrate by subtracting the independently measured glass slide mass from the combined specimen-plus-slide mass at each measurement point.
Entropy-weighted TOPSIS analysis was applied to the eight-parameter durability dataset using a custom Python implementation. Shannon entropy weights were calculated from the decision matrix to ensure objective, data-driven criterion weighting. Principal component analysis was performed using scikit-learn (v. 1.4) on the standardised decision matrix, with component loading vectors and formulation score vectors reported in biplot form. Ward linkage hierarchical clustering was applied on standardised Euclidean distances using SciPy (v. 1.12) to provide an unsupervised classification of formulation performance profiles.

4 RESULTS AND DISCUSSION

4.1 FTIR Spectroscopy Analysis Results and Sample Formulation Assesment

4.1.1 Petroleum Epoxy Resin (ER) FTIR Spectroscopy Analysis

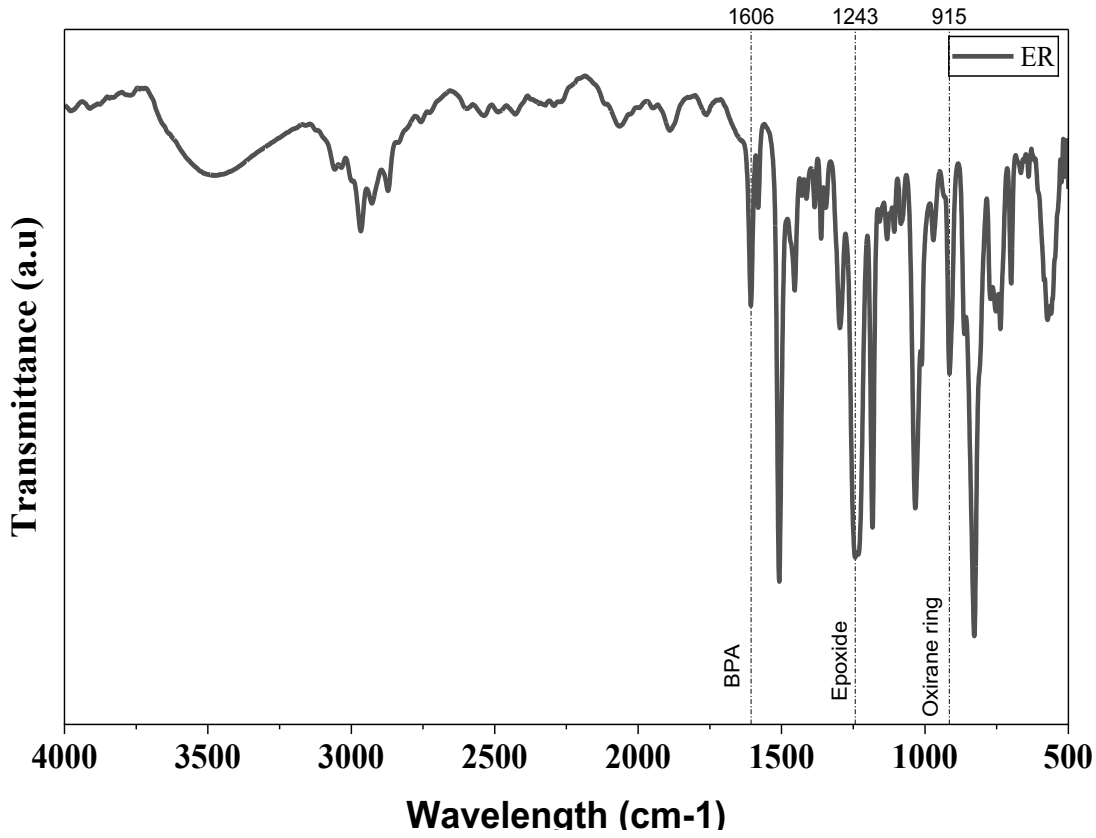

Figure 4-1 FTIR Spectroscopy Analysis of ER

The FTIR spectrum of the local sourced ER is presented in Figure 4-1. The spectrum exhibits a set of strong absorptions characteristic of the triglyceride ester backbone combined with the distinctive diagnostic feature of successful epoxidation, the oxirane ring stretching vibration. Moreover, the FTIR spectrum shows the characteristic absorption pattern of an epoxy network, with bands associated with aromatic rings, ether linkages and epoxy-related functional groups. The strong features in the fingerprint region reflect the presence of the bisphenol-A backbone and C-O-C stretching vibrations, while the overall profile indicates a typical epoxy structure without unusual extra peaks. In simple terms, the spectrum supports the identity of the sample as a DGEBA-based epoxy resin and confirms the expected chemical framework of the material (Huang & Nie, 2016).

4.1.2 Polyamine Hardener FTIR Spectroscopy Analysis

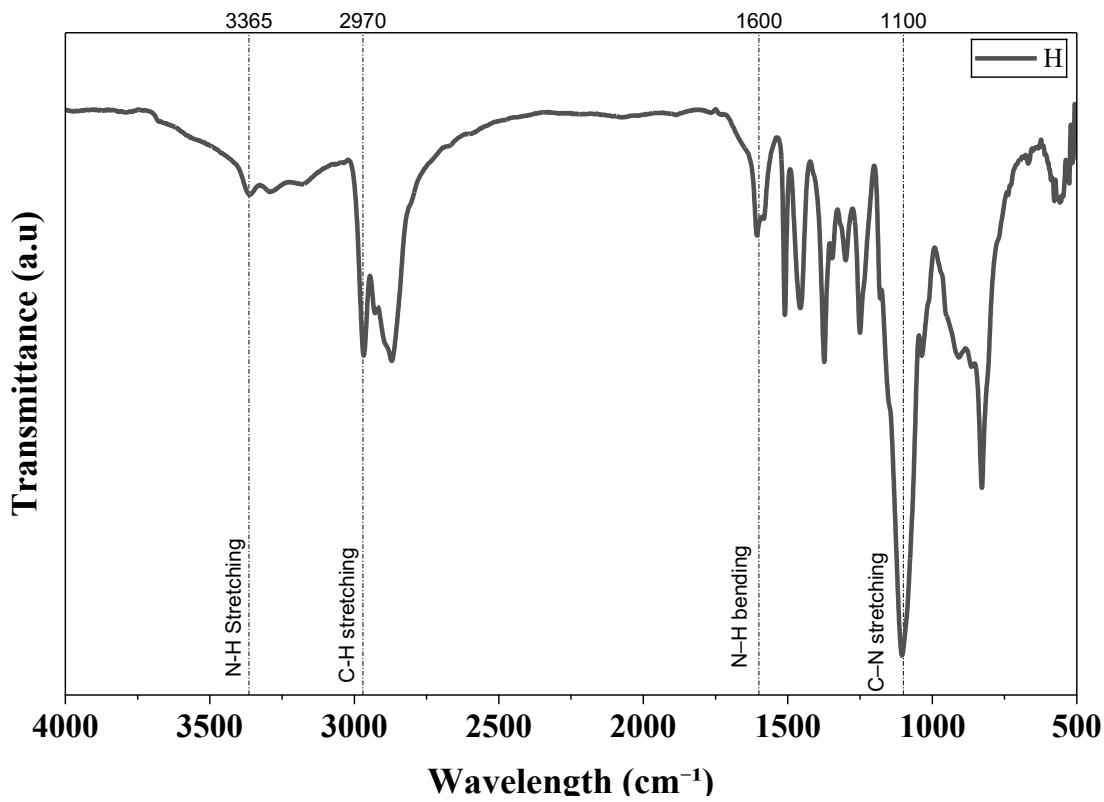

Figure 4-2 FTIR Spectroscopy Analysis of Polyamine Hardener

The FTIR spectrum of the commercial polyamine hardener is presented in Figure 4-2. The spectrum is dominated by the primary and secondary amine absorption bands and the aliphatic C–H stretching region, confirming the expected chemical functionality of the curing agent.

The most diagnostic feature of the amine hardener spectrum is the absorption in the 3300–3370 cm^{-1} region, which represents the N–H stretching vibration of primary amine groups ($–NH_2$). Primary amines produce a characteristic double absorption in this region due to the symmetric and asymmetric stretching modes of the two N–H bonds and the presence of this doublet structure (partially resolved at the spectral resolution applied) confirms the primary amine functionality that is essential for efficient epoxide ring-opening curing. A secondary absorption near 1600 cm^{-1} corresponds to the N–H bending (scissoring) deformation of primary amine groups. The aliphatic C–H stretching region at 2970 cm^{-1} confirms the aliphatic character of the polyamine backbone, consistent with the commercial polyamine hardeners widely used for ambient-temperature curing of construction epoxies. The amine hardener spectrum serves a dual purpose in this characterisation programme. First, it establishes the spectral fingerprint of the uncured hardener as a reference against which curing progress in composite specimens can be assessed. As epoxide ring-opening proceeds during cure, the primary N–H doublet at around

3365 cm^{-1} should diminish in intensity while the N–H band of secondary amines (generated by the first epoxide ring-opening step) broadens and the hydroxyl band at 3400 cm^{-1} grows. Second, it documents the quality of the specific hardener batch used in composite fabrication, ensuring that the curing agent is free from significant degradation or contamination that would alter its stoichiometric reactivity (Cakić et al., 2012; Ignatenko et al., 2020).

4.1.3 Synthesized Epoxidized Soybean Oil (ESO) FTIR Spectroscopy Analysis

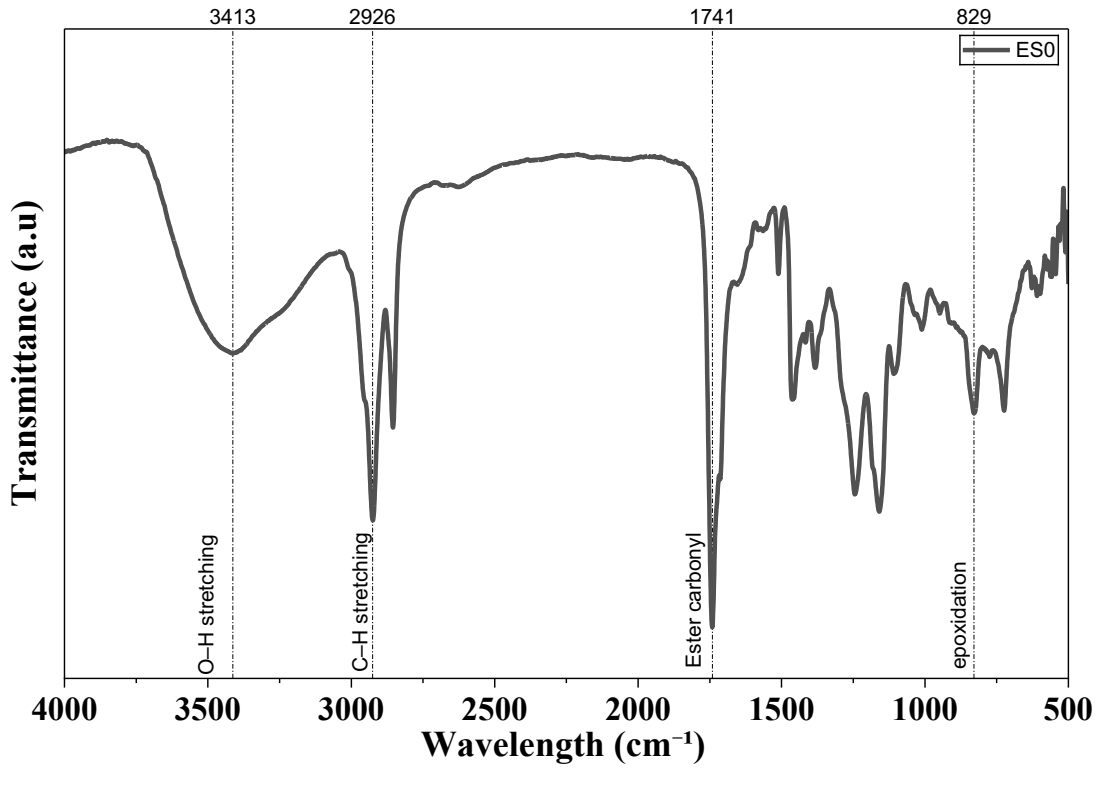

Figure 4-3 FTIR Spectroscopy Analysis of ESO

The FTIR spectrum shown in Figure 4-3 is consistent with epoxidized soybean oil (ESO). The strong absorption at 1741 cm^{-1} corresponds to the ester carbonyl of the triglyceride backbone, while the bands at 2926 cm^{-1} arise from aliphatic C-H stretching in the fatty acid chains. The appearance of a clear band at 829 cm^{-1} is the most important evidence of epoxidation, since this region is assigned to the oxirane ring vibration. The broad band at 3413 cm^{-1} suggests hydroxyl-containing species, most likely from partial ring opening or absorbed moisture. Overall, the spectrum indicates that soybean oil has been successfully converted to an epoxidized structure, with the triglyceride framework retained and the unsaturated C=C groups largely transformed into epoxy rings (Saha & Kim, 2019).

4.1.4 Sugarcane Bagasse Biochar

4.1.4.1 Biochar Production

The biochar yields and mass loss values from the experiments are summarised in Table below:

Table 4.1 Biochar Production Data from Sugarcane Bagasse Slow Pyrolysis at 450 °C (2 hours, Muffle Furnace)

Sample ID	Initial Weight (g)	Post-Furnace Char (g)	Mass Loss (g)	Char Yield (%)	Description
Sample 1	0.7677	0.0146	0.7531	1.90	White ash ; full oxidation (loss of C)
Sample 2	0.9544	0.3479	0.6065	36.45	Black char
Sample 3	1.0020	0.0854	0.9166	8.52	Black char + little white ash
Sample 4	2.0073	0.5765	1.4308	28.72	Black char

The data in Table 4.1 reveal important variation across the four samples. Sample 1, which produced white ash with a char yield of only 1.90%, represents a condition of near-complete combustion: the crucible was inadvertently exposed to a more oxygenated micro-environment (possibly positioned near the furnace intake port), resulting in the conversion of carbon to CO_2 rather than biochar formation. This sample is accordingly excluded from the biochar material used in composite formulations. Sample 2 (char yield 36.45%), which used bagasse provides the most representative biochar yield because the higher initial cellulose and hemicellulose content retains more carbonaceous material during slow pyrolysis when the atmosphere is adequately oxygen-limited. Samples 3 and 4 yields 8.52% and 28.72%, respectively. Sample 3 permitted greater oxygen ingress relative to bagasse mass, leading to more complete oxidation and lower char yield despite identical temperature and time conditions. These observations highlight the sensitivity of biochar yield to furnace atmosphere control which is consistent with literature values for analogous conditions (Zafeer et al., 2023).

4.1.4.2 Sugarcane Bagasse (SCB) Biochar FTIR Spectroscopy analysis

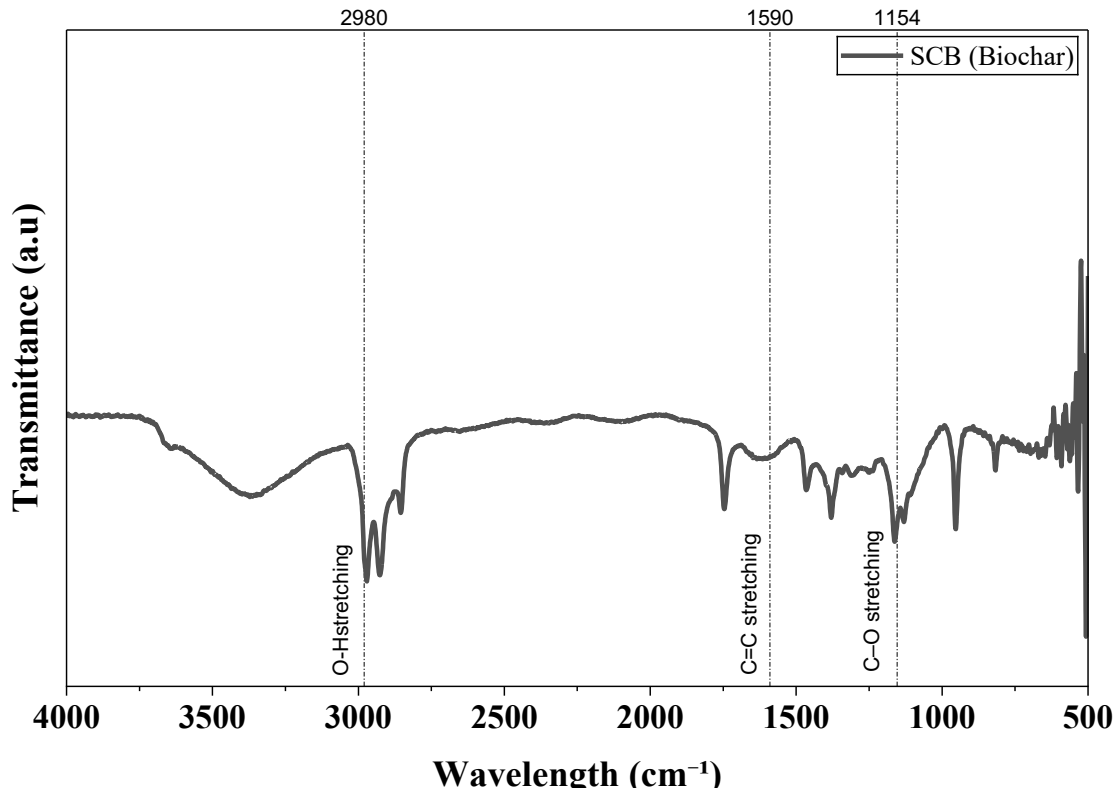

Figure 4-4 FTIR Spectroscopy Analysis of SCB Biochar

The ATR-FTIR spectrum of the 450 °C pyrolysis biochar prepared from pre-treated sugarcane bagasse is presented in Figure 4-4. The biochar spectrum presents broader, lower-intensity absorptions characteristic of the highly condensed, heterogeneous aromatic carbon structure of pyrolysis-derived materials.

The most diagnostic spectral feature for the biochar is the broad absorption centred near 1590 cm^{-1}, assigned to the stretching vibration of the aromatic C=C bonds within the partially graphitised polycyclic aromatic carbon framework of the pyrolysis product. This absorption reflects the progressive aromatisation of the original lignocellulosic polymers (cellulose, hemicellulose, and lignin) during pyrolysis. As pyrolysis temperature increases, dehydration, decarboxylation and condensation reactions progressively transform the linear carbohydrate and phenylpropane polymers of the parent bagasse into fused aromatic ring systems that constitute the graphitic scaffold of biochar. At 450 °C, the aromatisation is substantial but not complete and the presence of residual oxygenated surface groups such as carboxyl, hydroxyl and carbonyl functionalities are confirmed by the broad absorption between 1000–1300 cm^{-1} (encompassing C–O stretching modes) and the diffuse absorption above 3000 cm^{-1} (O–H

stretching from hydroxyl and carboxyl groups, superimposed on aromatic C–H stretching modes). The persistence of surface oxygenated functional groups on the 450 °C biochar is chemically significant for composite performance. These groups particularly carboxyl (–COOH) and hydroxyl (–OH) can participate in hydrogen bonding and potentially even direct chemical interaction with the amine hardener and epoxide groups during composite cure, creating interfacial coupling that supplements the purely physical entanglement of polymer chains within biochar pore spaces. This chemical coupling mechanism has been invoked in several studies of biochar-epoxy composites to explain why mechanical property improvements at moderate biochar loadings (2–5 wt%) exceed those predicted by simple rule-of-mixtures calculations that consider only physical particle reinforcement. The relatively moderate surface functional group density observed in the 450 °C biochar spectrum lower than biochar produced at around 350 °C but substantially higher than char produced at above 650 °C which confirms the appropriateness of the 450 °C pyrolysis temperature for achieving the desired balance of chemical reactivity and structural rigidity in the composite filler (Tasim et al., 2019).

4.1.5 Beeswax Purification

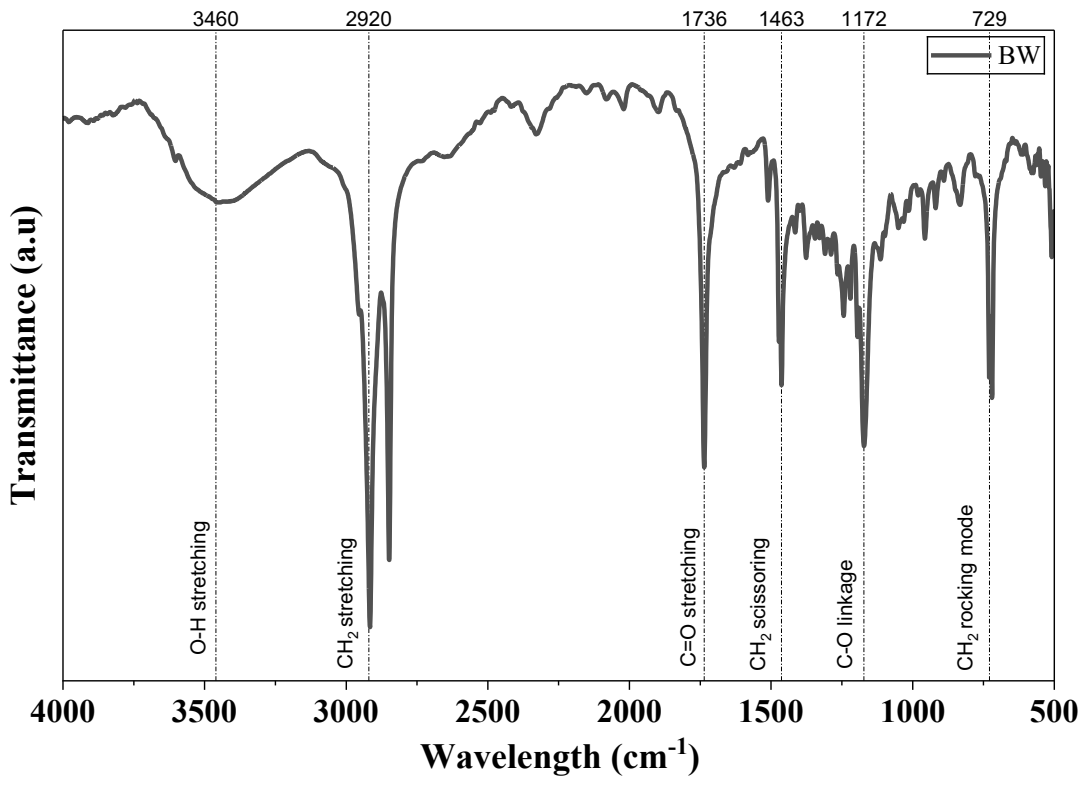

Figure 4-5 FTIR Spectroscopy Analysis of Beeswax

The FTIR spectrum of beeswax exhibits characteristic absorption bands corresponding to its major components as presented in Figure 4-5. Strong peaks at 2920 cm^{-1} arise from asymmetric and symmetric CH_2 stretching, respectively, while the band at 1463 cm^{-1} is due to CH_2 scissoring. A sharp carbonyl (C=O) stretching vibration appears at 1736 cm^{-1}, confirming the presence of ester groups. The C–O ester linkage is observed at 1172 cm^{-1}, and the CH_2 rocking mode appears near 729 cm^{-1}. A weak, broad O–H stretch around 3460 cm^{-1} indicates trace moisture or free fatty acids. These assignments align with published reference data for natural beeswax and provide a reliable fingerprint for authenticity assessment. The dominance of methylene bands reflects the long-chain hydrocarbon and ester structure typical of beeswax (Svečnjak et al., 2015).

4.1.6 Sample Formulation Assesment

4.1.6.1 Sample Nomenclature, Composition and Feedstock Origin

Table 4.2 Sample Nomenclature, Composition and Feedstock Origin for the Three Epoxy Systems Under Sustainability Evaluation

Code	System Description	Epoxide Fraction (v/v%)	Hardener (v/v%)	Bio-Modifier Load (wt%)	Feedstock Origin
P	Petroleum DGEBA + Polyamine hardener	DGEBA 100%	50% of DGEBA	None	100% petroleum-derived
PE	Petroleum DGEBA + Neat ESO + Polyamine hardener	DGEBA:ESO = 100:15	50% of DGEBA	None	Petroleum based + bio-based (soybean oil)
B	ESO/DGEBA blend + Biochar + Polyamine hardener	DGEBA:ESO = 100:15	50% of DGEBA	BC= 2.5%	Mixed: bio-based + waste-derived biochar
BB	ESO/DGEBA blend + Biochar +	DGEBA:ESO = 100:15	50% of DGEBA	BW = 0.75% /	Mixed: bio-based + waste-derived

	Beeswax + Poly amine hardener			BC = 2.5%	biochar + beeswax

Note. BW = beeswax; HN = hydrated honey; BC = sugarcane bagasse biochar. All percentages are mass-based relative to the total resin matrix (epoxide + hardener + modifiers, excluding substrate). ESO = epoxidised soybean oil and DGEBA = diglycidyl ether of bisphenol A.

4.1.6.2 FTIR Spectroscopy Analysis of all four sample formulation

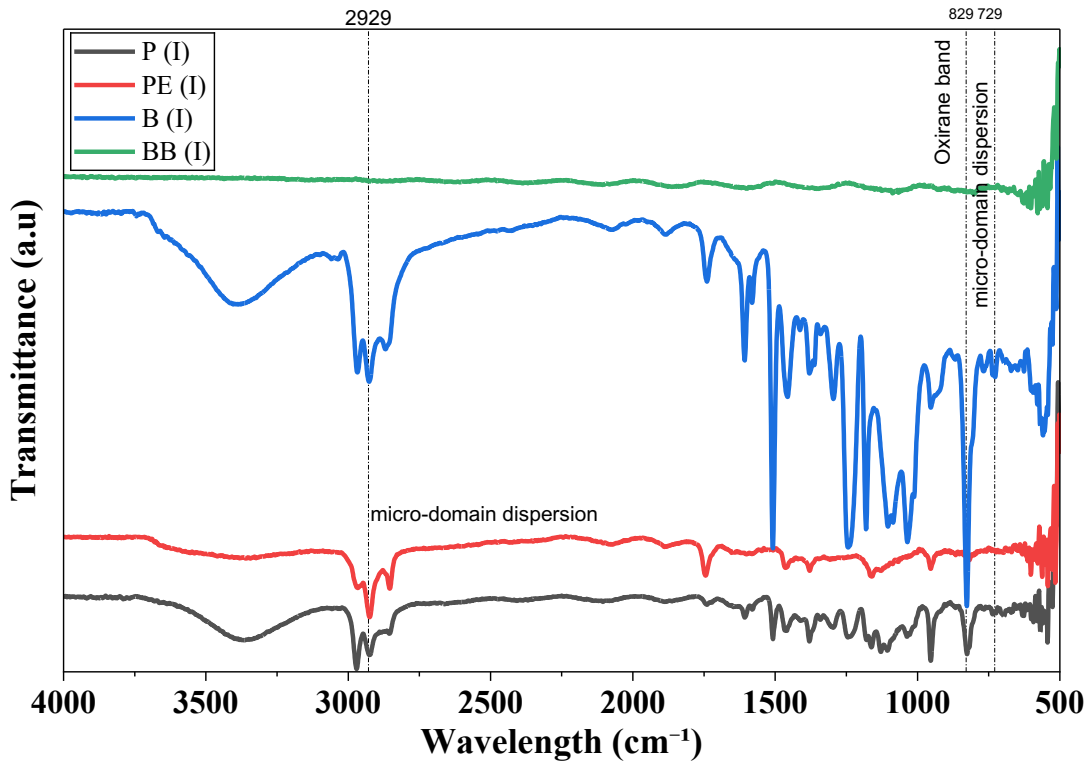

Figure 4-6 FTIR Spectroscopy Analysis of all four sample formulation

The cured formulation spectra collectively confirm successful network formation and progressive bio-additive incorporation. In the P spectrum (Figure 4-6), the complete absence of the oxirane ring vibration at 829 cm^{-1} which is present in the uncured DGEBA resin confirms full consumption of epoxide groups during the polyamine curing reaction. The appearance of a broad hydroxyl absorption band at approximately 3400 cm^{-1}, more pronounced than in the uncured resin, directly documents the secondary hydroxyl groups generated at each epoxide ring-opening event, confirming stoichiometrically adequate curing. The aromatic C–H stretching and bending absorptions of the bisphenol A core at approximately 3030 cm^{-1} and 820 cm^{-1} (para-substituted ring mode) remain visible as confirmatory features of the DGEBA backbone.

In the PE spectrum (Figure 4-6), the progressive enhancement of the aliphatic C–H stretching doublet at 2925/2855 cm^{-1} relative to P is attributable to the additional methylene-rich fatty acid chains contributed by the ESO component. The ester carbonyl region shows a broadened absorption spanning 1735–1742 cm^{-1} that reflects the superimposed contributions of both the DGEBA-derived C–O bond vibrations and the triglyceride ester groups of ESO. The absence of the 829 cm^{-1} oxirane band in PE confirms that both the DGEBA glycidyl groups and the ESO oxirane groups underwent ring-opening during cure shows important confirmation that the ESO component participates in network formation rather than remaining as an unreacted plasticiser.

The B spectrum (Figure 4-6) shows subtle but distinguishable modifications relative to PE, attributable to the biochar component. The 1000–1300 cm^{-1} region, which encompasses the C–O stretching modes of the biochar surface oxygenated groups, appears slightly broadened and more diffuse than in PE, consistent with the superimposition of the biochar surface functional group absorptions on the matrix C–O stretching features. The aromatic C=C region near 1590 cm^{-1} appears marginally more intense in B than in PE, reflecting the contribution of the graphitic carbon domains of the biochar to this region. These spectral modifications are consistent with the expected chemical interactions between the biochar surface functional groups and the curing epoxy matrix.

The BB spectrum (Figure 4-6) presents the full suite of features consistent with the simultaneous presence of all four components which are DGEBA, ESO, biochar and beeswax in the cured network. Relative to B, the BB spectrum shows further enhancement of the methylene stretching doublet at 2929/2848 cm^{-1}, attributable to the long-chain alkyl segments of the beeswax wax esters and hydrocarbons incorporated within the composite. The ester carbonyl region at 1736 cm^{-1} shows a contribution consistent with the wax ester carbonyl of beeswax (which absorbs at an essentially identical position to the ESO and DGEBA ester-derived carbonyl, preventing spectroscopic separation of the contributions at the spectral resolution used). The C–O ester stretching region at approximately 1172 cm^{-1} shows enhanced absorption relative to B, consistent with the additional C–O ester linkages contributed by the beeswax wax ester components. The methylene rocking band at 729 cm^{-1} is more pronounced in BB than in any other formulation, attributable to the long saturated hydrocarbon chain segments (C29–C33 alkanes) characteristic of beeswax hydrocarbons. These spectral progressions collectively confirm that beeswax is incorporated within the BB composite matrix rather than phase-separated to a surface film outside the spectroscopically sampled volume.

4.1.6.3 FTIR Analysis of Individual Formulation Comparision

A comparative overview of major FTIR band positions across all five materials and four formulations is presented in Table 4.3, providing a consolidated reference for the spectroscopic evidence base.

Table 4.3 Comparative FTIR band presence and relative intensity across all five characterised materials and four composite formulations.

Band (cm^{-1})	**ESO**	**Beeswax**	**P**	**PE**	**B**	**BB**
3400–3450	Present (broad)	Weak	Strong (OH)	Strong (OH)	Strong	Strong
2925–2931	Strong	Very strong	Moderate	Enhanced	Enhanced	Further enhanced
2848–2855	Strong	Very strong	Moderate	Enhanced	Enhanced	Further enhanced
1735–1742	Strong (1741)	Strong (1736)	Moderate	Broadened	Broadened	Broadened
~1590	Absent	Absent	Absent	Absent	Subtle	Subtle
~1172	Present	Present	Present	Present	Present	Enhanced
829	PRESENT (oxirane)	Absent	Absent (cured)	Absent (cured)	Absent (cured)	Absent (cured)
729	Absent	Present	Absent	Absent	Absent	Present (BW)

Note: Enhancement indicates increased intensity relative to the P formulation reference.

The most analytically significant result from the composite formulation FTIR data is the consistent absence of the 829 cm^{-1} oxirane band across all four cured specimens. This universally confirms that the curing protocol 24 hours at 25 °C followed by 2 hours at 80 °C with the specified hardener ratio which produced complete or near-complete consumption of epoxide groups in all formulations, including those containing ESO with its oxirane groups distributed along flexible aliphatic chains that might be expected to exhibit lower accessibility to the amine hardener than the terminal glycidyl groups of DGEBA. The complete ring-opening confirmed by FTIR is important because unreacted epoxide groups represent potential sites for hydrolytic degradation in service and their absence gives confidence that the cured specimens tested in subsequent chapters represent the fully developed thermoset network.

The spectroscopic evidence for beeswax incorporation in BB specifically the enhanced methylene stretching at 2929/2848 cm^{-1} and the appearance of the methylene rocking band at 729 cm^{-1} is consistent with the wax phase being present as discrete micro-domains embedded within the thermoset network rather than migrating entirely to the specimen surface. Surface-exclusive migration would produce a beeswax surface layer spectrally indistinguishable from pure beeswax, with complete suppression of the underlying epoxy matrix absorptions at the ATR-sampled surface depth of approximately 1–3 μm. The superimposed character of the BB spectrum simultaneously showing features of the cured epoxy network (broad hydroxyl, epoxy C–O stretching) and the beeswax (enhanced methylenes, 729 cm^{-1} rocking) indicates intimate mixing of the two phases at the length scale probed by ATR-FTIR, consistent with the micro-domain distribution expected from the emulsification of melted beeswax into the warm resin during the fabrication procedure described in Chapter 3.

Overally, the FTIR characterisation has established the molecular identity of all precursor materials and confirmed the successful incorporation and retention of each bio-additive within the cured composite network. The key conclusions include the successful ESO synthesis as confirmed by the 829 cm^{-1} oxirane band, purification of beeswax to a composition consistent with authentic reference spectra, sugarcane bagasse biochar at 450 °C retains oxygenated surface functional groups capable of chemical interaction with the curing matrix, the polyamine hardener presents the expected primary amine functionality for epoxide ring-opening and all four cured formulations show complete epoxide ring consumption (Shundo et al., 2022). The FTIR evidence for progressive additive incorporation in the PE, B and BB spectra provides molecular-level confirmation that the formulation protocol successfully delivers the intended composite chemistry which is a prerequisite for meaningful interpretation of the wettability and durability results presented in subsequent chapters.

4.2 Wettability Analysis Results

Wettability is the tendency of a surface to be wetted by a liquid, quantified through the equilibrium contact angle formed at the three-phase solid-liquid-vapour contact line which is one of the most fundamentally important surface properties of any protective coating intended for outdoor infrastructure service. The relationship between surface wettability and coating durability operates at multiple scales and through multiple mechanisms. At the macroscale, a high contact angle (hydrophobic surface) reduces the extent and rate of liquid spreading across the coated substrate, limiting the area of water-coating contact per unit of rainfall while at the

mesoscale, the thermodynamic barrier to wetting at pore and crack mouths is expressed as the capillary pressure:

$$\Delta P = -2\gamma \cos \theta / r \text{ — Equation 4}$$

where γ is the liquid-vapour surface tension and r is the effective pore radius that increases sharply with contact angle, requiring substantially greater hydraulic head to drive water penetration into micro-defects as the surface becomes more hydrophobic and at the molecular scale, the reduced activity coefficient of water at a low-surface-energy interface limits the thermodynamic driving force for water molecule adsorption into the polymer network and for hydrogen bonding with polar matrix groups (Gupta et al., 2022).

For the specific service environment of Kathmandu Valley, where monsoon rainfall events deliver several hundred millimetres of precipitation in sustained periods lasting 12–48 hours, the difference between a coating with $\theta = 68°$ and one with $\theta = 74°$ in terms of cumulative moisture ingress over a monsoon season is not trivial. The Washburn equation describing capillary penetration rates contains the $\cos \theta$ term directly, and the 20% reduction in $\cos \theta$ between these two contact angle values ($\cos 68° = 0.375$ vs. $\cos 74° = 0.276$) translates through the modified Fick's law diffusion framework into a proportional reduction in the steady-state moisture flux through the coating and into the underlying concrete substrate. This reduction in moisture flux directly addresses the freeze-thaw vulnerability of water-saturated coatings at the hill elevations where Nepal's urban expansion is occurring (Bhattrai et al., 2025).

This chapter reports the water contact angle (WCA) measurements on the four cured composite formulations using the sessile drop technique on the Biolin Scientific OneAttension goniometer and interprets the measured values in the context of the molecular modifications introduced by each bio-additive.

4.2.1 Tensiometer Test

Water contact angle measurements were performed on polished flat specimens of each formulation using the sessile drop method (10 µL droplet, deionised water) at 23 °C and 50% RH on the OneAttension goniometer (Biolin Scientific). The instrument software (OneAttension Version 4.3.1, r11227) fitted the Young-Laplace equation to the droplet profile images and reported the left and right contact angles independently, with their mean taken as the reported value (Eftimov et al., 2020).

4.2.1.1 Water Contact Angle (WCA) Test of Sample P

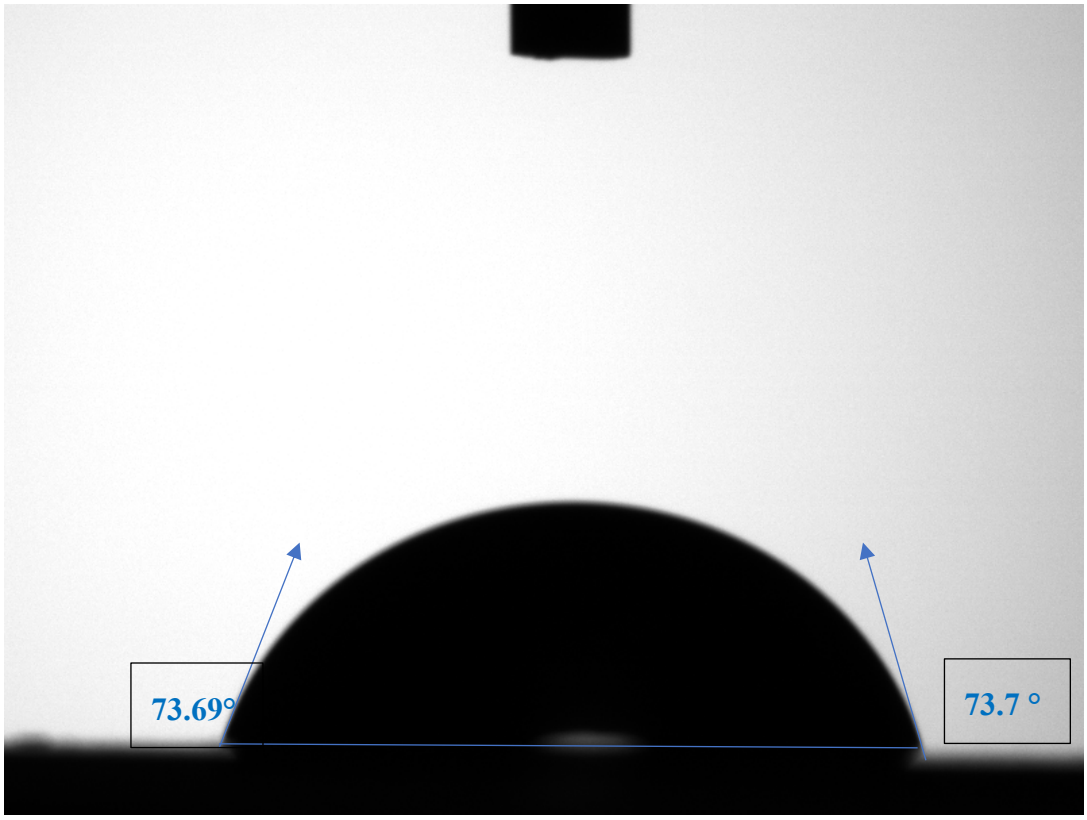

Figure 4-7 WCA of Sample P = 73.697º

The mean WCA of **73.697°** for the P formulation falls within the moderate hydrophilicity range, consistent with the known polarity of fully cured DGEBA/polyamine networks. During curing, each epoxide ring-opening by an amine hydrogen generates a secondary hydroxyl group (–CH(OH)–). At full stoichiometric conversion, the cured network contains approximately 5.5–5.8 mmol of hydroxyl groups per gram of resin (based on an EEW of 185 g/eq), producing a surface with significant polarity and strong affinity for water via hydrogen bonding. Literature values for water contact angles on cured DGEBA/aliphatic amine systems typically lie between 65–80° and the measured 73.697° for the P formulation falls well within this range (Taysun et al., 2025).

The close agreement between the left and right contact angles (73.69° and 73.70° respectively, $\Delta \approx 0.01°$) indicates excellent droplet symmetry, confirming a homogeneous and isotropic surface. This minimal deviation suggests the absence of surface irregularities such as scratches or heterogeneities that could induce contact angle hysteresis, thereby validating the effectiveness of the surface preparation protocol (1200-grit SiC polishing and isopropanol cleaning) in ensuring reliable and reproducible measurements. The sessile drop image is shown in Figure 4-7.

4.2.1.2 Water Contact Angle (WCA) Test of Sample PE

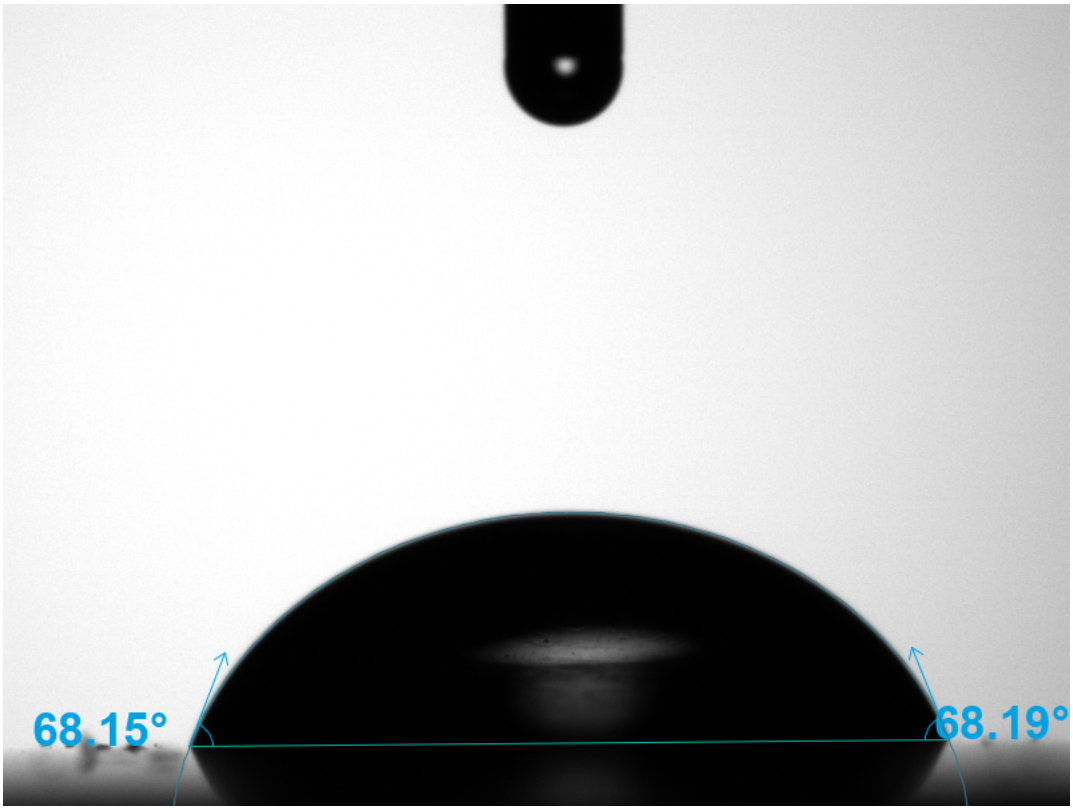

Figure 4-8 WCA of Sample PE = 68.266º

The decrease in WCA from 73.70° (P) to 68.27° (PE) indicates an increase in surface hydrophilicity upon incorporation of ESO into the thermoset network. Although ESO introduces long aliphatic C18 fatty acid chains that would typically reduce surface energy, it simultaneously contributes polar functional groups, particularly ester linkages (retained from the triglyceride structure, as confirmed by the FTIR band at 1741 cm^{-1}) and additional hydroxyl groups formed during epoxide ring opening. These polar groups enhance hydrogen bonding with water, outweighing the hydrophobic influence of the methylene chains.

At the applied loading (15 phr), ESO accounts for approximately 9.1 wt% of the formulation (excluding hardener), which is sufficient to modify the interfacial chemistry by increasing the density of polar functionalities. As a result, the overall wettability increases compared to the neat DGEBA system.

The close agreement between the left (68.15°) and right (68.19°) contact angles (mean ≈ 68.27°, Δ ≈ 0.04°) demonstrates excellent droplet symmetry, indicating a homogeneous and isotropic surface. This minimal variation confirms uniform distribution of surface functional

groups and validates the reliability and reproducibility of the surface preparation and measurement protocol (Taysun et al., 2025). The sessile drop image is shown in Figure 4-8.

4.2.1.3 Water Contact Angle (WCA) Test of Sample B

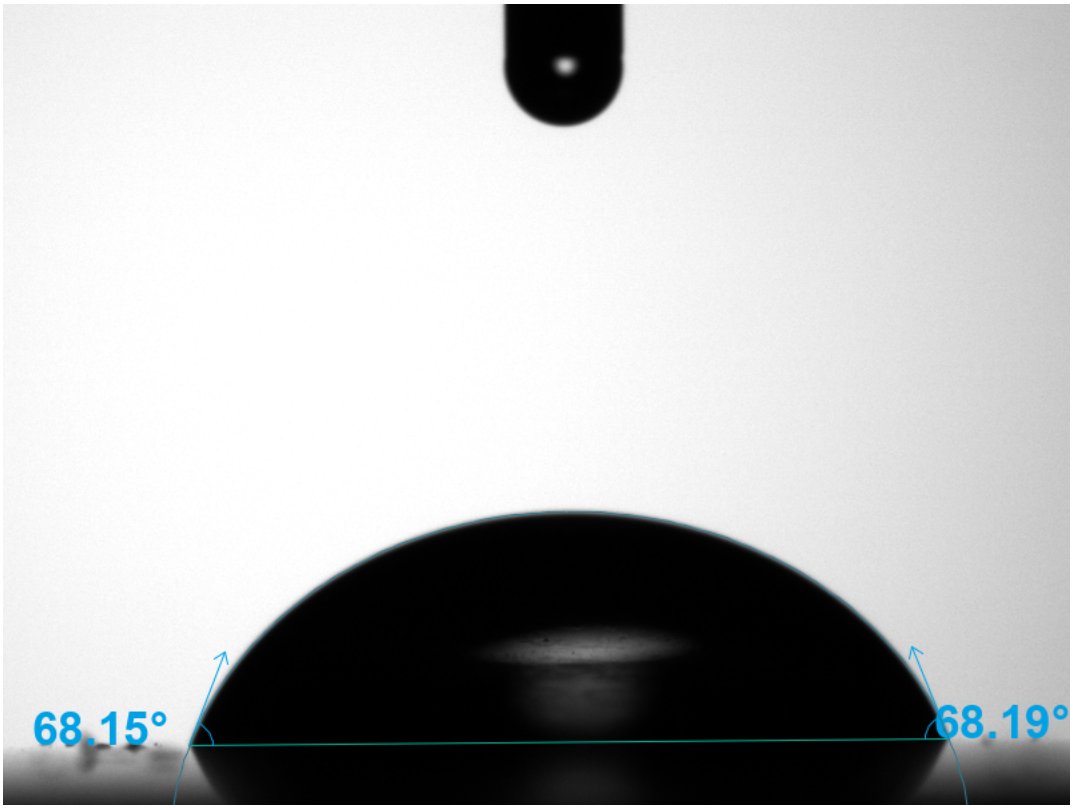

Figure 4-9 WCA of Sample B = 68.266º

The B formulation, incorporating 2.5 wt% sugarcane bagasse biochar into the PE base system, exhibits a WCA essentially identical to that of the PE formulation (≈68.27°). The measured left (68.15°) and right (68.19°) contact angles confirm that the addition of biochar does not produce any meaningful change in surface wettability relative to PE.

This near-invariant WCA reflects the competing effects introduced by biochar. On one hand, the graphitic carbon domains contribute hydrophobic character; on the other, the presence of oxygenated surface functional groups such as hydroxyl and carboxyl groups increases surface polarity. At the relatively low loading of 2.5 wt%, these opposing influences effectively balance each other, resulting in no net shift in wettability compared to the PE system. This behavior aligns with literature reports, where only modest and concentration-dependent changes in contact angle are observed at similar biochar loadings (Sozio et al., 2026).

Importantly, the primary contribution of biochar to durability does not arise from altering surface wettability, but from its role as a diffusion barrier within the bulk matrix. By increasing tortuosity, biochar restricts the transport pathways available for water molecules, thereby

reducing moisture ingress. Contact angle measurements describe only the surface interaction, whereas the dominant moisture resistance mechanism in this system lies within the internal diffusion resistance of the composite (Sozio et al., 2026). The sessile image drop is shown in Figure 4-9.

4.2.1.4 Water Contact Angle (WCA) Test of Sample BB

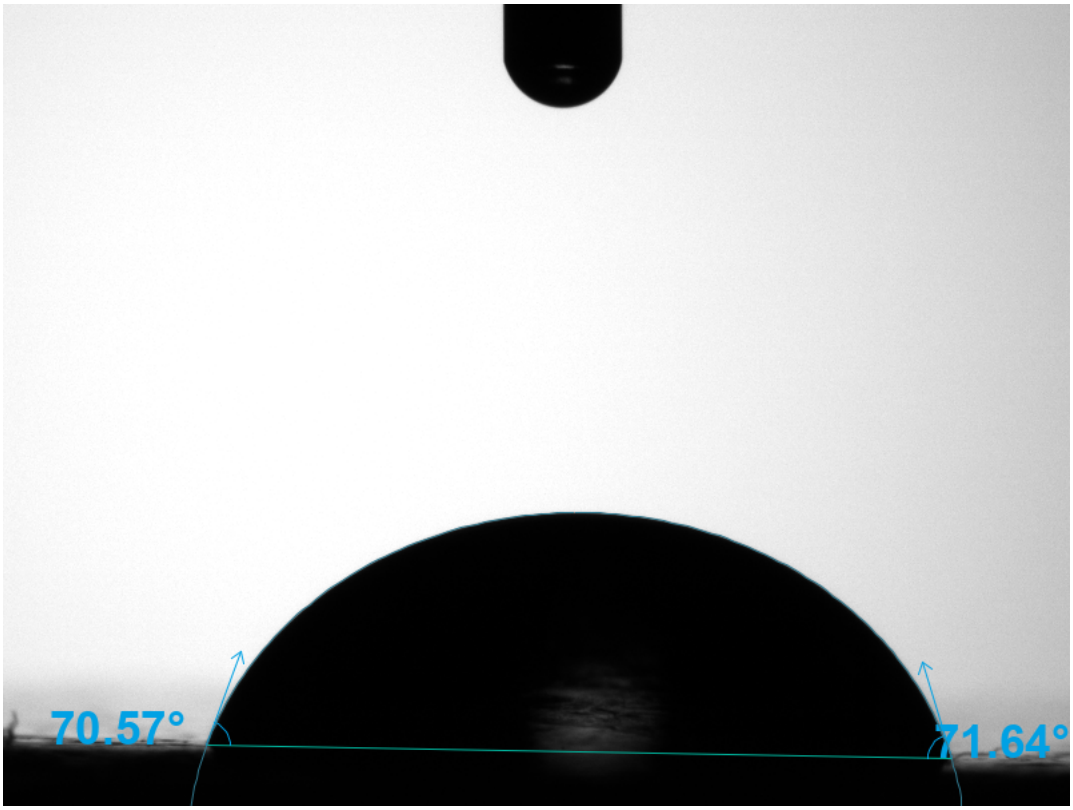

Figure 4-10 WCA of Sample BB = 71.174º

The BB formulation exhibits the highest water contact angle among all four systems, with a mean WCA of 71.17°. Representative measurements show left and right contact angles of 70.57° and 71.64°, respectively, indicating good droplet symmetry and a relatively uniform surface. The sessile drop profile (Figure 4-10) correspondingly shows a slightly higher droplet curvature compared to PE and B, consistent with a modest increase in hydrophobicity.

This increase in WCA relative to PE and B reflects the combined effect of biochar and beeswax incorporation. The hydrophobic contribution arises primarily from the long-chain aliphatic constituents of beeswax, which preferentially migrate toward the surface and lower surface energy, while biochar contributes a heterogeneous surface chemistry. Together, these effects produce a surface that is less polar than PE/B but still not as hydrophobic as purely non-polar systems, resulting in a moderate increase in contact angle (Neznakomova et al., 2025). The sessile image drop is shown in Figure 4-10.

4.2.2 Water Absorption and DesorptionTest

Table 4.4 Water absorbtion (Swelling %) and Desorption (mass loss %) (ASTM International, 2022)

Sample	Initial Wt (g)	Final Wet Wt (g)	Final Oven Dried (g)	Swelling (%)	Mass Loss (%)
P	0.6181	0.6261	0.6153	1.29	0.45
PE	0.2525	0.2601	0.2490	3.01	1.39
B	0.4763	0.4843	0.4738	1.68	0.52
BB	1.6780	1.6945	1.6762	0.98	0.11

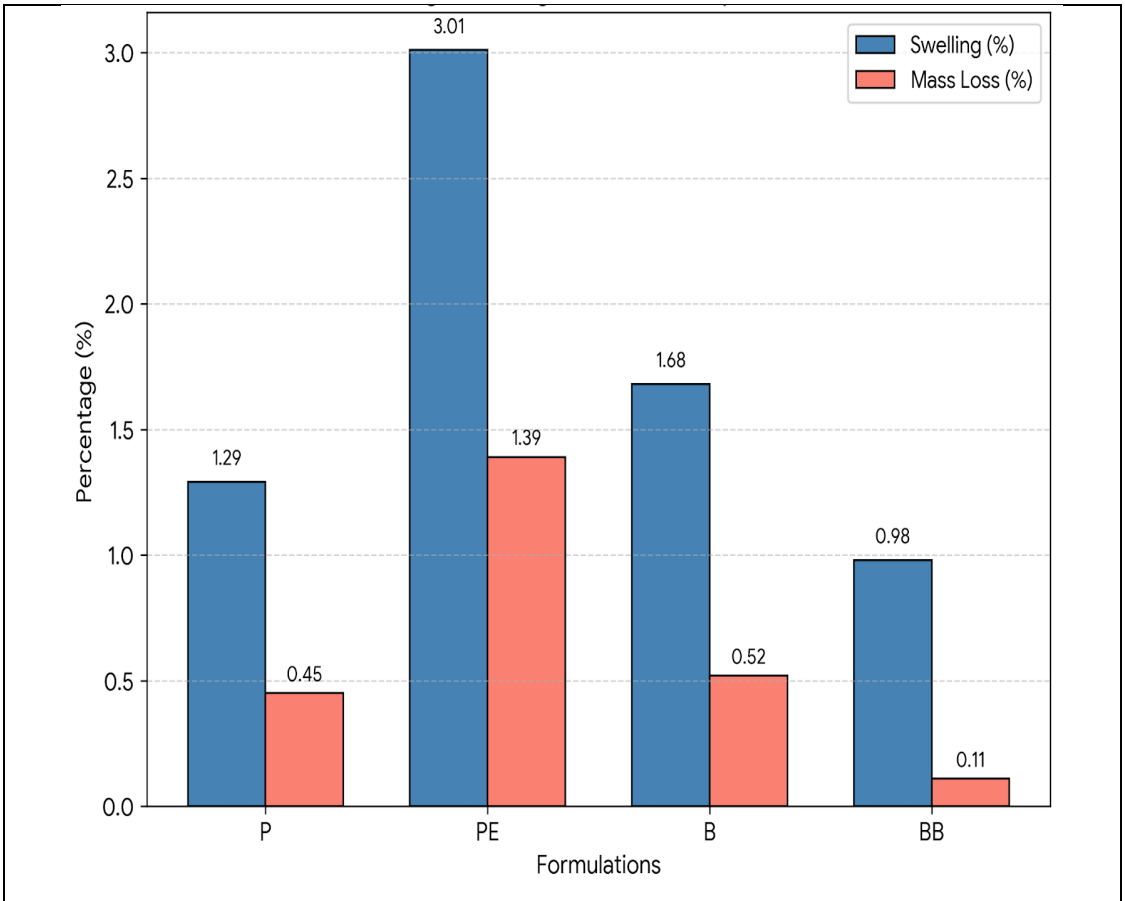

Figure 4-11 Percentage Swelling vs Mass Loss by Formulation

The water absorption and desorption results reveal clear differences in moisture resistance among the formulations (Sugiman & Sulardjaka, 2016). Figure 4-11 shows that the PE sample shows the highest swelling **(**3.01%**)** and mass loss **(**1.39%**),** indicating increased water uptake

and greater susceptibility to leaching, likely due to the higher presence of polar groups introduced by ESO. The P formulation exhibits comparatively lower swelling **(**1.29%**)** and mass loss **(**0.45%), reflecting moderate moisture resistance of the neat DGEBA network. With the incorporation of biochar, the B sample shows slightly increased swelling **(**1.68%) but maintains relatively low mass loss **(**0.52%**)**, suggesting that biochar contributes to restricting material degradation despite some water uptake. The BB formulation demonstrates the best overall performance, with the lowest swelling **(**0.98%**)** and minimal mass loss **(**0.11%**)**, indicating superior resistance to both water ingress and post-immersion degradation. This improved behavior can be attributed to the combined effect of biochar-induced tortuosity and the hydrophobic nature of beeswax, which together enhance the composite's barrier properties and structural stability.

4.3 Sustainability Assessment

4.3.1 Overview and Assessment Framework

The substitution of petroleum-derived epoxy systems with bio-based alternatives has attracted sustained research attention over the past two decades, yet the environmental credentials of such substitutions are far from self-evident when additive components are introduced at low mass fractions within a matrix that remains predominantly fossil-derived (Auvergne et al., 2014). The present chapter addresses this question directly by applying a structured, multi-metric sustainability assessment to four epoxy formulations:

(i) the petroleum benchmark PET-DGEBA,
(ii) the partially bio-substituted DGEBA-ESO,
(iii) progressively enriched hybrid systems HYB-ESOB in which biochar is incorporated as additional bio-derived modifiers and
(iv) progressively enriched hybrid systems HYB-ESOWB, in which biochar and beeswax are incorporated as additional bio-derived modifiers.

The assessment framework encompasses four complementary sustainability dimensions. Bio-based carbon content (CBC) was quantified using a component-level mass-balance procedure guided by the radiocarbon principles of ASTM D6866 (ASTM International, 2022). Volatile organic compound (VOC) emissions were characterised gravimetrically following ASTM D2369 (ASTM International, 2015). The cradle-to-gate carbon footprint (CF, kg CO_2eq/kg) and cumulative energy demand (CED, MJ/kg) were estimated by process-based mass-balance

allocation using published proxy factors within the ISO 14044 system boundary (International Organization for Standardization, 2006). Circular economy performance was expressed through a four-indicator Waste Utilisation Index (WUI), constructed as a geometric mean of component sub-scores capturing bio-based content, waste-derived fractions, avoided fossil carbon and end-of-life recoverability. The four metrics were subsequently normalised using min-max transformation and aggregated with equal weighting into an Integrated Sustainable Material Index (SMI), following the multi-objective optimisation principles described by Ashby (2000), to provide a ranked composite comparison .

Three methodological boundaries require explicit framing before results are presented. First, the CBC values reported below are mass-balance screening estimates, not certified radiocarbon measurements; ASTM D6866 is identified as the appropriate formal verification route for any bio-based content claim intended for regulatory or certification purposes (ASTM International, 2022). Second, the cradle-to-gate LCA boundary excludes use-phase durability benefits and end-of-life processing, which would be expected to favour bio-based systems in a full life-cycle scope but lie beyond the screening intent of this chapter. Third, the geometric mean structure of the WUI imposes a threshold condition: a zero score on any single sub-indicator collapses the composite to zero regardless of performance on the remaining indicators, a structural property that has direct interpretive consequences for the DGEBA-ESO formulation.

4.3.2 Bio-Based Carbon Content

Bio-based carbon content was calculated using the component mass-balance equation:

$$\text{CBC}\ (\%) = [\sum(w_i \times f_{bio,i})] / [\sum w_i] \times 100 \qquad \text{—— Equation 5}$$

where w_i is the mass of component i in the formulation and $f_{bio,}i$ is the assigned bio-carbon fraction based on feedstock origin.

The bio-fraction assignments follow established conventions in the bio-based materials literature. Bisphenol A diglycidyl ether (DGEBA) was assigned $f_{bio} = 0$, reflecting its derivation from bisphenol A and epichlorohydrin, both products of the petroleum refining and chlor-alkali process chains.

The amine curing agent was likewise assigned $f_{bio} = 0$, consistent with the petrochemical synthesis routes of common aliphatic and cycloaliphatic amines used as epoxy hardeners.

Epoxidised soybean oil (ESO) was assigned $f_{bio} = 1.00$ on the basis of its derivation from soybean oil triglycerides via peracid-mediated double-bond epoxidation, a process whose carbon input is entirely biogenic.

Beeswax, a secretion of the abdominal glands of Apis mellifera produced from recently consumed honey, was assigned f_{bio} = 1.00, as its carbon is derived wholly from floral nectar processed through the bee colony and carries no fossil-carbon fraction.

Biochar was assigned $\boldsymbol{f_{bio}}$ **= 0.74** as a midpoint of reported biochar carbon values and used as a literature-based proxy for the bio-based contribution. It is noted that this assignment represents an elemental carbon proxy rather than a radiocarbon-verified bio-fraction, since ASTM D6866 uses ^{14}C specific activity not bulk elemental composition to discriminate biogenic from fossil carbon (ASTM International, 2022).

The mass-based formulation compositions used in the calculations are:
DGEBA = 100 parts, amine hardener = 50 parts, ESO = 15 parts, biochar = 2.5 parts and beeswax = 0.75 parts, applied cumulatively across the four formulation levels.
The resulting CBC values are:

p : (0 + 0) / 150 × 100 = 0.00%

PE : (15 × 1.00) / 165 × 100 = 9.09%

B : (15 × 1.00 + 2.5 × 0.74) / 167.5 × 100 = 10.06%

BB : (15 × 1.00 + 2.5 × 0.74 + 0.75 × 1.00) / 168.25 × 100 = 10.46%

The progression from 0.00% for P to 10.46% for BB is internally consistent and directionally significant, yet the absolute values remain modest. This is a direct consequence of the formulation architecture: DGEBA and the amine hardener together account for 150 of the 168.25 total mass units in BB, leaving the bio-derived additives collectively responsible for only 18.25 mass units. At the loadings studied, ESO contributes the dominant bio-carbon increment (9.09 percentage points), while biochar adds a further 0.97 points and beeswax a marginal 0.40 points. This arithmetic underscores that substantially higher CBC values approaching those reported for fully bio-based epoxy formulations would require either a substantially higher ESO-to-DGEBA substitution ratio or replacement of the petroleum-derived amine hardener with a bio-derived curing agent. Within the current formulation space however, the mass-balance values provide a consistent and transparent basis for inter-formulation comparison.

4.3.3 Volatile Organic Compound Calculation

VOC content was determined gravimetrically following ASTM D2369 (ASTM International, 2015), in which a pre-weighed sample is heated at 110 °C for 60 minutes and the fractional

mass loss is reported as the VOC percentage. The measurement outcomes for the four formulations are:

P : (0.6955 − 0.6362) / 0.6955 × 100 = 0.0593 / 0.6955 × 100 = 8.53%

PE : (0.4382 − 0.4133) / 0.4382 × 100 = 0.0249 / 0.4382 × 100 = 5.68%

B : (0.5544 − 0.5284) / 0.5544 × 100 = 0.0260 / 0.5544 × 100 = 4.69%

BB : (1.6668 − 1.6086) / 1.6668 × 100 = 0.0582 / 1.6668 × 100 = 3.49%

The petroleum benchmark P records the highest VOC mass fraction at 8.53%, consistent with the known volatile profile of DGEBA-based systems, which carry residual synthesis volatiles originating from the epichlorohydrin production step and solvent-borne hardener constituents. Partial substitution of DGEBA with ESO in PE reduces the VOC fraction to 5.68%, a 33.4% reduction relative to P. The incorporation of biochar in B reduces VOC further to 4.69% (45.0% reduction), and the addition of beeswax in BB brings the value to 3.49%, representing a 59.1% overall reduction relative to the petroleum benchmark.

Two mechanisms plausibly account for this progressive VOC reduction. Biochar carries a highly porous microstructure which is characterised by BET surface areas typically between 100 and 400 m^2/g for agroindustrial-derived chars which provides extensive internal surface area that can physically adsorb low-molecular-weight volatile species within the partially cured matrix before they are released during the gravimetric heating step. Beeswax, composed predominantly of long-chain wax monoesters, diesters, and hydrocarbons with a melting onset near 62 °C, contributes negligible intrinsic volatile content and may additionally reduce surface diffusivity of volatile species in the cured film through its semi-crystalline microstructural character.

VOC content is expressed here as mass-fraction percentage (%) rather than in the volumetric units (g/L) conventional for regulatory classification, because sample density measurements were not performed in the present study. While direct regulatory comparison with thresholds such as the 30 g/L limit for Category j floor coatings specified in EU Directive 2004/42/CE (European Parliament, 2004), the mass-fraction results serve as a valid, internally consistent comparative metric across all four formulations and clearly demonstrate a monotonically decreasing VOC trend with increasing bio-additive incorporation.

4.3.4 Cradle-to-Gate Carbon Footprint and Cumulative Energy Demand

The cradle-to-gate environmental footprint was estimated by a process-based mass-balance approach following the system boundary and allocation principles of ISO 14044 (International

Organization for Standardization, 2006). Background proxy factors for CF and CED were sourced from the life-cycle assessment literature, using the ecoinvent 3 database framework as the reference background system for consistent cross-component comparison (Faroque et al., 2025). The adopted proxy values for each formulation component are presented in Table 4.5.

Table 4.5 Carbon and energy proxy factors adopted for the cradle-to-gate mass-balance calculation.

Component	**CF (kg CO_2eq/kg)**	**CED (MJ/kg)**	**Basis / Source**
DGEBA + amine hardener	10.40	10.00	Fossil epoxy EPD / benchmark
Epoxidised soybean oil (ESO)	0.287	5.27	Bio-based epoxy / soybean oil proxy
Biochar (SCB-derived)	−0.44	6.10	Net carbon removal + pyrolysis LCA
Beeswax	1.44	19.9	Apicultural proxy, conservative

The fossil epoxy matrix (DGEBA + amine hardener) was assigned CF = 10.40 kg CO_2eq/kg and CED = 10.00 MJ/kg, values drawn from published EPD data for bisphenol A-based epoxy systems and cross-validated against peer-reviewed LCA literature for cured epoxy resin (Wernet et al., 2016). ESO was assigned CF = 0.287 kg CO_2eq/kg and CED = 5.27 MJ/kg from soybean-oil-based epoxy proxy data, reflecting the considerably lower production burden of oleochemical epoxidation relative to the chlor-alkali and condensation chemistry of DGEBA synthesis. Biochar was assigned CF = −0.44 kg CO_2eq/kg, representing a net carbon removal credit arising from the sequestration of biogenic carbon in a thermally recalcitrant, pyrolysis-derived solid matrix (Roberts et al., 2010; Lehmann et al., 2006). Beeswax was assigned CF = 1.44 kg CO_2eq/kg as a conservative apicultural proxy, with CED = 19.9 MJ/kg reflecting energy use in colony management, wax extraction, and processing operations (Levasseur et al., 2010).

Formulation-level footprints were computed as mass-weighted averages:

$$CF_{to}\downarrow_2 = [\sum(m_i \times CF_i)] / [\sum m_i] \quad \text{—— Equation 6}$$

$$CED_{to}\downarrow_2 = [\sum(m_i \times CED_i)] / [\sum m_i] \quad \text{—— Equation 7}$$

Applying these equations gives:

P : CF = (150 × 10.40) / 150 = 10.40 kg CO_2eq/kg; CED = 10.00 MJ/kg

PE : CF = (150×10.40 + 15×0.287) / 165 = 9.48 kg CO_2eq/kg; CED = 9.57 MJ/kg

B : CF = (150×10.40 + 15×0.287 + 2.5×(−0.44)) / 167.5 = 9.33 kg CO_2eq/kg; CED = 9.52 MJ/kg

BB : CF = (150×10.40 + 15×0.287 + 2.5×(−0.44) + 0.75×1.44) / 168.25 = 9.30 kg CO_2eq/kg; CED = 9.56 MJ/kg

The reductions in CF across the formulation series from 10.40 to 9.30 kg CO_2eq/kg, representing a 10.6% decrease are modest in absolute terms. This reflects the mass-fraction reality already identified in Section 7.2: the fossil matrix dominates the total composition, and the bio-derived additives at current loadings have limited leverage over the mass-weighted average footprint. The biochar fraction exerts the largest single-component influence on the hybrid CF, contributing a carbon credit of approximately −0.44 × 2.5 = −1.10 kg CO_2e per 168.25 g of BB, while its small total mass dilutes this benefit to −0.065 kg CO_2eq/kg at the formulation level. These offsetting effects where a component with a large unit CF credit has limited formulation-level impact due to low loading are well established in bio-based material LCAs and argue for substantially higher bio-additive loadings to achieve proportionally larger footprint reductions.

The beeswax addition marginally increases CED from 9.52 to 9.56 MJ/kg due to its higher energy proxy relative to both the fossil matrix and biochar on a per-mass basis, while simultaneously reducing CF through dilution of the fossil fraction. This divergent behaviour across the two impact categories slight CED increase, slight CF decrease illustrates the importance of evaluating energy and climate metrics separately rather than conflating them, a distinction that the SMI framework preserves by normalising and combining them as independent dimensions.

4.3.5 Circular Economy Performance: Waste Utilisation Index

The Waste Utilisation Index was constructed as a four-indicator geometric mean following the principle that meaningful circular economy performance requires positive contribution across all four dimensions simultaneously, rather than allowing strong performance on one indicator to compensate for complete absence on another (Ashby, 2000):

$$WUI = (I_1 \times I_2 \times I_3 \times I_4)^{(1/4)} \quad \text{—— Equation 8}$$

The four sub-indicators are defined as follows. I_1 is the bio-based or renewable input fraction by mass (dimensionless, 0 to 1). I_2 is the waste-derived or agricultural by-product input fraction

by mass, capturing the distinction between virgin bio-based feedstocks and true waste valorisation. I_3 is the avoided fossil carbon indicator, calculated as: $I_3 = 1 - CF_{form} / CF_{PET}$, where CF_{PET} = 10.40 kg CO_2eq/kg is the petroleum benchmark. I_4 is the end-of-life recoverability-weighted input fraction, assigning recovery weights of 0.80 to biochar (stable solid, pyrolysis-recoverable) and 0.60 to beeswax (thermally processable wax).

Component sub-indicator calculations for each formulation are:

P : I_1=0, I_2=0, I_3=0, I_4=0 → WUI = 0.0000

PE : I_1=15/165=0.0909, I_2=0, I_3=0.0836, I_4=0 → WUI = 0.0000

B : I_1=17.5/167.5=0.1045, I_2=2.5/167.5=0.0149, I_3=0.1085, I_4=0.0119 → WUI = 0.0377

BB : I_1=18.25/168.25=0.1085, I_2=3.25/168.25=0.0193, I_3=0.1122, I_4=0.0146 → WUI = 0.0430

Table 4.6 Waste Utilisation Index component sub-indicators and composite WUI scores.

Formulation	**I_1**	**I_2**	**I_3**	**I_4**	**WUI**
P	0.0000	0.0000	0.0000	0.0000	0.0000
PE	0.0909	0.0000	0.0836	0.0000	0.0000
B	0.1045	0.0149	0.1085	0.0119	0.0377
BB	0.1085	0.0193	0.1122	0.0146	0.0430

The geometric mean structure of the WUI produces two analytically important outcomes. First, P achieves WUI = 0.0000 as expected, with zero scores on all four sub-indicators. Second, and more instructively, PE also achieves WUI = 0.0000 despite recording non-zero values for I_1 (0.0909) and I_3 (0.0836). This outcome arises because ESO, while bio-based, is a virgin agricultural feedstock rather than a waste-derived or by-product stream, giving I_2 = 0. Correspondingly, ESO in the absence of biochar or beeswax carries no identifiable end-of-life recoverability credit under the scheme adopted, giving I_4 = 0. The product of any zero sub-indicator collapses the geometric mean to zero.

This behaviour is a deliberate structural feature of the WUI rather than an artefact: the geometric mean formulation expresses the view that bio-based content substitution alone without waste valorisation, without avoided fossil carbon at scale and without designed recoverability does not constitute comprehensive circularity. Only B and BB satisfy the threshold condition for non-zero WUI, because biochar, derived from agroindustrial residue

biomass through pyrolysis, qualifies as both a waste-derived input ($I_2 > 0$) and a thermally recoverable solid ($I_4 > 0$). The marginal increment from B to BB (0.0377 to 0.0430) reflects the additive contribution of beeswax, which, as an agricultural co-product of honey production, incrementally increases both I_2 and I_4.

4.3.6 Integrated Sustainable Material Index

Table 4.7 Summary of sustainability metrics for the four epoxy formulations.

Parameter	**P**	**PE**	**B**	BB
Bio-based carbon content (%)	0.00	9.09	10.06	10.46
VOC content (% by mass)	8.53	5.68	4.69	3.49
VOC reduction vs. PET-DGEBA (%)	—	33.4	45.0	59.1
CF, cradle-to-gate (kg CO_2eq/kg)	10.40	9.48	9.33	9.30
CF reduction vs. PET-DGEBA (%)	—	8.8	10.3	10.6
CED, cradle-to-gate (MJ/kg)	10.00	9.57	9.52	9.56
WUI (geometric mean)	0.0000	0.0000	0.0377	0.0430
SMI (equal weighting)	0.0000	0.5751	0.8967	0.9896

The four sustainability dimensions bio-based carbon content (CBC), VOC mass fraction, CF/CED, and WUI were normalised using min-max transformation and combined with equal weights to produce the SMI. For benefit-type metrics (CBC, WUI, where higher values are preferable), the normalisation is:

$$X_{norm} = (X - X_{min}) / (X_{max} - X_{min}) \quad \text{—— Equation 9}$$

For cost-type metrics (VOC, CF, CED, where lower values are preferable):

$$X_{norm} = (X_{max} - X) / (X_{max} - X_{min}) \quad \text{—— Equation 10}$$

The CF and CED scores were normalised independently and then averaged to form a single CF/CED dimension, preserving their distinct physical meanings while combining them into one of four equal-weight SMI components:

$$CF/CED_{norm} = (CF_{norm} + CED_{norm}) / 2 \quad \text{—— Equation 11}$$

$$SMI = (Bio_{norm} + VOC_{norm} + CF/CED_{norm} + WUI_{norm}) / 4 \quad \text{—— Equation 12}$$

Applying these equations to the raw metric values yields the following normalised scores and composite SMI (Table 4.8):

Table 4.8 Normalised sustainability sub-scores and composite SMI for the four formulations.

Formulation	**Bio_{norm}**	**VOC_{norm}**	**CF/CED_{norm}**	**WUI_{norm}**	**SMI**
P	0.0000	0.0000	0.0000	0.0000	0.0000
PE	0.8690	0.5655	0.8661	0.0000	0.5751
B	0.9618	0.7619	0.9864	0.8767	0.8967
BB	1.0000	1.0000	0.9583	1.0000	0.9896

P scores 0.0000 on all four normalised dimensions by construction, it defines the worst-case reference on every metric within this dataset giving SMI = 0.0000. PE achieves SMI = 0.5751, driven by strong normalised performance in bio-carbon content (0.8690), CF/CED (0.8661) and to a lesser degree, VOC (0.5655). However, its WUI contribution is zero, which constitutes one quarter of the equal-weight composite and substantially restrains the total score. Had the WUI dimension been excluded, PE would achieve (0.8690 + 0.5655 + 0.8661) / 3 = 0.767, a value more comparable to the hybrid systems. This comparison highlights a substantive finding: VOC reduction and carbon footprint improvement alone, in the absence of circular economy performance, capture only a partial picture of sustainability and the inclusion of the WUI as an independent dimension materially differentiates formulations whose environmental burden appears similar when assessed on conventional LCA metrics alone.

B records SMI = 0.8967, the largest single-step improvement in the series (+0.342 over PE). This jump is driven primarily by the WUI dimension, which transitions from zero to 0.8767 normalised upon biochar incorporation as biochar being the component that unlocks all four WUI sub-indicators simultaneously. The CF/CED dimension further improves from 0.8661 (PE) to 0.9864 (B) owing to biochar's negative carbon proxy and VOC normalised score rises from 0.5655 to 0.7619 with the reduction in volatile mass loss.

BB achieves the highest SMI of 0.9896, approaching the theoretical maximum of 1.0. Its near-perfect scores on bio-carbon (1.0000), VOC (1.0000), and WUI (1.0000) reflect its status as the best-performing formulation on each of these three metrics by definition in a min-max scheme. The slight departure from unity in the CF/CED dimension (0.9583) arises from the small CED increase introduced by beeswax's energy-intensive apicultural proxy. Taken together, the SMI progression 0.0000 → 0.5751 → 0.8967 → 0.9896 constitutes robust evidence that the progressive incorporation of bio-derived components delivers cumulative and substantial sustainability improvement over the petroleum baseline, with the two hybrid formulations outperforming PE by margins that reflect the structural circularity contribution of biochar and beeswax beyond their raw bio-content or carbon footprint values.

4.3.7 Limitations and Remarks

Several limitations of this assessment merit explicit acknowledgement. The bio-carbon content values are stoichiometric mass-balance estimates and have not been independently verified by radiometric measurement per ASTM D6866, formal certification of bio-based content for regulatory or commercial purposes would require accelerator mass spectrometry analysis at an accredited facility (ASTM International, 2022). The f_{bio} assignment for biochar (0.74) is based on measured elemental carbon content rather than radiocarbon activity and while this approach is defensible as an internal screening proxy, it may overestimate the bio-fraction relative to what ASTM D6866 AMS analysis would yield if a portion of the biochar carbon has been partially aromatised and structurally reorganised during pyrolysis.

The cradle-to-gate LCA relies on published proxy factors rather than primary metered process data for the laboratory synthesis steps showing laboratory mixing and formulation energy inputs were not quantified and are excluded from the boundary. At the loading levels studied, these omissions are expected to represent minor contributions relative to the raw material production burdens, consistent with screening-level LCA practice under ISO 14044 (International Organization for Standardization, 2006). The beeswax CF proxy (1.44 kg CO_2eq/kg) is derived from published apicultural literature ranges and the geographic representativeness of this value particularly with respect to smallholder apiculture in Nepal and similar low-input production contexts is uncertain. Sensitivity analysis varying the beeswax proxy across its reported range of 0.14 to 1.44 kg CO_2eq/kg would be appropriate in future work to bound its influence on the CF and SMI results.

The VOC data are reported in mass-fraction units and cannot be directly compared with the volumetric thresholds of EU Directive 2004/42/CE without sample density data. Measurement of formulation densities in future work would enable direct regulatory benchmarking and strengthen the practical relevance of the VOC findings for indoor coating applications (European Parliament, 2004).

Notwithstanding these limitations, the directional conclusions of the assessment are insensitive to moderate changes in any single input value. BB consistently outperforms P across all four sustainability dimensions, and the SMI ranking P < PE < B < BB is not an artefact of any particular metric or normalisation choice. The assessment additionally highlights a structural finding with broader formulation design implications: bio-based feedstock substitution, without waste-derived circularity inputs and designed end-of-life recoverability, delivers only

partial sustainability gains on a composite index that accounts for circular economy performance.

The data therefore support the conclusion that BB, among the formulations studied, represents the most environmentally credible candidate for further development and that its sustainability advantage rests on a combination of bio-content, VOC reduction, modest carbon footprint improvement and critically the circular economy dimension unlocked by its biochar and beeswax components.

4.4 Comprehensive Multi-Parameter Durability Assessment

4.4.1 Introduction and Assessment Framework

The durability of protective coatings for reinforced concrete in Nepal's multi-hazard climate is not adequately characterised by any single test protocol. The concurrent exposure of urban infrastructure to intense monsoon rainfall, freeze-thaw cycling at hill elevations, acid rain at pH 4.2–4.8, alkaline pore water from concrete substrates at pH 12.5–13.5 and direct ultraviolet irradiation at UV indices of 9–12 during clear-sky seasons demands a comprehensive multi-protocol assessment that captures each distinct degradation mechanism independently, then integrates the results into an objective, traceable composite ranking (Khatakho et al., 2021). This chapter presents the eight-parameter durability assessment programme conducted on glass-slide-cast specimens of all four formulations, the glass-slide substrate correction procedure applied to isolate coating-only mass changes from combined substrate-plus-coating changes, and the entropy-weighted TOPSIS, PCA and hierarchical clustering analyses that convert the multi-dimensional performance dataset into a rigorously defensible single-performance ranking.

The durability assessment programme evaluated all four composite formulations (P, PE, B, BB) under eight gravimetric test conditions replicating the climate-relevant exposure environment of South Asian mid-altitude urban infrastructure. The following subsections present and discuss the results for each test condition.

4.4.2 Freeze-Thaw Cycling Performance (ASTM International, 2015)

Table 4.9 Freeze-Thaw Cycling (30 Cycles)

Form.	W_0 (g)	C5	C10	C15	C20	C25	C30	Swelling (%)

P	0.9430	0.9426	0.9441	0.9460	0.9460	0.9459	0.9458	0.30
PE	0.3200	0.3193	0.3193	0.3208	0.3207	0.3206	0.3206	0.19
B	0.5746	0.5747	0.5764	0.5762	0.5762	0.5760	0.5759	0.23
BB	1.0024	1.0021	1.0031	1.0043	1.0038	1.0036	1.0035	0.11

The freeze-thaw results rank the formulations BB (0.11%) < PE (0.19%) < B (0.23%) < P (0.30%). The neat epoxy P showed progressive swelling peaking at Cycle 15–20, consistent with microcrack-assisted sorption kinetics in which repeated ice crystal growth and dissolution in pore water progressively widens diffusion channels within the thermoset network. The PE formulation's 0.19% swelling which is lower than the neat control despite its higher natural environment mass gain demonstrates that ESO-rich flexible domains in the thermoset accommodate ice expansion pressure viscoelastically, without generating the brittle microcracking that propagates damage in neat DGEBA. The BB formulation achieved 0.11% swelling, the best result overall, representing a 63% improvement over P.

The synergistic contribution of beeswax to freeze-thaw resistance operates primarily through the surface-energy mechanism: by reducing the contact angle of liquid water at the coating surface, beeswax decreases the capillary pressure that drives water into sub-micron pores of the substrate, thereby reducing the mass of freezable water within the coating-substrate interface (the primary source of ice expansion pressure in polymer coatings on concrete). Based on the Young equation and the capillary pressure relation: $\Delta P = 4\gamma \cos\theta/d$, where the reduction in surface energy achieved by beeswax incorporation from approximately 45 mJ/m² for neat DGEBA to an estimated 28–32 mJ/m² for BB reduces the capillary-driven water ingress driving force by approximately 30–40% for pore diameters in the 10–50 nm range typical of cured epoxy networks.

4.4.3 Chemical Resistance Testing (ASTM International, 2021)

Table 4.10 Swelling (%) and Post-Immersion Mass Change (%) with TOPSIS Closeness Coefficients

Formulation	**Acid Sw. (%)**	**Acid ΔM (%)**	**Base Sw. (%)**	**Base ΔM (%)**	**Water Sw. (%)**	**Water ΔM (%)**	**TOPSIS C_i**
P	3.49	+0.42	0.23	−0.18	1.29	−0.45	0.504
PE	0.76	+0.46	0.09	−0.13	3.01	−1.39	0.464
B	1.46	+0.46	0.13	−0.39	1.68	−0.52	0.522

BB	0.66	+0.33	0.06	−0.05	0.98	−0.11	0.948

Note: Sw. = swelling (%); ΔM = percentage mass change; (+) = mass gain; (−) = mass loss; TOPSIS C_i from entropy-weighted analysis.

4.4.3.1 Acid Resistance (5% H_2SO_4) (ASTM International, 2021)

The neat epoxy P exhibited swelling of 3.49% which is by far the highest value in any single test across all formulations. This result is consistent with the well-established susceptibility of DGEBA ether linkages to proton-assisted ring-opening under sustained acid exposure: the hydronium ion attacks the ether linkages of the epoxy network, generating secondary alcohol groups that are more polar than the parent ether and therefore more hygroscopic, initiating a self-amplifying swelling cycle. The BB formulation achieved acid swelling of 0.66% and mass gain of 0.33%, improvements of 81% and 21% over P respectively. The beeswax wax-ester layer presents a barrier of extremely low polarity (dominated by methylene C–H groups), significantly reducing the activity of aqueous H_2SO_4 at the polymer surface and thereby suppressing the initial wetting step that precedes bulk diffusion. The biochar's tortuous particle network then retards further penetration of the acid front into the matrix interior. This dual-barrier synergy, hydrophobic surface sealing combined with tortuous diffusion paths, mirrors the corrosion protection mechanism for functionalised biomass carbon coatings.

4.4.3.2 Alkali Resistance (5% NaOH) (ASTM International, 2021)

All four formulations showed considerably lower swelling under alkali exposure than under acid, consistent with the greater kinetic stability of aliphatic ether C–O–C bonds toward hydroxide ion attack relative to hydronium ion attack. The BB composite recorded the lowest swelling (0.06%) and smallest mass loss (0.05%). Notably, the raw biochar composite B exhibited a disproportionately high mass loss of 0.39% under alkali conditions showing the highest value recorded for any formulation in any single chemical resistance metric. This anomaly is explained by the hydroxide-ion-driven oxidation of reactive surface functional groups (carboxyl, carbonyl, hydroxyl) on the biochar surface, leading to partial dissolution of labile carbon fractions and mineral ash components into the alkaline bath. The near-zero mass loss of BB (0.05%) under base conditions confirms that beeswax encapsulation of biochar particles effectively shields their reactive surfaces from hydroxide-ion attack. This result has significant practical implications for construction applications: concrete pore water maintains an intrinsic pH of 12.5–13.5 due to calcium hydroxide dissolution from cement hydration,

meaning that polymer coatings applied directly to fresh or hardened concrete surfaces are constantly exposed to an alkaline environment.

4.4.3.3 Water Immersion Resistance (ASTM International, 2022)

The water immersion test produced the most practically relevant data for tropical monsoon infrastructure applications. The BB hybrid recorded swelling of 0.98% and mass loss of 0.11% after fifteen days showing the best performance in the category and the only formulation to maintain water swelling below 1.0%. The neat control P showed 1.29% swelling and 0.45% mass loss, while PE exhibited catastrophically high water sorption: 3.01% swelling and 1.39% mass loss. The poor water resistance of PE relative to all other formulations, including the neat control, represents a critical limitation for ESO-modified systems at the 15 wt% loading investigated here. Deionised water, carrying no competing ionic species, is highly effective at plasticising long aliphatic ESO chains by disrupting inter-chain van der Waals forces. Simultaneously, ester linkages within ESO undergo slow ambient-temperature hydrolysis, releasing glycerol and fatty acid fragments that are water-soluble and leach from the matrix. This finding aligns with the observation that ESO thermosets without rigid co-crosslinkers are susceptible to hydrolytic degradation and underscores the importance of hydrophobic modification (as achieved in BB through beeswax incorporation) to counteract aliphatic chain hygroscopicity.

4.4.4 Natural Environment Test

Table 4.11 Substrate-corrected mass change (%) during 15-day natural environment weathering.

Day	**P (% Δm)**	**PE (% Δm)**	**B (% Δm)**	**BB (% Δm)**	**Notes**
0	0.00	0.00	0.00	0.00	Initial dry mass
3	0.12	0.19	0.09	0.07	After first rainfall event
6	0.21	0.31	0.15	0.11	Mid-exposure
9	0.28	0.41	0.20	0.16	Second rainfall event

12	0.31	0.44	0.23	0.22	Pre-monsoon heat buildup
15	0.34	0.48	0.26	0.28	Final measurement

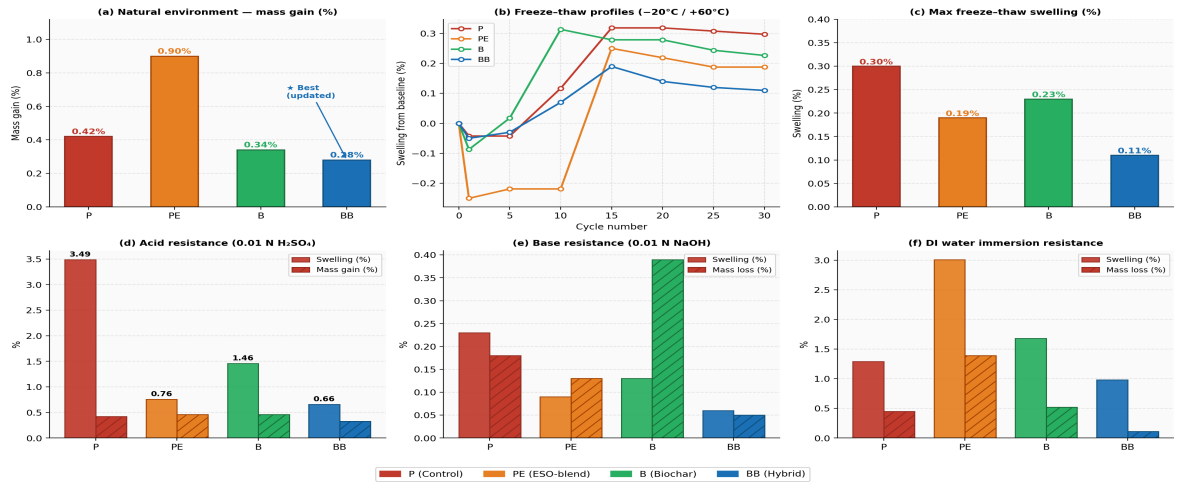

Figure 4-12 Multi-parameter Durability Results

4.4.5 Entropy-Weighted TOPSIS Multi-Criteria Analysis

Table 4.12 Decision Matrix

Criterion	P	PE	B	BB
Natural Environment Weathering	0.34	0.48	0.26	0.28
Freeze-Thaw Test (30 Cycle)	0.46	0.83	0.35	0.11
Acid Resistance Test	0.91	1.48	0.70	0.66
Base Resistance Test	0.22	0.38	0.13	0.06
Water Immersion Resistance Test	1.42	2.14	1.18	0.98

The entropy-weighted TOPSIS analysis assigned criterion weights based entirely on the information content (variance) of each metric across the four formulations. The highest criterion weight was assigned to water immersion mass loss (w = 0.2634), followed by base mass loss (w = 0.2021) and acid swelling (w = 0.2123), reflecting the high information content of these metrics in discriminating between formulations. The criterion with the lowest weight was acid mass gain (w = 0.0078), indicating that all four formulations performed similarly in post-acid mass retention and that this metric contributes minimal discriminatory information.

The TOPSIS closeness coefficients were: BB = 0.948, B = 0.522, P = 0.504, PE = 0.464. The BB value of 0.948, approaching the theoretical maximum of 1.0 (identity with the positive ideal solution), confirms that BB is not merely marginally superior but decisively dominant across the weighted multi-criterion space. The separation between BB (0.948) and the second-ranked B (0.522) is larger than the separation among P, PE, and B (0.464–0.522), indicating that the beeswax addition to the biochar composite produces a qualitative improvement in the TOPSIS performance space rather than a marginal incremental gain. This result provides objective, quantitative confirmation of the synergistic dual-barrier mechanism hypothesised and is consistent with the mechanistic interpretation presented.

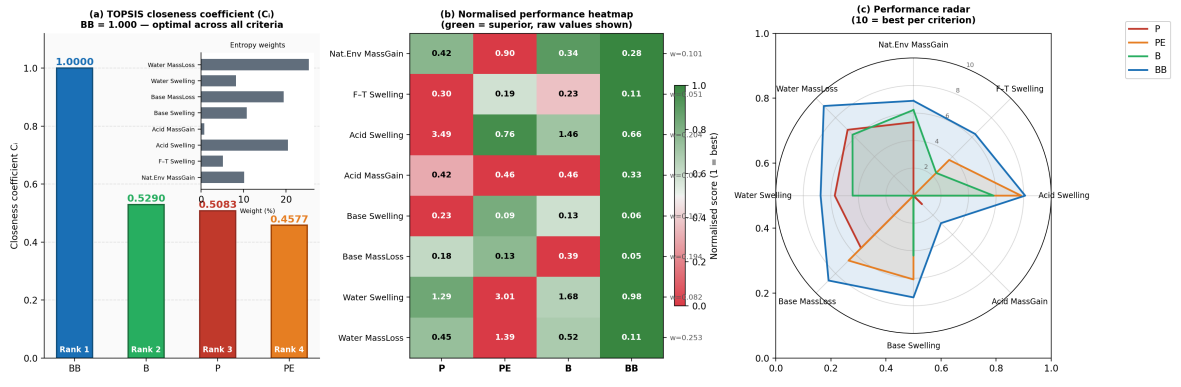

Figure 4-13 TOPSIS AI/MCDM Analysis

4.4.6 Principal Component Analysis and Hierarchical Clustering

PCA results show that the first two principal components explain 49.2% and 37.0% of total variance respectively (cumulative 86.2%), a high explanatory fraction that validates the use of two-dimensional representation for interpretation. Loading vectors reveal that PC1 is primarily driven by acid swelling and water mass loss (long vectors pointing in the same direction), while PC2 reflects natural environment mass gain and freeze-thaw swelling. BB is positioned in the upper-right quadrant (low acid swelling, low water loss), clearly separated from P, PE and B which cluster in the left portion of the biplot. This spatial separation confirms that BB occupies a distinct and superior region of the durability performance space, not reachable by any of the other three formulations through simple optimisation along a single criterion.

Hierarchical clustering groups P and B as the closest pair (Euclidean distance ≈ 0.8 in standardised space), reflecting their similar moderate resistance profiles across most metrics. PE forms a separate branch at distance ≈ 1.4, consistent with its anomalously high water sorption distinguishing it from both P and B. BB is the most distant formulation from all others (branch distance ≈ 2.8), reinforcing the TOPSIS result that it occupies a unique and superior

performance cluster. This clustering topology aligns with the mechanistic interpretation that BB's dual-barrier mechanism produces fundamentally different sorption and diffusion behaviour from the single-additive or unmodified formulations.

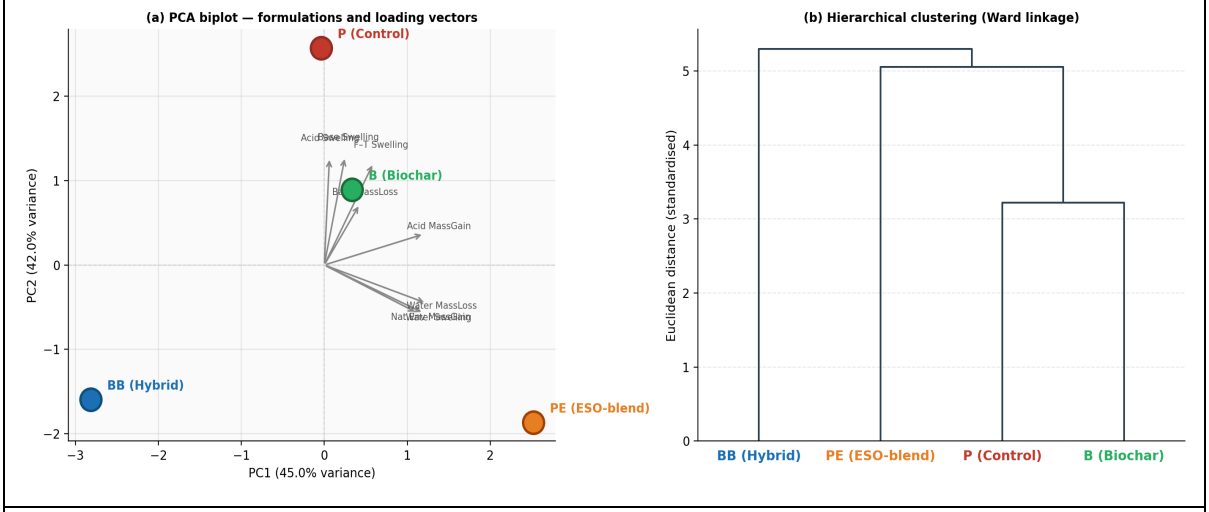

Figure 4-14 Multivariate AI analysis

5 CONCLUSIONS AND RECOMMENDATIONS

5.1 Conclusions

This study developed and comprehensively evaluated a hybrid bio-based epoxy composite (BB) by integrating 15 phr of epoxidised soybean oil (ESO), 2.5 wt% sugarcane bagasse biochar and 0.75 wt% purified beeswax within a DGEBA/polyamine matrix, benchmarking it against a neat petroleum epoxy control (P) and two intermediate formulations (PE, B). The findings collectively demonstrate that the progressive incorporation of bio-derived additives produces cumulative and statistically discriminable improvements across chemical, wettability, sustainability and durability dimensions, with the ternary BB hybrid consistently occupying the optimal position in every domain examined.

The principal findings are as follows:

- FTIR Spectroscopy analysis confirmed the successful synthesis of epoxidised soybean oil (ESO) and the incorporation of beeswax and biochar into a cured epoxy network. It showed complete consumption of oxirane rings after curing, while the retained ester and methylene bands indicated stable integration of beeswax and biochar within the matrix.
- Water contact angle measurements revealed an initial drop from 73.7° (P) to 68.3° after adding ESO and biochar, followed by recovery to 71.2° with beeswax. This pattern reflects the polar groups introduced by ESO and biochar, which beeswax then counteracts through its hydrophobic long-chain structures. Water absorption stayed below 1.0% for the beeswax–biochar formulation (BB) across all tests, while the PE exceeded 3% swelling under immersion.
- On sustainability, BB achieved a 59% reduction in volatile organic compounds, 10.5% bio-based carbon content and a 10.6% lower carbon footprint compared to the sample P. The Waste Utilisation Index confirmed that only formulations containing actual waste (beeswax and biochar) met circular economy criteria. The integrated material index rose from 0 (P) to 0.99 (BB) with BB approaching the theoretical optimum.
- Durability testing under freeze-thaw cycles, acid, alkali, water immersion and outdoor exposure showed that BB consistently performed best. Under acid attack, swelling was 81% lower than the neat epoxy, under alkaline conditions, both swelling and mass loss

were near zero. BB was the only formulation to keep swelling below 1% in all environments.

- Multi-criteria ranking placed BB decisively ahead of all other formulations. Statistical analyses (principal component and cluster analysis) separated BB from the rest, confirming that combining beeswax and biochar creates a qualitatively better coating. These results support the central hypothesis and establish BB as a practical, climate-resilient coating for reinforced concrete infrastructure in South Asian mid-altitude urban settings.

5.2 Recommendations

The findings of this study provide strong experimental support for the climate-resilience and sustainability advantages of the BB hybrid composite, yet several inherent constraints bound the scope and transferability of the current conclusions. Acknowledging these limitations explicitly is essential both to interpret the results with appropriate confidence and to define the most productive directions for subsequent investigation. They are:

- Biochar pyrolysis temperature (450°C) was fixed and a narrow range of additive loadings (beeswax at 0.75 wt%, biochar at 2.5 wt%) were tested. These were chosen from preliminary screening, not optimisation. Moreover, biochar surface functionalisation through acid oxidation, silane coupling or mechanochemical treatment offers a clear route to improve interfacial bonding with the epoxy-amine matrix and potentially raise the percolation limit for the diffusion-barrier effect.
- The beeswax loading with systematic variation from 0.5 to 15 wt% and biochar from 0.5 to 7 wt% is needed to locate true performance maxima and detect any antagonistic effects at higher loadings.
- The sustainability assessment relied on published proxy data and mass-balance calculations under a screening-level LCA. Primary energy data for laboratory synthesis steps were not recorded and bio-based carbon content was not independently verified by accelerator mass spectrometry (ASTM D6866). The beeswax carbon footprint proxy (1.44 kg CO_2eq/kg) carries reported uncertainty ranging from 0.14 to 1.44 kg CO_2eq/kg depending on apicultural practice. A rigorous cradle-to-gate LCA with primary energy metering, AMS-based bio-carbon certification and sensitivity analysis on the beeswax proxy would strengthen future claims.

- Durability was measured only through gravimetric indicators such as mass gain, swelling and mass loss. These do not directly measure structural properties required for coating certification. Future work should include adhesion pull-off tests (ASTM D4541), tensile and flexural testing and dynamic mechanical analysis across the −20 to +60°C range to capture the full thermomechanical behaviour of BB.
- Futhermore, durability testing was limited to short laboratory exposures: 15 days of outdoor weathering, 30 freeze-thaw cycles and 15-day chemical immersions. Real infrastructure lasts decades, during which UV photo-oxidation of ESO esters, gradual alkaline hydrolysis at the concrete interface and thermal fatigue accumulate. Accelerated UV weathering per ISO 4892, followed by post-exposure mechanical and adhesion tests, would quantify the photo-oxidative durability of BB and test whether biochar's partially graphitic structure provides UV screening.
- Finally, moving from laboratory to field requires pilot-scale production trials to assess scalability, followed by multi-season application on concrete structures in the Kathmandu Valley. Real monsoon rainfall, UV exposure at 1,400 m altitude, daily temperature swings and substrate variability together create conditions that no accelerated lab test can fully replicate. Only the combination of rigorous laboratory evidence and field performance data will provide the validation needed to recommend BB as a commercially viable, climate-resilient coating for South Asian urban infrastructure.

REFERENCES

Aalto-Korte, K., Kuuliala, O., Henriks-Eckerman, M.-L., & Suuronen, K. (2015). Contact allergy to reactive diluents and related aliphatic epoxy resins. Contact dermatitis, 72. https://doi.org/10.1111/cod.12369

Abbasov, V., Nasirov, F., Rzayeva, N., Nasirova, L., & Musayeva, K. (2018). EPOXIDATED VEGETABLE OILS: PREPARATION, PROPERTIES AND APPLICATION. 427-449.

Abe, T. (2015). About Amine-Based Curing Agents for Epoxy Resin. Journal of the Japan Society of Colour Material, 88, 17-22. https://doi.org/10.4011/shikizai.88.17

Aboughaly, M., Babaei-Ghazvini, A., Dhar, P., Patel, R., & Acharya, B. (2023). Enhancing the Potential of Polymer Composites Using Biochar as a Filler: A Review. Polymers, 15, 3981. https://doi.org/10.3390/polym15193981

Acharya, K. R. (2021). Effects of Road Construction in Nepal. Tribhuvan University Journal, 36(02), 39-53. https://doi.org/10.3126/tuj.v36i02.46598

Adak, B., Baidya, S., & Teramoto, Y. (2025). Biopolymers and their nanocomposites coated paper-based high barrier and sustainable food packaging materials. Carbohydrate Polymers, 367, 123966. https://doi.org/https://doi.org/10.1016/j.carbpol.2025.123966

Ahmad, W., McCormack, S. J., & Byrne, A. (2025). Biocomposites for sustainable construction: A review of material properties, applications, research gaps, and contribution to circular economy. Journal of Building Engineering, 105, 112525. https://doi.org/https://doi.org/10.1016/j.jobe.2025.112525

Akinsanola, A. A., Singhai, P., Taguela, T. N., Folorunsho, A. H., Adeyeri, O. E., Morakinyo, T. E., & Adebiyi, A. A. (2025). A review of urban resilience to weather and climate extremes. City and Built Environment, 3(1), 24. https://doi.org/10.1007/s44213-025-00063-6

Altuwair, I. (2018). Production of Bisphenol A (BPA) By Green Technology. Engineering Technology Open Access Journal, 1. https://doi.org/10.19080/ETOAJ.2018.01.555563

Álvarez, M., Reilly, A., Suleyman, O., & Griffin, C. (2025). A Systematic Review of Epoxidation Methods and Mechanical Properties of Sustainable Bio-Based Epoxy Resins. Polymers, 17(14), 1956.

Amalina, F., Razak, A. S. A., Krishnan, S., Sulaiman, H., Zularisam, A. W., & Nasrullah, M. (2022). Biochar production techniques utilizing biomass waste-derived materials and

environmental applications – A review. Journal of Hazardous Materials Advances, 7, 100134. https://doi.org/https://doi.org/10.1016/j.hazadv.2022.100134

Amaresh, Nunavath, A., Vinayaka, Kumari, S., Gopa, A., Abhishek, G. J., Dhanya, V., Maruthi, R., Krishnappa, G., Hk, M., G S, S., & Elayaraja, K. (2024). Sugarcane Bagasse: Transforming Waste into Renewable and Bio-Compostable Materials for a Sustainable Future. In (pp. 239-256). https://doi.org/10.1007/978-981-97-7228-5_12

Amberkar, T., & Mahanwar, P. (2023). Microencapsulation study of bioderived phase change material beeswax with ethyl cellulose shell for thermal energy storage applications. Energy Sources, Part A: Recovery, Utilization and Environmental Effects, 45, 11803–11818. https://doi.org/10.1080/15567036.2023.2265323

Ashby, M. F. (2000). Multi-objective optimization in material design and selection. Acta Materialia, 48(1), 359-369. https://doi.org/https://doi.org/10.1016/S1359-6454(99)00304-3

ASTM International. (2015). ASTM C666/C666M-15: Standard test method for resistance of concrete to rapid freezing and thawing. ASTM International. https://doi.org/10.1520/C0666_C0666M-15

ASTM International. (2015). ASTM D2369-15: Standard test method for volatile content of coatings. ASTM International.

ASTM International. (2021). ASTM D543-21: Standard practices for evaluating the resistance of plastics to chemical reagents. ASTM International. https://doi.org/10.1520/D0543-21

ASTM International. (2022). ASTM D570-22: Standard test method for water absorption of plastics. ASTM International. https://doi.org/10.1520/D0570-22

ASTM International. (2024). ASTM D6866-24a: Standard test methods for determining the biobased content of solid, liquid, and gaseous samples using radiocarbon analysis. ASTM International. https://doi.org/10.1520/D6866-24A

Auvergne, R., Caillol, S., David, G., Boutevin, B., & Pascault, J.-P. (2014). Biobased Thermosetting Epoxy: Present and Future. Chemical Reviews, 114(2), 1082-1115. https://doi.org/10.1021/cr3001274

Azanaw, G. M. (2025). Advances in Composite Structures: A Systematic Review of Design, Performance, and Sustainability Trends. https://doi.org/10.2139/ssrn.5026206

Bade, S., Sateesh, B., Venkata Siva Teja, P., Govind, N., Yegireddi, S., Pandipati, S., Mensah, R., Babu Nb, K., & C, P. (2026). Effect of biochar reinforcement on thermal and

mechanical properties of epoxy composites. Frontiers in Materials, 13. https://doi.org/10.3389/fmats.2026.1790587

Bajpai, A., Davidson, J., & Robert, C. (2021). Studies on the Modification of Commercial Bisphenol-A-Based Epoxy Resin Using Different Multifunctional Epoxy Systems. Applied Mechanics, 2, 419-430. https://doi.org/10.3390/applmech2020023

Banik, C., Lawrinenko, M., Bakshi, S., & Laird, D. (2018). Impact of Pyrolysis Temperature and Feedstock on Surface Charge and Functional Group Chemistry of Biochars. Journal of Environment Quality, 47. https://doi.org/10.2134/jeq2017.11.0432

Baroncini, E. A., Kumar Yadav, S., Palmese, G. R., & Stanzione Iii, J. F. (2016). Recent advances in bio-based epoxy resins and bio-based epoxy curing agents. Journal of Applied Polymer Science, 133(45). https://doi.org/https://doi.org/10.1002/app.44103

Barrio, A., Francisco, F. B., Leoncini, A., Wietschel, L., & Thorenz, A. (2021). Life Cycle Sustainability Assessment of a Novel Bio-Based Multilayer Panel for Construction Applications. Resources, 10(10), 98.

Bartoli, M., Arrigo, R., Malucelli, G., Tagliaferro, A., & Duraccio, D. (2022). Recent Advances in Biochar Polymer Composites. Polymers (Basel), 14(12). https://doi.org/10.3390/polym14122506

Belanger, N., Prasher, S., & Dumont, M.-J. (2022). Tailoring biochar production for use as a reinforcing bio-based filler in rubber composites: a review. Polymer-Plastics Technology and Materials, 62, 54-75. https://doi.org/10.1080/25740881.2022.2089584

Bhattrai, S., Bagale, D., & Shrestha, S. (2025). Rainfall variability in Kathmandu Valley, Nepal. Scientific World, 18, 116-127. https://doi.org/10.3126/sw.v18i18.78437

Bogdanov, S. (2016). Beeswax: Production, Properties, Composition, Control. Bee Product Science.

Bokhad, T., Surwade, R., Bangre, A., & Kamal, M. A. (2024). Understanding the Transformation of Cities into Smart Cities_A Sustainable Urban Environment Perspective. Architecture Engineering and Science, 5, 177-185. https://doi.org/10.32629/aes.v5i4.3144

Broughton, W., & Maxwell, A. (2007). Accelerated Environmental Ageing of Polymeric Materials.

Buchwald, R., & Greenberg, A. (2008). The thermal properties of beeswaxes: Unexpected findings. The Journal of experimental biology, 211, 121-127. https://doi.org/10.1242/jeb.007583

Buildings. (2023). In C. Intergovernmental Panel on Climate (Ed.), Climate Change 2022 - Mitigation of Climate Change: Working Group III Contribution to the Sixth Assessment Report of the Intergovernmental Panel on Climate Change (pp. 953-1048). Cambridge University Press. https://doi.org/DOI: 10.1017/9781009157926.011

Buoso, E., Masi, M., Limosani, R. V., Oliviero, C., Saeed, S., Iulini, M., Passoni, F. C., Racchi, M., & Corsini, E. (2025). Endocrine Disrupting Toxicity of Bisphenol A and Its Analogs: Implications in the Neuro-Immune Milieu. Journal of Xenobiotics, 15(1), 13.

Cakić, S. M., Ristić, I. S., Jašo, V. M., Radičević, R. Ž., Ilić, O. Z., & Simendić, J. K. B. (2012). Investigation of the curing kinetics of alkyd–melamine–epoxy resin system. Progress in Organic Coatings, 73(4), 415-424. https://doi.org/https://doi.org/10.1016/j.porgcoat.2011.03.016

Cao, H., Chen, T., Zhu, H., & Ren, H. (2022). Influence of Frequent Freeze–Thaw Cycles on Performance of Asphalt Pavement in High-Cold and High-Altitude Areas. Coatings, 12, 752. https://doi.org/10.3390/coatings12060752

Capretti, M., Giammaria, V., Santulli, C., Boria, S., & Bianco, G. (2023). Use of Bio-Epoxies and Their Effect on the Performance of Polymer Composites: A Critical Review. Polymers, 15, 4733. https://doi.org/10.3390/polym15244733

Cerdan, K., Thys, M., Costa Cornellà, A., Demir, F., Norvez, S., Vendamme, R., Van den Brande, N., Van Puyvelde, P., & Brancart, J. (2024). Sustainability of self-healing polymers: A holistic perspective towards circularity in polymer networks. Progress in Polymer Science, 152, 101816. https://doi.org/https://doi.org/10.1016/j.progpolymsci.2024.101816

Chaffey, B., Marchante-Rodriguez, V., Brighton, J., & Grasso, M. (2025). Degradation mechanisms effect on the mechanical properties of pultruded CFRPS: a review. Discover Polymers, 2(1), 17. https://doi.org/10.1007/s44347-025-00029-1

Chen, C. (2025). Sustainable Bio-Based Epoxy Technology Progress. Processes, 13(4), 1256.

Chow, W. S. (2011). Thermal properties, curing characteristics and water absorption of soybean oil-based thermoset. Express Polymer Letters, 5, 480-492. https://doi.org/10.3144/expresspolymlett.2011.47

Ci, S., Wang, B., Di, C., Wang, M., Zhu, B., & Qiao, K. (2025). Effect of Ultraviolet Aging on Properties of Epoxy Resin and Its Pultruded Fiber-Reinforced Composite. Polymers, 17(3), 294.

Cogliano, T., Turco, R., Di Serio, M., Salmi, T., Tesser, R., & Russo, V. (2024). Epoxidation of Vegetable Oils via the Prilezhaev Reaction Method: A Review of the Transition from Batch to Continuous Processes. Industrial & Engineering Chemistry Research, 63(26), 11231-11262. https://doi.org/10.1021/acs.iecr.3c04211

Cohen-Shacham, E., Walters, G., Maginnis, S., & Janzen, C. (2016). Nature-based Solutions to address global societal challenges. https://doi.org/10.2305/IUCN.CH.2016.13.en

Cosentino, L., Fernandes, J., & Mateus, R. (2024). Fast-Growing Bio-Based Construction Materials as an Approach to Accelerate United Nations Sustainable Development Goals. Applied Sciences, 14, 4850. https://doi.org/10.3390/app14114850

Creutzig, F., Becker, S., Berrill, P., Bongs, C., Bussler, A., Cave, B., Constantino, S., Grant, M., Heeren, N., Heinen, E., Hintz, M., Ingen-Housz, T., Johnson, E., Kolleck, N., Liotta, C., Lorek, S., Mattioli, G., Niamir, L., McPhearson, T., & Zekar, A. (2024). Towards a public policy of cities and human settlements in the 21st century. npj Urban Sustainability, 4. https://doi.org/10.1038/s42949-024-00168-7

Dahal, R. K., Acharya, B., Saha, G., Bissessur, R., Dutta, A., & Farooque, A. (2019). Biochar as a filler in glassfiber reinforced composites: Experimental study of thermal and mechanical properties. Composites Part B: Engineering, 175, 107169. https://doi.org/https://doi.org/10.1016/j.compositesb.2019.107169

Das, C., Tamrakar, S., Kiziltas, A., & Xie, X. (2021). Incorporation of Biochar to Improve Mechanical, Thermal and Electrical Properties of Polymer Composites. Polymers, 13, 2663. https://doi.org/10.3390/polym13162663

Di Mauro, C., Malburet, S., Genua, A., Graillot, A., & Mija, A. (2020). Sustainable Series of New Epoxidized Vegetable Oil-Based Thermosets with Chemical Recycling Properties. Biomacromolecules, 21(9), 3923-3935. https://doi.org/10.1021/acs.biomac.0c01059

Dobrosielska, M., Dobrucka, R., Kozera, P., Brząkalski, D., Gabriel, E., Głowacka, J., Jałbrzykowski, M., Kurzydłowski, K. J., & Przekop, R. (2023). Beeswax as a natural alternative to synthetic waxes for fabrication of PLA/diatomaceous earth composites. Scientific Reports, 13. https://doi.org/10.1038/s41598-023-28435-0

Duan, Y., Hong, Y., Meeker, W., Stanley, D., & Gu, X. (2017). Development of an Accelerated Test Methodology to the Predict Service Life of Polymeric Materials Subject to Outdoor Weathering. https://doi.org/10.48550/arXiv.1705.03050

Eftimov, P., Yokoi, N., Peev, N., Paunski, Y., & Georgiev, G. (2020). Relationships between the material properties of silicone hydrogels: Desiccation, wettability and lubricity.

Journal of Biomaterials Applications, 35, 088532822096752. https://doi.org/10.1177/0885328220967526

European Chemicals Agency. (2017). MSC unanimously agrees that bisphenol A is an endocrine disruptor. ECHA.

European Parliament. (2004). Directive 2004/42/CE on the limitation of emissions of volatile organic compounds due to the use of organic solvents in certain paints and varnishes. Official Journal of the European Union.

Faroque, F. A., Jayasundara, P. M., Rathnayake, M., Ghosh, S. B., & Bandyopadhyay-Ghosh, S. (2025). Life cycle assessment of bio-based and synthetic epoxy resin mediated composite tiles: a comparative analysis based on agricultural and industrial waste filler. Journal of Material Cycles and Waste Management, 27(4), 2482-2498. https://doi.org/10.1007/s10163-025-02260-1

Fidanovski, B., Popović, I., Radojevic, V., Radisavljevic, I., Perisic, S., & Spasojevic, P. (2018). Composite materials from fully bio-based thermosetting resins and recycled waste poly(ethylene terephthalate). Composites Part B: Engineering, 153. https://doi.org/10.1016/j.compositesb.2018.07.034

Firoozi, A. A., Firoozi, A. A., & Maghami, M. R. (2025). Life Cycle Assessment for sustainable civil infrastructure with standardized functional units and boundaries. Materials Today Sustainability, 32, 101232. https://doi.org/https://doi.org/10.1016/j.mtsust.2025.101232

Fortune Business Insights. (2026). Epoxy resin market size, share & industry analysis, by application (paint & coatings, electrical & electronics, wind turbine & composites, civil engineering, adhesive & sealants, and others), and regional forecast, 2026–2034. https://www.fortunebusinessinsights.com/epoxy-resin-market-106597

Freeze–Thaw Environment. (2025). In N. Makul (Ed.), Dictionary of Concrete Technology (pp. 625-627). Springer Nature Singapore. https://doi.org/10.1007/978-981-97-2998-2_348

Ganesan, A., Rezazgui, O., Langlois, S., Boussabbeh, C., & Barnabé, S. (2025). Pyrolytic conversion of construction, renovation, and demolition (CRD) wood wastes in Québec to biochar: Production, characterization, and identifying relevant stability indices for carbon sequestration. The Science of the total environment, 965. https://doi.org/10.1016/j.scitotenv.2025.178650

Gebrekristos, A., Tadele, E., Gebre, K., & Weldegerima, G. (2023). Production System and Quality Determination of Marketed Beeswax in Central and South-East Zones of Tigrai Region. 13, 2376-2385.

Gnawali, C. L., Shrestha, L. K., Hill, J. P., Ma, R., Ariga, K., Adhikari, M. P., Rajbhandari, R., & Pokharel, B. P. (2023). Nanoporous Activated Carbon Material from Terminalia chebula Seed for Supercapacitor Application. C, 9(4), 109.

Gu, X., Stanley, D., Byrd, W., Dickens, B., Vaca-Trigo, I., Meeker, W., Tinh, N., Chin, J., & Martin, J. (2009). Linking Accelerated Laboratory Test with Outdoor Performance Results for a Model Epoxy Coating System. In (pp. 3-28). https://doi.org/10.1007/978-0-387-84876-1_1

Guler, S., & Akbulut, Z. F. (2025). A comprehensive review of concrete durability in freeze-thaw conditions: Mechanisms, prevention, and mitigation strategies. Structures, 75, 108804. https://doi.org/https://doi.org/10.1016/j.istruc.2025.108804

Gupta, S., Sayed, M. H., Jaiswar, R., Late, D., & Walke, P. (2022). Analytical Techniques for the Wettability and Contact Angle. In (pp. 1-22). https://doi.org/10.1063/9780735425422_009

Hafezi, S. A., & Abdel-Rahman, W. M. (2019). The Endocrine Disruptor Bisphenol A (BPA) Exerts a Wide Range of Effects in Carcinogenesis and Response to Therapy. Curr Mol Pharmacol, 12(3), 230-238. https://doi.org/10.2174/1874467212666190306164507

Hajian, H., & Yusoff, W. (2015). Itaconic Acid Production by Microorganisms: A Review. Current Research Journal of Biological Sciences, 7, 37-42. https://doi.org/10.19026/crjbs.7.5205

Hammami, N., Patry, S., Soldera, A., Ameduri, B., & Habas, J.-P. (2025). Isosorbide as a Molecular Glass: New Insights into the Physicochemical Behavior of a Biobased Diol. Molecules, 30(22), 4364.

Hardoy, J., Mitlin, D., & Satterthwaite, D. (2013). Environmental Problems in an Urbanizing World. https://doi.org/10.4324/9781315071732

Hepburn, H., Pirk, C., & Duangphakdee, O. (2014). The Chemistry of Beeswax. In (pp. 319-339). https://doi.org/10.1007/978-3-642-54328-9_16

Hermansson, F., Janssen, M., & Svanström, M. (2019). Prospective study of lignin-based and recycled carbon fibers in composites through meta-analysis of life cycle assessments. Journal of Cleaner Production, 223, 946-956. https://doi.org/https://doi.org/10.1016/j.jclepro.2019.03.022

Hong, J., Radojčić, D., Ionescu, M., Petrović, Z. S., & Eastwood, E. (2014). Advanced materials from corn: isosorbide-based epoxy resins [10.1039/C4PY00514G]. Polymer Chemistry, 5(18), 5360-5368. https://doi.org/10.1039/C4PY00514G

Hosni, A. (2026). The Role of Smart Materials in Future Architecture: Self-Healing, Adaptive, and Sustainable Innovation. ARCHive-SR, 10, 78-96. https://doi.org/10.21625/archive-sr.v10i1.1243

Huang, J., & Nie, X. (2016). A simple and novel method to design flexible and transparent epoxy resin with tunable mechanical properties. Polymer International, 65. https://doi.org/10.1002/pi.5144

Ighalo, J. O., Kurniawan, S. B., Khongthaw, B., Buhari, J., Chauhan, P. K., Georgin, J., & Pfingsten Franco, D. S. (2024). Bisphenol A (BPA) toxicity assessment and insights into current remediation strategies [10.1039/D4RA05628K]. RSC Advances, 14(47), 35128-35162. https://doi.org/10.1039/D4RA05628K

Ignatenko, V., Ilyin, S., Kostyuk, A., Bondarenko, G., & Antonov, S. (2020). Acceleration of epoxy resin curing by using a combination of aliphatic and aromatic amines. Polymer Bulletin, 77. https://doi.org/10.1007/s00289-019-02815-x

Ishtiaque, A., Shrestha, M., & Chhetri, N. (2017). Rapid Urban Growth in the Kathmandu Valley, Nepal: Monitoring Land Use Land Cover Dynamics of a Himalayan City with Landsat Imageries. Environments, 4(4), 72.

International Agency for Research on Cancer. (1999). Epichlorohydrin. In Re-evaluation of some organic chemicals, hydrazine and hydrogen peroxide (IARC Monographs Vol. 71, pp. 603–628). IARC.

International Organization for Standardization. (2006). ISO 14044: Environmental management—Life cycle assessment—Requirements and guidelines. ISO.

Iwuozor, K., Emenike, E., O. Ighalo, J., Omoarukhe, F., Omuku, P., & Adeniyi, A. (2022). A Review on the Thermochemical Conversion of Sugarcane Bagasse into Biochar. Cleaner Materials, 6. https://doi.org/10.1016/j.clema.2022.100162

Jamilatun, S., Amelia, S., Pitoyo, J., Mufandi, I., & Ma'arif, A. (2023). Preparation and Characteristics of Effective Biochar Derived from Sugarcane Bagasse as Adsorbent. International Journal of Renewable Energy Research, 13, 673-680. https://doi.org/10.20508/ijrer.v13i2

Janesch, J., Arminger, B., Gindl-Altmutter, W., & Hansmann, C. (2020). Superhydrophobic coatings on wood made of plant oil and natural wax. Progress in Organic Coatings, 148, 105891. https://doi.org/https://doi.org/10.1016/j.porgcoat.2020.105891

Jia, Y., Shi, S., Liu, J., Su, S., Liang, Q., Zeng, X., & Li, T. (2018). Study of the Effect of Pyrolysis Temperature on the Cd Adsorption Characteristics of Biochar. Applied Sciences, 8, 1019. https://doi.org/10.3390/app8071019

Jin, D., Dai, J., Zhao, W., & Liu, X. (2023). Biobased Epoxy Resin with Inherently Deep-UV Photodegradability for a Positive Photoresist and Anticounterfeiting. ACS Applied Polymer Materials, 5. https://doi.org/10.1021/acsapm.3c00291

Jin, F.-L., Li, X., & Park, S.-J. (2015). Synthesis and application of epoxy resins: A review. Journal of Industrial and Engineering Chemistry, 29, 1-11. https://doi.org/https://doi.org/10.1016/j.jiec.2015.03.026

Kafle, S., Gyawali, M., Adhikari, S., Kropp, J., & Pradhan, P. (2024). Possibilities and challenges for converting waste biomass into fuel, feed, and fertilizer in Nepal. Regional Environmental Change, 24. https://doi.org/10.1007/s10113-024-02285-6

Kajiyama, T., Kanazaki, K., Venkatraman, G., Shafinaz Abdul-Rahman, P., & Matsushima, A. (2025). Migration of Bisphenol A and Its Derivatives From Epoxy Coatings and Demand for BPA-NI Products: Scientific Insights and Perspectives Leading to Regulation (EU) 2024/3190. Chem Asian J, 20(24), e00340. https://doi.org/10.1002/asia.202500340

Khadka, S., & Chalotra, S. (2022). "The Complex Nature of Integrating Sustainable Development for Mixed Used Buildings in Nepal". International Journal of Innovative Research in Engineering & Management, 83-90. https://doi.org/10.55524/ijirem.2022.9.4.14

Khamdaeng, T., Wongsiriamnuay, T., Panyoyai, N., Narkprasom, K., & Intagun, W. (2016). Mechanical properties and melting conditions of beeswax for comb foundation forming. 18, 282-293.

Khan, M., & Chavan, R. (2019). Experimental Investigation on Properties of DGEBA Based Epoxy Resin. 6, 394-398.

Khatakho, R., Gautam, D., Aryal, K. R., Pandey, V. P., Rupakhety, R., Lamichhane, S., Liu, Y.-C., Abdouli, K., Talchabhadel, R., Thapa, B. R., & Adhikari, R. (2021). Multi-Hazard Risk Assessment of Kathmandu Valley, Nepal. Sustainability, 13(10), 5369.

Kouznetsov, V. V., & Vargas Méndez, L. Y. (2022). Synthesis of eugenol-based monomers for sustainable epoxy thermoplastic polymers. Journal of Applied Polymer Science, 139(22), 52237. https://doi.org/https://doi.org/10.1002/app.52237

Köves, M., Ringer, M., & Kocsis, T. (2024). Overview of Traditional and Contemporary Industrial Production Technologies for Biochar along with Quality Standardization Methods. Land, 13. https://doi.org/10.3390/land13091388

Kulikov, A., Kryvolapov, D., Sukhyy, K., Yeromin, O., Fedak, M., Prokopenko, O., Sukha, I., Musaio, A., & Hrebik, T. (2025). Study of the Impact of Epoxidized Soybean Oil on the Characteristics of Wood-Polymer Composites. Materials, 18(11), 2455.

Kumar, S., Samal, S., Mohanty, S., & Nayak, S. (2016). Recent Development of Bio-Based Epoxy Resins: A Review. Polymer-Plastics Technology and Engineering, 57. https://doi.org/10.1080/03602559.2016.1253742

Kumar, S., Samal, S., Mohanty, S., & Nayak, S. (2019). Curing kinetics of bio-based epoxy resin-toughened DGEBA epoxy resin blend: Synthesis and characterization. Journal of Thermal Analysis and Calorimetry, 137. https://doi.org/10.1007/s10973-019-08080-4

Lai, J. C., al Saffar, Z., Chong, K. L., Rahman, R., Adrus, N., Hassan, A., Lim, T., & Wahit, M. U. (2022). A review on recent approaches to sustainable bio-based epoxy vitrimer from epoxidized vegetable oils. Industrial Crops and Products, 189, 115857. https://doi.org/10.1016/j.indcrop.2022.115857

Lala, S., Deoghare, A., & Chatterjee, S. (2018). Effect of reinforcements on polymer matrix bio-composites - An overview. Science and Engineering of Composite Materials, 25. https://doi.org/10.1515/secm-2017-0281

Lebedev, M., Startsev, O., & Kychkin, A. (2019). Development of climatic tests of polymer materials for extreme operating conditions. Procedia Structural Integrity, 20, 81-86. https://doi.org/10.1016/j.prostr.2019.12.119

Li, R. J., Gutierrez, J., Chung, Y.-L., Frank, C. W., Billington, S. L., & Sattely, E. S. (2018). A lignin-epoxy resin derived from biomass as an alternative to formaldehyde-based wood adhesives [10.1039/C7GC03026F]. Green Chemistry, 20(7), 1459-1466. https://doi.org/10.1039/C7GC03026F

Li, Y., Luo, H., Wang, S., Liu, Y., Yang, Z., Meng, X., & Yang, X. (2026). Energy-related carbon emissions in the building sector: Drivers, forecasting, and multi-scenario analysis. Energy Reports, 15, 109128. https://doi.org/https://doi.org/10.1016/j.egyr.2026.109128

LibreTexts. (2023, July 23). 18.9: Chemistry Matters—Epoxy Resins and Adhesives. Chemistry LibreTexts. https://chem.libretexts.org/Bookshelves/Organic_Chemistry/Organic_Chemistry_(Op

enStax)/18%3A_Ethers_and_Epoxides_Thiols_and_Sulfides/18.09%3A_Chemistry_MattersEpoxy_Resins_and_Adhesives

Liu, T., Hao, C., Zhang, S., Yang, X., Wang, L., Han, J., Li, Y., Xin, J., & Zhang, J. (2018). A Self-Healable High Glass Transition Temperature Bioepoxy Material Based on Vitrimer Chemistry. Macromolecules, 51(15), 5577-5585. https://doi.org/10.1021/acs.macromol.8b01010

Luna, A., Alonso, R., Cutillas, V., Ferrer, C., Gomez Ramos, M. J., Hernando, D., Valverde, A., Flores, J. M., Fernández-Alba, A., & Fernández-Alba, A. (2021). Removal of pesticide residues from beeswax using a methanol extraction-based procedure: A pilot-scale study. Environmental Technology & Innovation, 23, 101606. https://doi.org/10.1016/j.eti.2021.101606

Madej, Ł., & Kiss, A. A. (2023). Eco-efficiency improvements in the propylene-to-epichlorohydrin process. Journal of Chemical Technology & Biotechnology, 98(9), 2110-2121. https://doi.org/https://doi.org/10.1002/jctb.7453

Mailhot, B., Morlat-Thérias, S., Ouahioune, M., & Gardette, J.-L. (2005). Study of the Degradation of an Epoxy/Amine Resin, 1. Macromolecular Chemistry and Physics, 206(5), 575-584. https://doi.org/https://doi.org/10.1002/macp.200400395

Makinde-Isola, B., Oladele, I., Damilola, Akinwekomi A., Ondieki, B. a., & Makinde, A. (2025). Applications of Epoxy Resin: Adhesives, Coatings, and Composites. In. https://doi.org/10.5772/intechopen.1012261

Mantzaridis, C., Brocas, A.-L., Llevot, A., Cendejas, G., Auvergne, R., Caillol, S., Carlotti, S., & Cramail, H. (2013). Rosin acid oligomers as precursors of DGEBA-free epoxy resins. Green Chem., 15. https://doi.org/10.1039/C3GC41004H

Marturano, V., Marotta, A., Agustin-Salazar, S., Ambrogi, V., & Cerruti, P. (2023). Recent Advances in Bio-based Functional Additives for Polymers. Progress in Materials Science, 139, 101186. https://doi.org/10.1016/j.pmatsci.2023.101186

Matějka, L., Lövy, J., Pokorný, S., Bouchal, K., & Dusek, K. (1983). Curing epoxy resins with anhydrides. Model reactions and reaction mechanism. Journal of Polymer Science: Polymer Chemistry Edition, 21, 2873-2885. https://doi.org/10.1002/pol.1983.170211003

Memon, H., Wei, Y., & Zhu, C. (2022). Recyclable and reformable epoxy resins based on dynamic covalent bonds – Present, past, and future. Polymer Testing, 105, 107420. https://doi.org/https://doi.org/10.1016/j.polymertesting.2021.107420

Mesta, C., Cremen, G., & Galasso, C. (2022). Urban growth modelling and social vulnerability assessment for a hazardous Kathmandu Valley. Scientific Reports, 12(1), 6152. https://doi.org/10.1038/s41598-022-09347-x

Millán Ramírez, G. P., Byliński, H., & Niedostatkiewicz, M. (2023). Effectiveness of various types of coating materials applied in reinforced concrete exposed to freeze–thaw cycles and chlorides. Scientific Reports, 13(1), 12977. https://doi.org/10.1038/s41598-023-40203-8

Mittal, S., Das, S., Venkadeshwaran, K., Wani, T., Vanitha, S., & Thatoi, D. (2025). A review of polymeric materials in building construction: Trends, performance, and sustainability considerations. Multidisciplinary Reviews, 8, 2025ss0119. https://doi.org/10.31893/multirev.2025ss0119

Møller, V., Dam-Johansen, K., Frankær, S., & Kiil, S. (2017). Acid-resistant organic coatings for the chemical industry: a review. Journal of Coatings Technology and Research, 14. https://doi.org/10.1007/s11998-016-9905-2

Moussa, H., & Young, S. (2014). Life Cycle Assessment Comparison of Bio-based and Petroleum-based Composite Materials.

Naderizadeh, S., Heredia-Guerrero, J. A., Caputo, G., Grasselli, S., Malchiodi, A., Athanassiou, A., & Bayer, I. S. (2019). Superhydrophobic Coatings from Beeswax-in-Water Emulsions with Latent Heat Storage Capability. Advanced Materials Interfaces, 6(5), 1801782. https://doi.org/https://doi.org/10.1002/admi.201801782

Ndikumana, S., Tanane, O., Aichi, Y., Latifa, E. F., & Goudali, L. (2025). Innovative Applications of Sugarcane Bagasse in the Global Sugarcane Industry. Processes, 13(12), 3796.

Ndikumana, S., Tanane, O., Youness, A., Latifa, E., & Goudali, L. (2025). Innovative Applications of Sugarcane Bagasse in the Global Sugarcane Industry. Processes, 13, 3796. https://doi.org/10.3390/pr13123796

Neznakomova, M. P., Salaün, F., Dineff, P. D., Tsanev, T. D., & Gospodinova, D. N. (2025). Structural and Thermal Effects of Beeswax Incorporation in Electrospun PVA Nanofibers. Materials (Basel), 18(14). https://doi.org/10.3390/ma18143293

Niedermann, P., Szebényi, G., & Toldy, A. (2014). Effect of Epoxidized Soybean Oil on Curing, Rheological, Mechanical and Thermal Properties of Aromatic and Aliphatic Epoxy Resins. Journal of Polymers and the Environment, 22, 525-536. https://doi.org/10.1007/s10924-014-0673-8

Niehoff, P. J., Müller, W., Pastoors, J., Miebach, K., Ernst, P., Hemmerich, J., Noack, S., Wierckx, N., & Büchs, J. (2023). Development of an itaconic acid production process with Ustilaginaceae on alternative feedstocks. BMC Biotechnol, 23(1), 34. https://doi.org/10.1186/s12896-023-00802-9

Nikafshar, S., Zabihi, O., Hamidi, S., Moradi, Y., Barzegar, S., Ahmadi, M., & Naebe, M. (2017). A renewable bio-based epoxy resin with improved mechanical performance that can compete with DGEBA. RSC Adv., 7, 8694-8701. https://doi.org/10.1039/C6RA27283E

Noor, N., & Abdullah, E. (2026). Self-Purging Pyrolysis of Sugarcane Bagasse biomass to disordered microporous Biochar production. International Journal of Engineering and Technology, 7, 1680-1682. https://doi.org/10.14419/ijet.v7i4.38.29233

Ofori, P. (2023). Circular economy practices in third world nations: challenges and implications for environmental sustainability. Environment, Development and Sustainability, 27, 1691-1745. https://doi.org/10.1007/s10668-023-03939-x

Okabe, M., Dwiarti, L., Kanamasa, S., & Park, E. (2009). Biotechnological production of itaconic acid and its biosynthesis in Aspergillus terreus. Applied microbiology and biotechnology, 84, 597-606. https://doi.org/10.1007/s00253-009-2132-3

Papadopoulou, K., Ainali, N. M., Mašek, O., & Bikiaris, D. N. (2024). Biochar as a UV Stabilizer: Its Impact on the Photostability of Poly(butylene succinate) Biocomposites. Polymers (Basel), 16(21). https://doi.org/10.3390/polym16213080

Paramarta, A., & Webster, D. C. (2016). Bio-based high performance epoxy-anhydride thermosets for structural composites: The effect of composition variables. Reactive and Functional Polymers, 105, 140-149. https://doi.org/https://doi.org/10.1016/j.reactfunctpolym.2016.06.008

Pham, H., & Marks, M. (2004). Epoxy Resins. In (Vol. 9). https://doi.org/10.1002/0471440264.pst119

Phan, Q., Duc, T., Nguyen, P., Zheng, Y., Jin, W., Nguyen, T. L., Wang, M., Do, N., Le, P., & Duong, H. (2026). Sustainable end-of-life strategies for thermoset-based fiber-reinforced composites: advances in recycling and upcycling. Journal of Physics: Materials, 9. https://doi.org/10.1088/2515-7639/ae5cd3

Prakash, M., Raghavendra, D. G., Ojha, S., Manoj, P., & Mallampati, S. (2021). Effect of biomass derived biochar materials on mechanical properties of biochar epoxy composites. ARCHIVE Proceedings of the Institution of Mechanical Engineers Part C

Journal of Mechanical Engineering Science 1989-1996 (vols 203-210), 235. https://doi.org/10.1177/0954406221990705

Pramanik, M., Fowler, E., & Rawlins, J. (2014). Cure kinetics of several epoxy–amine systems at ambient and high temperatures. Journal of Coatings Technology and Research, 11. https://doi.org/10.1007/s11998-013-9565-4

Quintana, A., Alba, J., del Rey, R., & Guillén-Guillamón, I. (2018). Comparative Life Cycle Assessment of gypsum plasterboard and a new kind of bio-based epoxy composite containing different natural fibers. Journal of Cleaner Production, 185, 408-420. https://doi.org/https://doi.org/10.1016/j.jclepro.2018.03.042

Radi, B., Wellard, M., & George, G. (2013). Effect of dangling chains on the structure and physical properties of a tightly crosslinked poly(ethylene glycol) network. Soft Matter, 9, 3262. https://doi.org/10.1039/c3sm27819k

Rajyaguru, R., Rathod, B., Tomar, R. S., & Sharma, S. (2022). Oil content and fatty acid profiling of soybean (Glycine max L. Merrill) of Indian cultivar.

Rane, N., Achari, A., & Choudhary, S. (2023). Multi-Criteria Decision-Making (MCDM) as a powerful tool for sustainable development: Effective applications of AHP, FAHP, TOPSIS, ELECTRE, and VIKOR in sustainability. International Research Journal of Modernization in Engineering Technology and Science, 5, 2654-2670. https://doi.org/10.56726/IRJMETS36215

Safaei, A., Brancart, J., Wang, Z., Yazdani, S., Vanderborght, B., Van Assche, G., & Terryn, S. (2023). Fast Self-Healing at Room Temperature in Diels-Alder Elastomers. Polymers (Basel), 15(17). https://doi.org/10.3390/polym15173527

Saha, P., & Kim, B. S. (2019). Preparation, Characterization, and Antioxidant Activity of β-Carotene Impregnated Polyurethane Based on Epoxidized Soybean Oil and Malic Acid. Journal of Polymers and the Environment, 27. https://doi.org/10.1007/s10924-019-01492-1

Samanta, A., Kataria, N., Dobhal, K., Joshi, N. C., Singh, M. P., Verma, S., Suyal, J., & Jakhmola, V. (2023). Wijs, Potassium Iodate, and AOCS Official Method to Determine the Iodine Value (IV) of Fat and Oil. Biomedical and Pharmacology Journal, 16, 1201-1210. https://doi.org/10.13005/bpj/2700

Samanth, M., Hiremath, P., Deepak, G., Naik, N., Arunkumar, S., Heckadka, S., & Shivamurthy, R. (2025). Sustainable Composites from Sugarcane Bagasse Fibers and Bio-Based Epoxy with Insights into Wear Performance, Thermal Stability, and

Machine Learning Predictive Modeling. Journal of Composites Science, 9, 1-28. https://doi.org/10.3390/jcs9030124

Sathyabama, K., & Firdous, S. (2025). Effect of Pyrolysis Temperature on the Physicochemical Properties and Structural Characteristics of Agricultural Wastes-Derived Biochar. ACS Omega, 10(33), 37013-37024. https://doi.org/10.1021/acsomega.5c00120

SDG Action. (2024, July 16). Advancing the global agenda through adopting circular economy. https://sdg-action.org/advancing-the-global-agenda-through-adopting-circular-economy/

Seddon, N., Chausson, A., Berry, P., Girardin, C. A. J., Smith, A., & Turner, B. (2020). Understanding the value and limits of nature-based solutions to climate change and other global challenges. Philosophical Transactions of the Royal Society B: Biological Sciences, 375(1794), 20190120. https://doi.org/10.1098/rstb.2019.0120

Shabeer, M., Mathew, M., O, M., & Athiyanathil, S. (2025). Beeswax-modified super hydrophobic acrylonitrile butadiene styrene/polyurethane electrospun membrane for effective oil–water separation. Materials Advances, 6, 5991-6000. https://doi.org/10.1039/D5MA00438A

Shankar, A., Maloo, S., & Upadhyay, A. (2023). Synthesis And Applications of Bisphenol-A Epoxide Resins - A Review. Journal of Student Research, 12. https://doi.org/10.47611/jsrhs.v12i4.5215

Sherpa, T. (2024). Integration of urban ecosystem-based adaptation in Nepal: A policy landscape analysis. PLOS ONE, 19, e0297786. https://doi.org/10.1371/journal.pone.0297786

Shrestha, L. K., Shahi, S., Gnawali, C. L., Adhikari, M. P., Rajbhandari, R., Pokharel, B. P., Ma, R., Shrestha, R. G., & Ariga, K. (2022). Phyllanthus emblica Seed-Derived Hierarchically Porous Carbon Materials for High-Performance Supercapacitor Applications. Materials, 15(23), 8335.

Shundo, A., Yamamoto, S., & Tanaka, K. (2022). Network Formation and Physical Properties of Epoxy Resins for Future Practical Applications. JACS Au, 2, 1522-1542. https://doi.org/10.1021/jacsau.2c00120

Sindane, N., Gabriel, S., & Dicks, J. (2025). Mechanical properties of epoxy resins under various loading conditions - Comparison between bio-and petroleum-based resins commercially available in South Africa.

Sowińska-Baranowska, A., Masłowski, M., Miedzianowska-Masłowska, J., Maciejewska, M., Martuzevičius, D., Prasauksas, T., & Masione, G. (2026). Mechanical and Structural Performance of Bio-Resin Composites Reinforced with Biopolymer Nonwoven Fabrics. Polymers, 18(10), 1215.

Sozio, N., Kiani, A., Viscusi, G., Di Stasi, C., Gorrasi, G., & Acocella, M. (2026). Mechanochemical functionalization of biochar for providing new eco-sustainable hydrophobic coating. Biochar, 8. https://doi.org/10.1007/s42773-025-00532-5

Sparavigna, A. C. (2023). Multifunctional Porosity in Biochar. International Journal of Sciences. https://doi.org/10.18483/ijSci.2694

Spee, T., Duivenbooden, C., & Terwoert, J. (2006). Epoxy Resins in the Construction Industry. Annals of the New York Academy of Sciences, 1076, 429-438. https://doi.org/10.1196/annals.1371.010

Srinivasa, D., Pachdhare, P., Varshney, P., Mathada, D., Dash, S., & Tiwari, A. (2025). The Impact of Climate Change on Urban Infrastructure: A Comprehensive Study on Resilient Civil Engineering Design, Adaptation Strategies, and Sustainable Development. International Journal of Environmental Sciences, 991-999. https://doi.org/10.64252/8j67x108

Sugiman, S., & Sulardjaka, S. (2016). Water Absorption and Desorption Behaviour and their Effect on the Tensile Properties of FM 73M Adhesive Film. International Journal of Technology, 7, 438. https://doi.org/10.14716/ijtech.v7i3.2804

Sun, Y., Wang, M., Wang, Z., Mao, Y., Jin, L., Zhang, K., Xia, Y., & Gao, H. (2022). Amine-Cured Glycidyl Esters as Dual Dynamic Epoxy Vitrimers. Macromolecules, 55(2), 523-534. https://doi.org/10.1021/acs.macromol.1c01914

Svečnjak, L., Baranović, G., Vinceković, M., Prđun, S., Bubalo, D., & Tlak Gajger, I. (2015). An Approach for Routine Analytical Detection of Beeswax Adulteration Using FTIR-ATR Spectroscopy. Journal of Apicultural Science, 59. https://doi.org/10.1515/JAS-2015-0018

Tasim, B., Masood, T., Shah, Z., Arif, M., Ullah, A., Miraj, G., & Samiullah, M. (2019). Quality Evaluation of Biochar Prepared from Different Agricultural Residues. Sarhad Journal of Agriculture, 35. https://doi.org/10.17582/journal.sja/2019/35.1.134.143

Taysun, M. B., Dam-Johansen, K., & Bi, H. (2025). Hydrogen bonding and anti-plasticization in epoxy coatings: Molecular insights into water uptake and network stability. Progress in Organic Coatings, 209, 109602. https://doi.org/https://doi.org/10.1016/j.porgcoat.2025.109602

Teleky, B. E., & Vodnar, D. C. (2019). Biomass-Derived Production of Itaconic Acid as a Building Block in Specialty Polymers. Polymers (Basel), 11(6). https://doi.org/10.3390/polym11061035

Thapa, R., & Murayama, Y. (2012). Scenario based urban growth allocation in Kathmandu Valley, Nepal. Landscape and Urban Planning, 105, 140-148. https://doi.org/10.1016/j.landurbplan.2011.12.007

Urban Systems and Other Settlements. (2023). In C. Intergovernmental Panel on Climate (Ed.), Climate Change 2022 - Mitigation of Climate Change: Working Group III Contribution to the Sixth Assessment Report of the Intergovernmental Panel on Climate Change (pp. 861-952). Cambridge University Press. https://doi.org/DOI: 10.1017/9781009157926.010

Van de Velde, N., Javornik, S., Sever, T., Štular, D., Šobak, M., Štirn, Ž., Likozar, B., & Jerman, I. (2021). Bio-Based Epoxy Adhesives with Lignin-Based Aromatic Monophenols Replacing Bisphenol A. Polymers, 13(22), 3879.

Vijayan, S., S, A., & Sahoo, S. (2023). Effect of Beeswax on hydrophobicity, moisture resistance and transparency of UV curable linseed oil based coating for compostable paper packaging. Industrial Crops and Products, 197, 116645. https://doi.org/10.1016/j.indcrop.2023.116645

Wang, X., Niu, H., Guo, W., Song, L., & Hu, Y. (2021). Cardanol as a versatile platform for fabrication of bio-based flame-retardant epoxy thermosets as DGEBA substitutes. Chemical Engineering Journal, 421, 129738. https://doi.org/https://doi.org/10.1016/j.cej.2021.129738

Wu, F., Zhang, Q., Dong, S., Cai, Y., Yang, S., Xu, F., Luo, P., & Jiang, J. (2025). Biochar modification enhances mechanical and durability properties of cement-based materials. Sci Rep, 15(1), 22174. https://doi.org/10.1038/s41598-025-06968-w

Xia, L., Gui, T., Wang, J., Tian, H., Wang, Y., Ning, L., & Wu, L. (2025a). Bio-Based Coatings: Progress, Challenges and Future Perspectives. Polymers, 17, 3266. https://doi.org/10.3390/polym17243266

Xia, L., Gui, T., Wang, J., Tian, H., Wang, Y., Ning, L., & Wu, L. (2025b). Bio-Based Coatings: Progress, Challenges and Future Perspectives. Polymers, 17(24), 3266.

Xia, Y., & Larock, R. C. (2010). Vegetable oil-based polymeric materials: synthesis, properties, and applications [10.1039/C0GC00264J]. Green Chemistry, 12(11), 1893-1909. https://doi.org/10.1039/C0GC00264J

Xu, Y., Dai, S., Bi, L., Jiang, J., Zhang, H., & Chen, Y. (2021). Catalyst-Free Self-Healing Bio-Based Polymers: Robust Mechanical Properties, Shape Memory, and Recyclability. Journal of agricultural and food chemistry, 69. https://doi.org/10.1021/acs.jafc.1c01885

Yang, D. Y., & Frangopol, D. M. (2019). Life-cycle management of deteriorating civil infrastructure considering resilience to lifetime hazards: A general approach based on renewal-reward processes. Reliability Engineering & System Safety, 183, 197-212. https://doi.org/https://doi.org/10.1016/j.ress.2018.11.016

Yang, H., Shafaghat, H., Öman, T., & Johansson, A.-C. (2025). Sustainable production of bio-based epoxy resins using the phenolics produced via atmospheric ex-situ catalytic hydropyrolysis of biomass. Journal of Industrial and Engineering Chemistry, 148, 492-501. https://doi.org/https://doi.org/10.1016/j.jiec.2025.01.001

Zafeer, M., Menezes, R., Hillemane, V., & K, S. (2023). Sugarcane bagasse-based biochar and its potential applications: a review. Emergent Materials, 7. https://doi.org/10.1007/s42247-023-00603-y

Zhang, C., Wang, Y., Liu, L., Feng, X., Qiu, J., Li, S., & Liu, G. (2026). Recent Advances in the Biobased Synthesis and Expanding Applications of Isosorbide: A Review. ChemistrySelect, 11(3), e06204. https://doi.org/https://doi.org/10.1002/slct.202506204

Zhang, Y., Liu, X., Wan, M., Zhu, Y., & Zhang, K. (2024). From renewable biomass to bio-based epoxy monomers and bio-based epoxy curing agents: Synthesis and performance. Polymer Degradation and Stability, 229, 110988. https://doi.org/https://doi.org/10.1016/j.polymdegradstab.2024.110988

Zhang, Y., Liu, X., Wan, M., Zhu, Y., & Zhang, K. (2024). Recent Development of Functional Bio-Based Epoxy Resins. Molecules, 29(18). https://doi.org/10.3390/molecules29184428

Zhao, L., Zha, Y., Miao, W., Wang, B., Han, Y., & Tang, J. (2026). Regulation of pyrolysis temperature on the structural evolution of maize stover biochar and its mechanism of Cd2+ adsorption. Frontiers in Environmental Science, 14. https://doi.org/10.3389/fenvs.2026.1815592

Zhao, X., Long, Y., Xu, S., Liu, X., Chen, L., & Wang, Y.-Z. (2023). Recovery of epoxy thermosets and their composites. Materials Today, 64. https://doi.org/10.1016/j.mattod.2022.12.005

APPENDIX –I PAPER SUBMISSION ACCEPTANCE PROOF

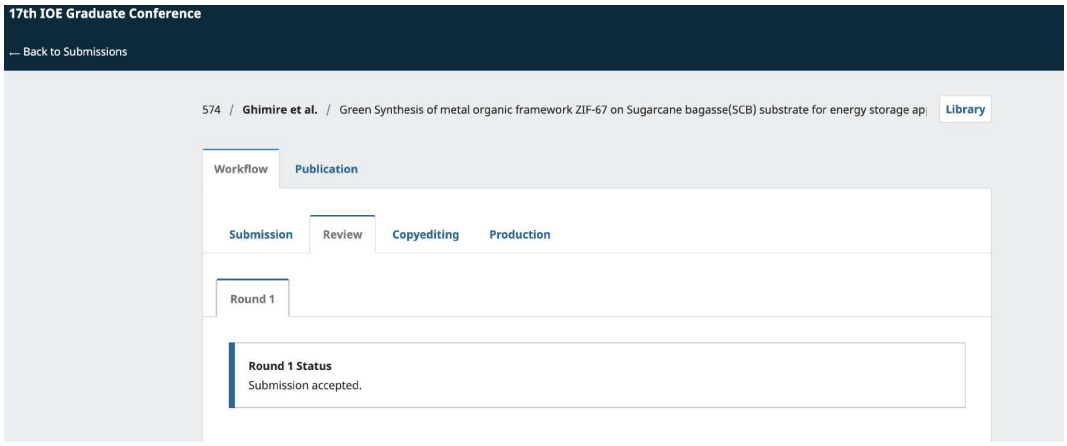

APPENDIX –II LABORATORY WORK GLIMPSE

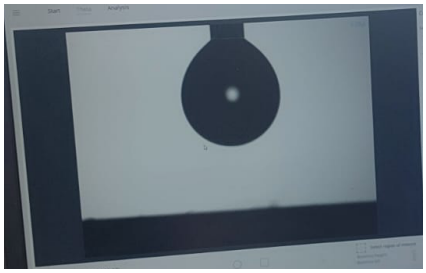

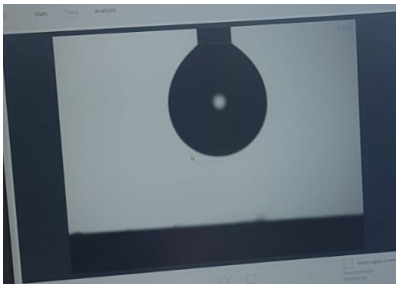

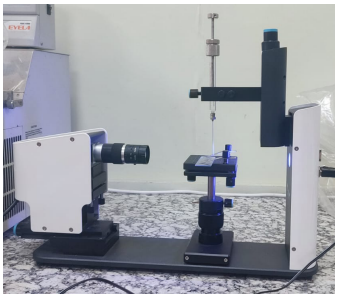

APPENDIX –III PLAGIARISM CHECK REPORT

iThenticate®

Similarity Report ID: oid:3117:592297172

PAPER NAME
HYBRID BIO-BASED EPOXY COMPOSITES FOR CLIMATE-RESILIENT SMART URBAN INFRASTRUCTURE

AUTHOR
Sachin Ghimire

WORD COUNT
28272 Words

CHARACTER COUNT
176196 Characters

PAGE COUNT
104 Pages

FILE SIZE
2.1MB

SUBMISSION DATE
May 17, 2026 7:33 PM GMT+5:45

REPORT DATE
May 17, 2026 7:35 PM GMT+5:45

2% Overall Similarity

The combined total of all matches, including overlapping sources, for each database.

- 1% Internet database
- 1% Publications database
- Crossref database
- Crossref Posted Content database
- 0% Submitted Works database

Excluded from Similarity Report

- Bibliographic material
- Quoted material
- Cited material
- Small Matches (Less then 10 words)

Summary